Analysis of the EDF family of schedulers

Stefan Martin Scriba

22 February 2009

Submitted in fulfillment of the academic requirements
for the degree of PhD
in the School of Electrical, Electronic and Computer Engineering
at the University of KwaZulu-Natal, Durban, South Africa

To my wife Mia

Preface

The research work presented in this thesis was performed by Stefan Martin Scriba, under the supervision of Prof. Fambirai Takawira, at the University of KwaZulu-Natal's School of Electrical, Electronic and Computer Engineering, in the Research Centre for Radio Access and Rural Technologies. This work was partially sponsored by Telkom S.A. Ltd, Alcatel-Lucent, and THRIP as part of the Centre of Excellence programme.

Parts of this thesis were presented by the author at the SATNAC 2003 conference held at George, South Africa, the SATNAC 2004 conference at Spier, Stellenbosch, South Africa, the SATNAC 2005 conference at the Champagne Sports Resort, South Africa, and the IEEE ICT 2005 conference at Cape Town, South Africa.

DECLARATION

I, Stefan Martin Scriba, declare that

1. The research reported in this thesis, except where otherwise indicated, is my original work.
2. This thesis has not been submitted for any degree or examination at any other university.
3. This thesis does not contain other persons' data, pictures, graphs or other information, unless specifically acknowledged as being sourced from other persons.
4. This thesis does not contain other persons' writing, unless specifically acknowledged

as being sourced from other researchers. Where other written sources have been quoted, then:

(a) their words have been re-written but the general information attributed to them has been referenced;

(b) where their exact words have been used, their writing has been placed inside quotation marks, and referenced.

5. Where I have reproduced a publication of which I am an author, co-author or editor, I have indicated in detail which part of the publication was actually written by myself alone and have fully referenced such publications.

6. This thesis does not contain text, graphics or tables copied and pasted from the Internet, unless specifically acknowledged, and the source being detailed in the thesis and in the References sections.

Signed: _____

Acknowledgements

I wish to thank my supervisor, Prof. Fambirai Takawira, for the guidance and the many hours of discussion that have made this thesis possible. He showed interest and support in my personal life, thereby creating a relaxed and enjoyable work environment.

I wish to thank Dr. Xu from Electronic Engineering, Dr Moolman from Statistics, Dr Scribani from Mathematics, and Prof Zaverdinos from Applied Mathematics at the Pietermaritzburg campus, for sharing their insights and answering all my peculiar e-mail requests.

Many thanks to Telkom South Africa, Alcatel-Lucent, and THRIP who partially financed this research project. A special word of thanks to my manager Johan Myburgh, and fellow employees Jaco Schutte, Joe van Zyl and everyone else in Technical Product Development, for their friendship and encouragement during the last few months.

And last, but definitely not least, a great thank you to my wife, Mia, and our beautiful little boys, Alexander and Timothy, who had to endure my lack of sleep after many late nights.

Abstract

Modern telecommunications companies are moving away from conventional circuit-switched architectures to more versatile packet-switched infrastructures. Traditional First-In-First-Out (FIFO) queues that are currently multiplexing IP traffic are not able to meet the strict Quality-of-Service (QoS) requirements of delay sensitive real-time traffic.

Two main solution families exist that separate heterogeneous traffic into appropriate classes. The first is known as Generalized Processor Sharing (GPS), which divides the available bandwidth among the contending classes, proportionally to the throughput guarantee negotiated with each class. GPS and its myriad of packetised variants are relatively easy to analyse, as the service rate of individual classes is directly related to its throughput guarantee. As GPS splits the arriving traffic into separate queues, it is useful for best-effort traffic, supplying each class of traffic with either a maximum or minimum amount of bandwidth that it deserves.

The second solution is the Earliest Deadline First (EDF) scheduler, also known as Earliest Due Date (EDD). Each traffic class has a delay deadline, by which the individual packets need to be served in order to meet their heterogeneous QoS requirements. EDF selects packets that are closest to their deadline. It is therefore primarily useful for delay sensitive real-time traffic. Although this is a simple algorithm, it turns out to be surprisingly difficult to analyse. Several papers attempted to analyse EDF. Most of them found either discrete bounds, which lie far away from the mean, or stochastic bounds which tend to capture the delay behaviour of the traffic more accurately.

After the introductory first chapter, this thesis simulates a realistic cellular environment,

where packets of various classes of service are transmitted across an HSDPA air interface. The aim is to understand the behaviour of EDF and its channel aware Opportunistic EDF scheduler compared to other scheduling families commonly used in HSDPA environments. In particular, Round Robin is simulated as the most simplistic scheduler. Max C/I chooses packets solely based on the best channel conditions. Finally, PF-T is a scheme that tries to maximise the overall transmission rate that packets experience, but this metric gets divided by the throughput that each class already achieved. This introduces a form of long-term fairness that prevents the starvation of individual classes.

The third chapter contains the main analysis, which uses Large Deviation principles and the Effective Bandwidth theory to approximate the deadline violation probability and the delay density function of EDF in a wired network. A definition for the fairness of EDF is proposed. The analysis is extended to approximate the stochastic fairness distribution.

In the fourth chapter of the thesis an opportunistic EDF scheduler is proposed for mobile legs of a network that takes advantage of temporary improvements in the channel conditions. An analytical model is developed that predicts the delay density function of the opportunistic EDF scheduler. The channel propagation gain is assumed to be log-normally distributed, which requires graphical curve fitting, as no closed-form solution exists.

Contents

List of Figures

List of Tables

List of Acronyms

16QAM	16 Quadrature Amplitude Modulation
3G	Third Generation
3GPP	3rd Generation Partnership Project
4G	Fourth Generation
AF	Assured Forwarding
AMC	Adaptive Modulation and Coding
AMPS	Advanced Mobile Phone Systems
AOS	Aggregate Opportunistic Scheduling
APAOS	Access Probability-based Assignment Opportunistic Scheduling
ARQ	Automatic Repeat-reQuest
BE	Best Effort
BER	Bit Error Rate
BTS	Base Transceiver Station
CDF	Cumulative Distribution Function
CDMA	Code Division Multiple Access
CE	Customer Edge
CoS	Class of Service
CQS	Capacity Queue Scheduling
CSI	Channel State Information
D-AMPS	Digital Advanced Mobile Phone Systems
DS-CDMA	Direct-Sequence Code Division Multiple Access
DSCP	DiffServe Code Points

EDF	Earliest Deadline First
EF	Expedited Forwarding
ETSI	European standardization body
FIFO	First In First Out
FPLMTS	Future Public Land Mobile Telecommunication Systems
FTP	File Transfer Protocol
GGSN	Gateway GPRS Support Node
GPS	Generalized Processor Sharing
GSM	Global Systems for Mobile communications
HPF	Hybrid Proportional Fair
HS-DSCH	High-Speed Downlink Shared Channel
HSDPA	High Speed Downlink Packet Access
HSPA	High Speed Packet Access
HSUPA	High Speed Uplink Packet Access
HTTP	Hyper Text Transfer Protocol
IEEE	Institute of Electrical and Electronics Engineers
IET	International Conference on Telecommunications
IMSL	International Mathematics and Statistics Library
IMT-2000	International Mobile Telephony 2000
IP	Internet Protocol
ITU	International Telecommunications Union
LAN	Local Area Network
LFI	Link Fragmentation and Interleaving
MAC	Medium Access Control
Max-rSNR	Maximum relative Signal-to-Noise Ratio
MaxC/I	Maximum Carrier to Interference Ratio
MCS	Modulation and Coding Scheme
MPLS	Multi-Protocol Label Switching
NMT	Nordic Mobile Telephone
O-EDF	Opportunistic-Earliest Deadline First
PCS	Personal Communication Systems

PDC	Personal Digital Cellular
PDF	Probability Density Function
PE	Provider Edge
PER	Packet Error Rate
PFQ-OS	Packet Fair Queueing-based Opportunistic Scheduling
PF-T	Proportional Fair Throughput
PG	Propagation Gain
QoS	Quality of Service
QPSK	Quadrature Phase Shift Keying
RNC	Radio Network Controller
SATNAC	South African Telecommunication Network and Applications Conference
SGSN	Serving GPRS Support Node
SIR	Signal-to-Interference power Ratio
SLA	Service Level Agreement
SNR	Signal-to-Noise Ratio
TACS	Total Access Communication Systems
TBF	Time-Between-Failures
TCP	Transmission Control Protocol
TTI	Transmission Time Interval
TTR	Time-To-Repair
UHF	Ultra-High Frequency
UMTS	Universal Mobile Telecommunications System
UPT	Universal Personal Telecommunication
VoIP	Voice over Internet Protocol
VPN	Virtual Private Network
VRF	Virtual Routing/Forwarding
W-CDMA	Wideband Code Division Multiple Access
WARC	World Administrative Radio Conference
WiFi	Wireless Fidelity

List of Symbols

a	Exponent of the auto-covariance
A_i	Total number of class i packets that arrive over a time period of $d_i - d_j$
$A_{ji}[0,t]$	Amount of EDF work of class j that source i produces in the time interval $[0,t]$
b	Large buffer asymptotic buffer space per source
B	Large buffer asymptotic total buffer length
$B(t_1,t_2)$	Golestani definition of set of sessions that are backlogged during interval $(t1,t2)$
BER	Bit error rate
C	Bandwidth capacity available to EDF scheduler
c	Large buffer asymptotic bandwidth per source
CDF_N	Cumulative distribution function of Normal distribution
CDF_{log-N}	Cumulative distribution function of Log-normal distribution
d	Delay deadline of class of traffic
d_i	Delay deadline of class i traffic
D_i	Delay experienced by head-of-line packet of queue containing class i traffic
$\frac{E_b}{I_0}$	Energy-to-interference spectral density
$\left(\frac{E_b}{I_0}\right)_{Threshold}$	Maximum Packet error rate threshold
$F(x)$	Cumulative distribution function with respect to x
$f(x)$	Probability density function with respect to x
$f \sim \text{log-N}(\mu,\sigma)$	Log-normal distribution with mean μ and standard deviation σ
$f \sim \text{N}(\mu,\sigma)$	Normal distribution with mean μ and standard deviation σ
F^S	Upper fairness bound
$F_i(t)$	Cumulative distribution function of the delay of class i traffic

$F_{D_i}(t)$	O-EDF cumulative distribution function of the queueing delay of traffic class i
$f_{D_i}(t)$	O-EDF probability density function of the queueing delay of traffic class i
$f_{\lvert\frac{D_a}{d_a}-\frac{D_b}{d_b}\rvert}(t)$	Stochastic fairness distribution probability density function
$g(k)$	partial expectation of the left truncated density $f(x)$
G_c	CDMA user channel gain
$G_c^{P_{Extra}}$	CDMA user channel gains of the extra-cell interference
$G_c^{P_{Inter}}$	CDMA user channel gains of the intra-cell interference
$G_c^{P_{RX}}$	CDMA user channel gains of the transmission
$h_i(t)$	Class boundary events for class i traffic
I_{Extra}	CDMA extra-cell interference
I_{Inter}	CDMA intra-cell interference
J	Total number of traffic classes being produced for EDF
k	Golestani definition of the session
k_j	Number of class j traffic sources
L	Packet Length
$L(t)$	Path-loss component of a UHF signal over flat terrain
$L_n(x)$	Laguerre polynomials of degree n
$l_{\max}$	Maximum Web packet length
$l_{\min}$	Minimum Web packet length
M	Number of video and voice independent ON-OFF Markov mini-sources
N_0	CDMA Noise spectral density
n_i	Number of transmission slots that should be assigned to traffic class i
p	Number of TTIs that Video and Voice mini-sources are in the ON-state
P_D	CDMA Node B available power
$p(x)$	Probability density function with respect to x
PER	Packet error rate
PG	CDMA processing gain
p_j	Packet of traffic class j
P_{RX}	CDMA useful received power
P_{TX}	CDMA transmitted power to the user
P_{vio}^i	Deadline violation probability of class i traffic

Q	Large Buffer asymptotic queue length
q	Number of TTIs that video and voice mini-sources are in the OFF-state
$Q(T-d_i)$	Queue length of packets that will be served before packet p_i by EDF
Q_{Total}	Total number of packets that will be served by EDF before packet p_i
r	Distance from Node B (in km)
R_b	CDMA bit-rate
R_i	Transmission rate assigned to class i traffic by GPS scheduler
r_k	Golestani definition of the service share allocated to session k
s	Effective bandwidth theory space parameter
$s(t)$	CDMA shadowing component
SIR	Signal-to-interference power ratio
t	Effective Bandwidth Theory time parameter
T0	EDF Audio traffic class
T1	EDF Video Conference traffic class
T2	EDF Stored Video traffic class
T_j	Time at which packet of class j arrives in EDF queue
TTI	Transmission Time Interval of HSDPA
$u(\cdot)$	Unitary step function
V	Constant rate ON-state at which Video and Voice mini-sources produce traffic
W	CDMA spreading bandwidth
w_i	Gauss-Laguerre / Gauss-Hermite quadrature weights
$W_k(t_1,t_2)$	Golestani definition of number of bits of session k transmitted during $(0,t)$
$X[0,t]$	Amount of work that arrives from a source in the interval $[0,t]$
x_i	Gauss-Laguerre / Gauss-Hermite quadrature nodes
α	CMDA intra-cell non-orthogonality coefficient
$\alpha(s,t)$	Effective Bandwidth of a source
$\bar{G}_c$	Short-term mean channel gain
$\bar{P}$	Mean of geometrically distributed number of packets produced by Web traffic
$\bar{\Psi}_m$	O-EDF mean channel gain of wireless channel m
ΔT	Packet Inter-Arrival Time
$\delta(\cdot)$	Dirac delta function

δ_i	Class-based violation probability requirement of LWDF and M-LWDF
ϵ	CDMA extra-cell interference power-to-the total received power ratio
λ_j	Mean arrival rate of Poisson source of class j
Φ	CDF of the standard normal, with a mean of 0 and standard deviation of 1
Ψ_m	O-EDF channel gain of wireless channel m
ρ_i	Throughput guarantee of class i of a GPS scheduler
τ	Scheduling interval when previously chosen packet has completed transmission
ξ	Pareto constant

Chapter 1

Introduction

1.1 MPLS-based Virtual Private Networks and their need for Quality of Service

With the use of Local area networks (LANs), branches in remote areas or separate cities could only be interconnected using point-to-point leased-line circuits. These were built using technologies such as Frame Relay, MARTIS, or ATM. As technology improved, it became possible to connect multiple sites to a core network, which formed the first instances of Virtual Private Networks (VPNs). At this time, links were exclusively circuit-switched, which offered perfect separation of traffic across the core network.

With the advent of IP communication, telecommunication operators realised that multiplexing packet-switched traffic implied a huge reduction in capacity requirements, as portions of the available bandwidth no longer had to be exclusively reserved per virtual circuit. This in turn resulted in a reduction in capital expenditure. The problem with IP-based networking is that packets originating from various customers travel across the network together. Separation of traffic is no longer possible. Security therefore becomes a concern. Furthermore, packets would queue at each router, which implied that one customer could affect another customer's experience.

1.1.1 MPLS networking [1]

The advent of Multi-Protocol Label Switching (MPLS) solved both these problem, as packets traversing the core are separated into VPNs using Virtual Routing/Forwarding (VRF) instances on the Provider Edge (PE) routers. Figure 1.1 shows how a PE router is connected to a Customer Edge (CE) router, which is usually situated on the customer's premises. Note that with MPLS, customers are not able to affect the experience of other customers, but the various classes of services of single customers will still affect each other. Hence the need for Quality of Service (QoS).

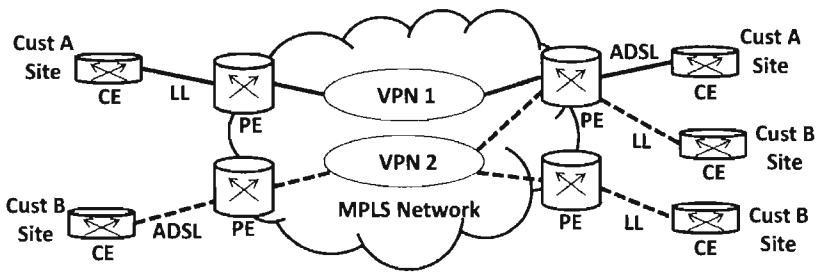

Figure 1.1: Basic VPN Architecture

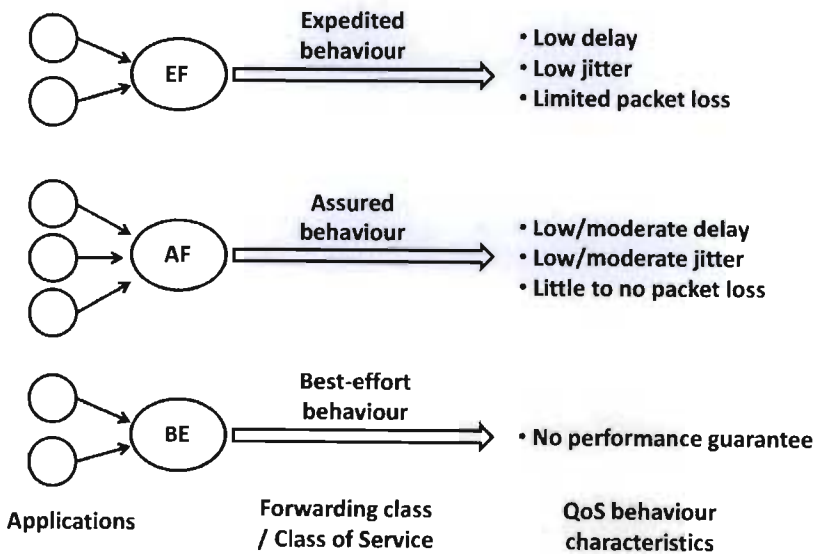

Figure 1.2: The mapping of application traffic into CoS

1.1.2 Quality of Service [2]

Packets traversing a VPN will all be treated the same, unless QoS has been configured in every core and access router where traffic converges and ends up queueing. Figure 1.2 shows how the traffic generated by the applications running on the LAN environment will be mapped into various Classes of Service (CoS). Every packet that enters the VPN is marked with the CoS that it belongs to. Typically the DiffServe Code Points (DSCP) bits in the IP header are used for this purpose.

As the traffic traverses the VPN, every router must be configured with a QoS profile that will interact with the traffic in various ways. Figure 1.3 shows the possible enforcement points that must be considered when configuring QoS on the access routers. Note that the core routers too must be configured to achieve QoS. Although, telecommunication operators will often collapse some of the CoS into a smaller set, while the traffic travels across the core.

Figure 1.4 gives an overview of the various QoS mechanisms that can be enforced in a typical router. These include:

- Classification — grouping packets into CoS
- Marking — setting the DSCP or IP Precedence bits
- Rate limiting — discarding packets
- Queueing — packets are buffered before transmission
- Scheduling — controls the allocation of resources to queues
- Congestion avoidance — avoiding congestion by dropping random packets
- Shaping — delaying packets to conform to a traffic profile
- Link Fragmentation and Interleaving (LFI) - breaking large packets into smaller fragments and interleaving smaller packets

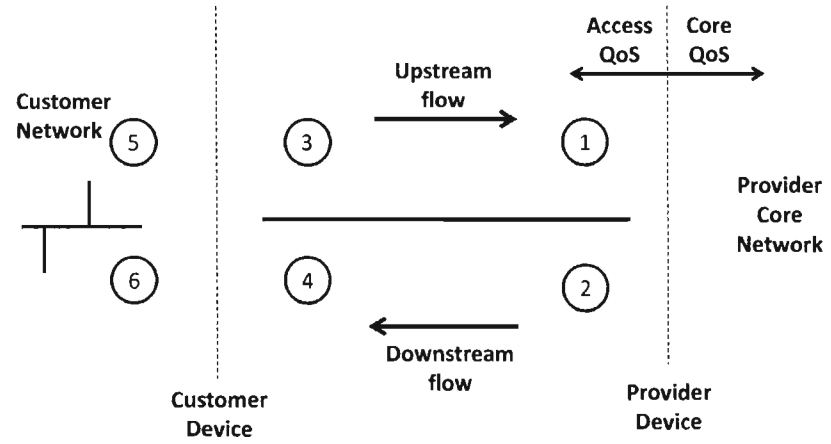

Figure 1.3: QoS Policy Enforcement Points on the access link

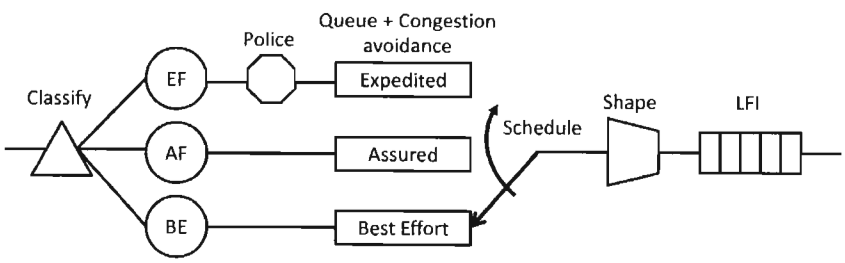

Figure 1.4: QoS Mechanisms

1.2 Mobile networks

Traditionally, the largest investment a telecommunications operator would make, was in the so-called last-mile, the last section of the network that usually connects a customer to the closest exchange. For the telephonic requirements of residential and small business customers, the last mile consisted of copper pairs. For larger corporate customers that require much more bandwidth, fibre cables would be laid. The installation and maintenance of these millions of kilometers of cables formed by far the largest portion of a telecommunication operator's budget.

With the advent of cellular technology, this significantly changed. It was suddenly possible to serve a large number of customers from a single base station. Although not a suitable solution for the requirements of corporate customers, the reduction in infrastructure and maintenance costs of narrow-band users is staggering. As a result telecommunications companies are looking at replacing as much of their fixed-line infrastructure and replacing this with wireless and mobile solutions. The challenge though, is how to maximise the capacity and offer effective QoS across these air interfaces. Specialised cross-layer designs can, in theory, greatly enhance the performance of these technologies. As an example, the fourth chapter of this thesis models the queueing delay of the Opportunistic EDF scheduler, which is a QoS-enabling scheduler, which is aware of the state of the underlying physical layer.

1.2.1 First Generation Communication Systems

Cellular systems started in the analogue domain. Examples of such systems are Nordic Mobile Telephone (NMT), Advanced Mobile Phone Systems (AMPS) and Total Access Communication Systems (TACS) [3]. These are commonly referred to as the first generation systems [4], which enabled voice communications to go wireless.

1.2.2 Second Generation Communication Systems

Cellular technology advanced into the digital domain with systems such as Global Systems for Mobile communications (GSM), Digital Advanced Mobile Phone Systems (D-AMPS), Japan's Personal Digital Cellular (PDC) and a derivative of GSM operating at 1800MHz, known as DCS1800 [3]. Further examples are cdmaOne (IS-95) and US-TDMA (IS-136), which collectively are referred to as the second generation systems [4]. The current wireless communication system commercially available in South Africa is GSM, which is an international standard, enabling GSM-enabled devices to operate in virtually every country around the world. In GSM, multiple base stations provide wireless coverage. Frequencies are reused in non-adjacent cells. Apart from just wireless voice communications, the digital nature of second generation systems enabled further services such as text messaging and access to data networks [4].

1.2.3 Third Generation Communication Systems

With *third generation* (3G) systems, more emphasis has been placed on multimedia communication. High quality images and video capabilities are added to normal person-to-person communication. Higher data rates and new flexible communication capabilities enhance access to information and services on public and private networks.

Wide-band CDMA (WCDMA) has emerged as the most widely adopted air interface for 3G systems. European research on WCDMA was initiated at the start of the 1990's by the European Union research projects CODIT and FRAMES. The *International Telecommunications Union* (ITU) decided at the *World Administrative Radio Conference* (WARC) in 1992 that the available frequencies around 2GHz would be used to implement the 3G systems. It was named the *International Mobile Telephony 2000* (IMT-2000). In January 1998 the European standardization body ETSI decided upon WCDMA as the third generation air interface. The first commercial network was opened in Japan during 2001 for commercial use in key areas, followed by Europe at the beginning of 2002. The specification of the standardization forums was created in 3GPP (the 3^{rd} Generation Partnership

Project), which is a standardization body comprised of Europe, Japan, Korea, the USA and China [4].

An example of a 3G system is the *Universal Mobile Telecommunications System* (UMTS), which promises circuit-switched connections with data rates of 384kbps and packet-switched connections up to 2Mbps. The high data rates make video telephony and quick downloading of data possible. UMTS supports a wide range of applications that possess different *Quality of Service* (QoS), that make it possible for the network to be sensitive to the throughput, transfer delay, and data error rate requirements of the various applications. To achieve such differentiated services, four traffic classes have been identified that applications can fit into:

- conversational
- streaming
- interactive
- background

The main difference between these classes is the delay sensitivity of the traffic. The conversational class is the most delay-sensitive, while the background class is the least [4].

As an extension to the third generation cellular systems, 3GPP has proposed the High Speed Downlink Packet Access (HSDPA) and High Speed Uplink Packet Access (HSUPA) standards, which together are referred to as High Speed Packet Access. These standards are considered to fall into the 3.5 generation of cellular communication. Chapter 2 presents a simulation model, in which HSDPA is discussed in more detail.

1.3 Motivation for research

In the past, networks contained only one type of data, making it possible to optimise the architecture of the network according to its specific needs. For example, the telephone

network is a rigid structure with good performance guarantees, while packet switched networks are more flexible but only provide marginal performance guarantees [5]. Modern integrated services networks carry a large number of different data types, each with its own requirements. The problem is how to address the varying requirements of the classes of traffic sharing the network infrastructure. One of the most important Quality of Service enforcement mechanisms is the scheduler. Advanced scheduling has therefore become an inevitable component of modern Quality-of-Service (QoS)-based data networks.

The scheduler is usually located inside every router of a packet-switched network. When the router has decided what the next destination of the various packets should be, the scheduler decides in what order the packets should be transmitted and at what rate, so that delay and throughput guarantees are met.

Wireless and mobile networks pose an additional problem since the channel conditions, through which information is transmitted, are constantly changing. HSDPA is an example of "last-mile" mobile technology in the access network.

The bulk of this research focusses specifically on the analysis of the delay-aware family of scheduling algorithms. An analytical model is derived that is able to predict the delay and fairness distributions of Earliest Deadline First (EDF). The model is then extended to predict the delay behaviour of the Opportunistic-Earliest Deadline First (O-EDF) scheduler, which not only considers the delay experienced by traffic, but also takes the current channel conditions into account. The scheduling algorithm of O-EDF can be summarised as follows:

$$\text{Next packet} = \min_i d_i \cdot \frac{\bar{G}_c}{G_c} - D_i, \tag{1.1}$$

where G_c is equivalent to the user channel gain $G_c^{P_{RX}}$ which in this context is abbreviated, while $\bar{G}_c$ is its short-term average.

As part of their service portfolio, modern Telecommunications Operators offer various forms of Service Level Agreements. At their most basic level, these will offer guarantees on the availability of a network, which will involve variables in the form of Time-To-Repair (TTR), Time-Between-Failures (TBF), and Accumulated Downtime per month.

But customers also expect network performance guarantees. These can include metrics such as jitter (the variation of the delay that packets experience) and packet-loss, but will most prominently focus on delay guarantees. The delay distribution models presented in this thesis can be used by telecommunication operators to find the risk of scheduled traffic under given load conditions. Based on the risk that the operator is willing to take, suitable delay guarantees can be found.

Note though, that even the most advanced routers in the world, as for example the high-end Cisco 12000 router, offer at most a hierarchical combination of deficit round-robin and strict-priority schedulers. As will be shown in this thesis, the problem with these two schedulers is that they are completely unaware of the latency that packets have already endured and are thus unable to alter their behaviour to attempt to meet the deadlines of delay sensitive and business critical data. The result is that the QoS designs of telecommunication operators must rely on the exclusive use of random early dropping and traffic policing algorithms, to keep the queue lengths in check and thereby achieve the desired delay behaviour. Although random dropping and traffic policers will always remain measures of last resort, improved scheduling can dramatically reduce the number of packets dropped. This, in turn, will keep the TCP window open, resulting in better throughput.

1.4 Thesis overview

The thesis has been divided into five chapters. In Chapter 1 an overview is given of the evolution of VPN and wireless networks, followed by the motivation of this work and a list of original contributions.

Chapter 2 presents the simulated behaviour of traffic belonging to 3 classes of service that was transmitted across an HSDPA air interface. The main aim of this chapter was to measure the performance of EDF and Opportunistic-EDF (O-EDF), compared to Round Robin, Max C/I, and PF-T, which are commonly used as HSDPA schedulers.

Chapter 3 extends an analytical model that is able to derive the violation probability of traffic scheduled by an Earliest Deadline First (EDF) scheduler. This model is modified

to be able to predict the violation probability per class of service. The rest of the chapter presents a novel approach that builds on the concepts of the violation probability analysis and is able to predict the delay distribution per CoS of the EDF scheduler. This result is further expanded by finding an expression for the fairness of EDF.

Chapter 4 extends Chapter 3's analysis into the mobile domain. The O-EDF scheduler is introduced. The analytical model of Chapter 3 is extended to be able to predict the delay distribution of O-EDF.

Chapter 5 presents the conclusions drawn in this thesis.

1.5 Original contributions

The original contributions in this thesis include:

1. An HSDPA air interface is simulated, where EDF is shown to be the only investigated scheduler that is able to achieve differentiated queueing delay, proportional to the delay deadlines.
2. An analytical model is presented that is able to predict the cumulative distribution function and probability density function of the delay and fairness per class of service of Earliest Deadline First-scheduled traffic.
3. The cumulative distribution function and probability density function of the queueing delay per class of service of Opportunistic Earliest Deadline First-scheduled traffic are analytically derived.

Parts of the work presented in this thesis have been presented by the author at the following conferences:

1. S.M. Scriba and F. Takawira, "The Fairness of CDMA-based Wireless Packet Schedulers", *Proceedings of the Southern African Telecommunication Networks and Applications Conference (SATNAC 2003)*, South Africa, 2003.

2. S.M. Scriba and F. Takawira, "Packet violation probability analysis of the Earliest Deadline First scheduler", *Proceedings of the Southern African Telecommunication Networks and Applications Conference (SATNAC 2004)*, South Africa, 2004.

3. S.M. Scriba and F. Takawira, "An Approximate Statistical Model of the Sojourn Time of the Earliest Deadline First Scheduler", *Proceedings of the IEEE International Conference on Telecommunications, (IET2005)*, Cape Town, South Africa, 2005.

4. S.M. Scriba and F. Takawira, "An Approximate Statistical Model of the Fairness of the Earliest Deadline First Scheduler", *Proceedings of the Southern African Telecommunication Networks and Applications Conference (SATNAC 2005)*, South Africa, 2005.

Chapter 2

HSDPA Simulation

2.1 Introduction

High Speed Downlink Packet Access (HSDPA) is becoming an important last-mile access technology used to give customers access to their Quality of Service (QoS)-enabled Virtual Private Network (VPN). The aim of this chapter is to compare the performance of several schedulers. This is achieved by means of a custom built simulator, which shows how the Earliest Deadline First (EDF) scheduler fills an essential role in providing QoS for delay sensitive traffic. The model was made as realistic as possible, as this chapter does not contain an analysis and simplifying assumptions are thus not required.

The network that is simulated is a mobile cellular network, with one base-station serving traffic to several mobile units. It focuses on the downlink, as this poses the main scheduling problem. Note that the uplink and downlink transmission problems can be separated, as in most modern cellular systems they use independent frequency ranges. To simulate the problem as realistically as possible, 3GPP's new HSDPA protocol is used as the air interface.

2.1.1 HSDPA background [6]

As part of the UMTS standard, the third generation partnership project (3GPP) included HSDPA in Release 5. The UMTS standard is built on the second generation network architecture. It essentially consists of the UMTS Radio Access Network (UTRAN) that handles all radio related functionalities, and the core network, which performs the routing and switching of traffic generated by user equipment (UE) [7]. As indicated in Fig. 2.1, the UTRAN can be further subdivided into the Radio Network Controller (RNC) and Node-B, which acts as a base station and is traditionally called the base transceiver station (BTS). The core network consists of the Serving GPRS Support Node (SGSN) and the Gateway GPRS Support Node (GGSN). The SGSN is connected to the RNC via the IuPS interface, while the GGSN provides access to external packet switched networks via the Gi interface.

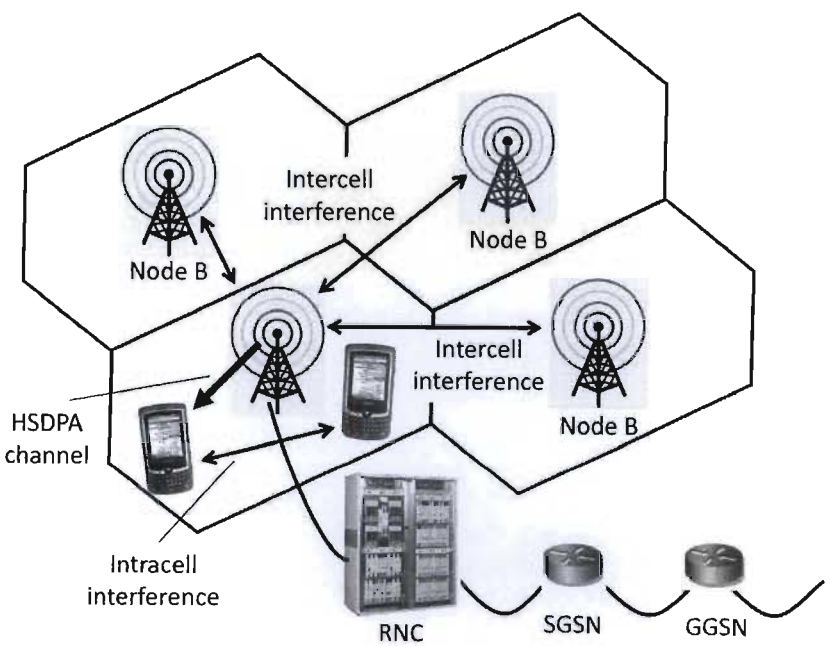

Figure 2.1: HSDPA Architecture

High Speed Downlink Packet Access (HSDPA) uses techniques such as adaptive modulation and hybrid ARQ. It is able to achieve a throughput of up to 10Mb/s with high peak rates, thereby reducing delay. HSDPA relies on the HS-DSCH transport channel, which is terminated in Node-B. Scheduling has been moved from the RNC to Node-B.

In HSDPA, all resources are usually made available to a single user on a Transmission Time Interval (TTI) basis [8]. HSDPA distinguishes itself from the previous WCDMA standard, by using an Adaptive Modulation and Coding (AMC) scheme, which enables it to respond rapidly to channel fluctuations, without the need for fast power control, which is disabled in HSDPA. Furthermore, Variable Spreading Factors have also been disabled, while the TTI has been decreased from 10ms to 2ms, allowing for much faster scheduling responses. Finally, the model makes use of a Fast Physical Layer Hybrid ARQ scheme. The most commonly used scheduling algorithms for HSDPA, which will be discussed further in Section 2.6, include [7]:

- Round Robin (RR)
- Maximum Carrier to Interference ratio (Max C/I)
- Proportional Fair (PF) scheduling

The second phase of HSDPA was specified in 3GPP release 7 [9]. It has been named HSPA evolved and can achieve data rates up to 42Mbps. Beamforming and Multiple-Input Multiple Output Communications (MIMO) antenna array technologies are used. Using these, the transmitted power can be focussed as a beam towards the user. In subsequent releases, a further dual 5MHz carrier operation has been introduced, which allows for peak data rates of 84Mbps. Finally, in 3GPP release 8 the Long Term Evolution initiative is introduced, which offers data rates of over 320Mbps for downlink and over 170Mbps for uplink using OFDMA modulation.

A number of papers have investigated the impact of using a variety of schedulers in the HSDPA environment. In [7], a new Hybrid Proportional Fair (HPF) scheduling algorithm is compared under Pedestrian A, Vehicular A and Vehicular B conditions, with Round Robin, Maximum Carrier to Interference Ratio (MaxC/I), and Proportional Fair Throughput (PFT). The new scheme was shown to have higher throughput and better fairness than PFT and MaxC/I.

In [10], the author proposes a scheduling scheme that uses a channel-dependent adaptive delay barrier function to maximise throughput of Best Effort (BE) traffic, while still

achieving QoS for VoIP services. The simulations used to evaluate the schedulers contained a regular hexagonal 19 cellular model, where the distance between Node B stations was 1km.

Finally, in [11] the effect of not having perfect Channel State Information (CSI) is studied, as perfect CSI requires high overhead. Integer programming and simulated annealing approaches are proposed to solve the optimisation problems. The resulting solution is able to achieve a similar performance, but at much lower complexity.

This chapter compares the behaviour of EDF and Opportunistic-EDF (O-EDF) with that of Round Robin, PFT, and MaxC/I. Video, voice and web traffic are transmitted through an HSDPA air interface. The resultant service rate, deadline violations, transmission corruptions, and queueing delay are measured and compared for each scheduler.

2.2 Traffic generation model

The simulation model assumes that multiple sources are producing voice, video, and web traffic that will arrive at the base station, enter the queueing system and is then transmitted via a channel to the mobile stations. Note that each physical mobile unit can simultaneously generate voice, video and web traffic, in other words, it can consist of several traffic sources. The same traffic generating models for video and web traffic will be used as [8], while the video generating model will be extended to give a realistic voice generating model. The scheduling intervals are defined in terms of the TTI. In other words, a new packet is scheduled every TTI. In an HSDPA system, the TTI is fixed at 2ms.

2.2.1 Video traffic source

A video source can be modeled as M independent ON-OFF Markov mini-sources. As was the case in [8], this model assumes that $M = 10$. In the ON state, a mini-source produces a constant rate of Vbps, while in the OFF state, a mini-source produces no traffic. Each mini-source spends a mean time of p TTIs in the ON state and q TTIs in the OFF state,

where their respective random variables P and Q are geometrically distributed.

Parameters p, q and V are obtained as follows:

$$p = \frac{1}{a \cdot TTI}\left(1 + \frac{\mu^2}{M\sigma^2}\right) \quad \text{[TTIs]} \tag{2.1}$$

$$q = \frac{1}{a \cdot TTI}\left(1 + \frac{M\sigma^2}{\mu^2}\right) \quad \text{[TTIs]} \tag{2.2}$$

$$V = \frac{\mu}{M} + \frac{\sigma^2}{\mu} \quad \text{[bps]} \tag{2.3}$$

A video source has a mean bit rate of μbps, a standard deviation of σbps, and exponent of the auto-covariance with coefficient $a\text{s}^{-1}$. As was the case in [8], μ=128kbps, σ=8kbps and a=3.9s^{-1}. Video packets are chosen to have a fixed packet length of 1500 Bytes = 12kb. Video traffic is considered to have a deadline of d=100ms, after which it will be dropped.

The result is that the mean ON-time is

$$\begin{aligned} p &= \frac{1}{3.9 \cdot 0.002}\left(1 + \frac{128^2}{10 \cdot 8^2}\right) = 3410.26 \text{ TTI} \\ &= 6,820,513 \ \mu\text{s} \end{aligned} \tag{2.4}$$

Similarly, the mean OFF-time is

$$\begin{aligned} q &= \frac{1}{3.9 \cdot 0.002}\left(1 + \frac{10 \cdot 8^2}{128^2}\right) = 133.21 \text{ TTI} \\ &= 266,420 \ \mu\text{s} \end{aligned} \tag{2.5}$$

And finally, the transmission rate of each mini-source is

$$\begin{aligned} V &= \frac{128 \cdot 10^3}{10} + \frac{\left(8 \cdot 10^3\right)^2}{128 \cdot 10^3} \\ &= 13,300 \text{ bps} \end{aligned} \tag{2.6}$$

2.2.2 Voice traffic source

For the voice traffic generation, exactly the same model is used as for video traffic generation, except that M=1. In other words, every source no longer consists of 10 mini-sources. For voice traffic, μ=64,000bps and σ=4,000bps. Voice packets have a fixed packet length of 80 Bytes = 640b. Voice traffic has a deadline of d=50ms, after which it will be dropped.

Once again, the mean ON-time is calculated to be

$$\begin{aligned} p &= \frac{1}{3.9 \cdot 0.002}\left(1 + \frac{64^2}{4^2}\right) = 32,948.7 \text{ TTI} \\ &= 65,897,436 \ \mu\text{s} \end{aligned} \tag{2.7}$$

Similarly, the mean OFF-time is given by

$$\begin{aligned} q &= \frac{1}{3.9 \cdot 0.002}\left(1 + \frac{4^2}{64^2}\right) = 128.71 \text{ TTI} \\ &= 257,412 \ \mu\text{s} \end{aligned} \tag{2.8}$$

And finally, the source transmission rate is

$$\begin{aligned} V &= 64 \cdot 10^3 + \frac{\left(4 \cdot 10^3\right)^2}{64 \cdot 10^3} \\ &= 64,250 \text{ bps} \end{aligned} \tag{2.9}$$

2.2.3 Web traffic source

Although it is fairly difficult to find a statistical distribution that accurately describes web traffic generation patterns, creating simulated web-traffic is fairly straight forward. We use the same model as in [8], where an end-user can be seen to oscillate between two states while browsing. He is either requesting a new webpage or reading. The reading state has a geometric distribution with an average duration of T_{OFF}=1000TTIs = 2s. During this time no traffic is generated. Web traffic has a virtual deadline of d=500ms. It is virtual because the packet is still served and not dropped when the delay exceeds d and creates a deadline violation.

When in the request state, the addressed data source will produce a geometrically distributed number of packets, with a mean of $\bar{P}$=300 packets. The packet inter-arrival time too is geometrically distributed, with a mean of $\triangle T$=200TTIs = 0.4s. The packet length L can be found by finding the floor of a truncated Pareto pdf, in other words, $L = \lfloor x \rfloor$, where:

$$p(x) = \frac{\zeta \cdot l_{\min}{}^{\zeta}}{x^{\zeta+1}} [u(x - l_{\min}) - u(x - l_{\max})] + \delta(x - l_{\max}) \left(\frac{l_{\min}}{l_{\max}}\right)^{\zeta} \quad \text{[bits]} \tag{2.10}$$

Here $\zeta = 1.1$ is a constant, $u(\cdot)$ is the unitary step function, $\delta(\cdot)$ is the Dirac Delta function, while $l_{\min} = 80$ Bytes = 640b and $l_{\max} = 1500$ Bytes = 12kb are respectively the minimum and maximum message lengths. The values of $l_{\min}$ and $l_{\max}$ are different to those proposed in [8] and were chosen to lie within the bounds of the packet lengths of voice and video packets.

The problem with generating web traffic is that the IMSL library that was used to perform statistical tasks does not include a function for generating Pareto distributed random numbers. To solve this problem, it was noted that the Pareto density function is given by

$$p(x) = \frac{ab^a}{x^{a+1}} \quad \text{[bits]}, \tag{2.11}$$

while the Pareto cumulative distribution is given by

$$F(x) = 1 - \left(\frac{l_{\min}}{x}\right)^{\zeta} \quad \text{[bits]}. \tag{2.12}$$

Pareto distributed random numbers can be obtained, by generating random numbers for a uniform distribution with limits [0,1]. For every uniformly distributed random u generated in this fashion, $F(x) = u$. One may then solve for x, as follows:

$$x = \frac{l_{\min}}{(1-u)^{1/\zeta}} \quad \text{[bits]}. \tag{2.13}$$

The result is that one is able to translate every uniformly distributed random number u into a Pareto distributed random number x.

2.3 Queueing model

To be able to compare all schedulers, identical conditions must be created in each case. The only difference may be the way the data is scheduled, in other words, the order in which it is transmitted. As described earlier, traffic that has violated its delay deadline is either physically dropped or virtually dropped, depending on whether it is real-time traffic (voice and video) or best-effort traffic (web). Because the real-time traffic can be dropped, its queue-length is indirectly limited to the product of the average service rate and the delay deadline. Under high enough load conditions, the best-effort queue could, on the other hand, grow to a significant size, which in turn drastically affects its delay behaviour. Limiting the queue size in any way would also indirectly cap the possible maximum delay. The result is that infinitely long buffers were chosen for all queues.

2.4 Channel model

HSDPA uses Direct-Sequence Code Division Multiple Access (DS-CDMA). The bit energy-to-interference spectral density $\frac{E_b}{I_0}$ that the User Equipment (UE) measures is fed back to Node-B using 5 bits, known as the Channel Quality Indicator (CQI) value. The CQI value is used to decide on the highest transmission rate that can be chosen.

The $\frac{E_b}{I_0}$ value that the UE measures, can be modeled as follows [8]:

$$\frac{E_b}{I_0} = \text{SIR} \cdot \text{PG}, \tag{2.14}$$

where SIR is the signal-to-interference power ratio, PG is the gain ratio, which is defined by the ratio $\frac{W}{R_b}$, where W is the spreading bandwidth and R_b is the bit-rate that depends on the used modulation and coding scheme (MCS). The SIR value can be estimated as

$$\text{SIR} = \frac{P_{RX}}{I_{Inter} + I_{Extra} + N}, \tag{2.15}$$

where P_{RX} is the useful received power, I_{Inter} is the intra-cell interference, I_{Extra} is the extra-cell interference and N is the noise power. Note that P_{RX}, I_{Inter}, I_{Extra} and N can

be characterized as follows [8]:

$$P_{RX} = P_{TX} G_c^{P_{RX}}, \quad I_{Inter} = \alpha G_c^{P_{Inter}} P_D, \tag{2.16}$$

$$I_{Extra} = \varepsilon G_c^{I_{Extra}} P_D, \quad N = N_0 W \tag{2.17}$$

where P_{TX} is the transmitted power to the user, $G_c^{P_{RX}}$, $G_c^{P_{Inter}}$, and $G_c^{I_{Extra}}$ are the user channel gains of the transmission, the intra-cell interference, and the extra-cell interference, respectively. P_D is the Node B available power, N_0 is the noise spectral density, α is the intra-cell non-orthogonality coefficient and ε is the extra-cell interference power-to-the total received power ratio. Note that all powers must be converted to Watts and cannot be left as dBs.

P_{TX} can be found quite simply, by assuming that all of Node B's power will be used during transmissions. Node B's power is therefore divided amongst each of the transmission codes. If one assumes that 15 codes are used for transmission, then P_{TX} becomes:

$$P_{TX} = \frac{P_D}{15} \quad [\text{W}]. \tag{2.18}$$

Hence

$$\frac{E_b}{I_0} = \frac{P_{TX} G_c^{P_{RX}} W/R_b}{(\alpha G_c^{P_{Inter}} + \varepsilon G_c^{P_{Extra}}) P_D + N_0 W} \tag{2.19}$$

per CDMA code.

From [12], one can derive that the channel gain for the transmission, the intra-cell interference, and the extra-cell interference are given by:

$$G_{c(\text{dB})} = -L(t)_{(\text{dB})} + s(t)_{(\text{dB})}, \quad [\text{dBW}] \tag{2.20}$$

where $s(t)$ is the shadowing component, which will be discussed later. $L(t)$ is the path-loss component of a UHF signal over flat terrain (in a semi-urban environment), which is given by [12]:

$$L(t)_{(\text{dB})} = K + \gamma \log_{10} r \quad \text{dBW}. \tag{2.21}$$

Here K is the signal strength measured at 1km from the base-station, with r in km, while γ is the rate at which $L(t)_{(\text{dB})}$ changes as r changes. Both K and γ may vary as distance

r between a mobile and the base-station changes. In the case of this thesis the convention proposed in [8] is adopted, as listed in Table 2.7 in Section 2.7.

Assuming that mobile units cannot be located on top of the base station, the pdf of r is given by:

$$F(r) = P(r \leq R) = 1 = \frac{\pi r^2}{\pi R^2} \tag{2.22}$$

The probability of a user being located within a disc with radius r, is directly related to the size of the area in relation to the total area with radius R. Hence:

$$f_r(r) = \frac{dP(X \leq r)}{dr} = \frac{2r}{R^2} \tag{2.23}$$

To generate random number r, one can generate a uniformly [0,1] distributed random number x and let:

$$F(r) = \frac{r^2}{R^2} = x. \tag{2.24}$$

Solving for r, results in:

$$r = \sqrt{x} \cdot R. \tag{2.25}$$

The shadowing term $s(t)$ (in dB) is usually modeled as a zero-mean stationary Gaussian process, which when expressed in Watts has a log-normal pdf:

$$f_{s(t)} = \frac{1}{\sigma\sqrt{2\pi t}} \cdot \exp\left[-(\ln t - \mu)^2/(2\sigma^2)\right] \tag{2.26}$$

$$= \frac{1}{\sigma\sqrt{2\pi t}} \cdot \exp\left[-\frac{\ln^2 t}{2\sigma^2}\right], \tag{2.27}$$

since $\mu = 0$.

2.5 HSDPA transmission rates

When a packet is selected for transmission to the j-th user, the bit-error-rate (BER) plays an important role. The applications using the various classes of service have different sensitivities to the BER.

Table 2.1: HSDPA MCS modes

MCS mode m	**Data rate (15 codes)** R_b
1. QPSK, rate $\frac{1}{4}$	1.8Mbps
2. QPSK, rate $\frac{1}{2}$	3.6Mbps
3. QPSK, rate $\frac{3}{4}$	5.3Mbps
4. 16QAM, rate $\frac{1}{2}$	7.2Mbps
5. 16QAM, rate $\frac{3}{4}$	10.7Mbps

The BER thresholds that were used in this chapter are $9.6 \cdot 10^{-6}$ for video and voice traffic, and $8.4 \cdot 10^{-7}$ for web traffic, as listed in Table 2.7 in Section 2.7. These values were chosen to correspond to a packet-error-rate (PER) proposed in [8] of 10^{-1} for video traffic and a mean PER of 10^{-2} for web traffic, which varies as the packet length of the web packets vary. The BER of the voice traffic is kept the same as video, but corresponds to a much lower PER, as can be calculated using the following expression:

$$PER = 1 - (1 - BER)^L, \tag{2.28}$$

where L in this context is the packet length, measured in bits.

The BER can be controlled directly by varying the transmission power. In the 3GPP's UMTS standard, power control therefore plays an important role. One of the improvements that HSDPA offers, is to track a BER by varying the modulation and coding scheme (MCS) as the channel conditions change. This enables the base station to keep its transmission power constant, simplifying the design.

In order to obtain high transmission rates, 15 codes were used with the MCS modes listed in Table 2.1. As the channel quality varies, a different MCS will have to be used, which effectively varies the transmission rate.

To determine which of these MCS modes should be used at any time, the indirect relationship between BER and transmission rate needs to be considered. Note that the BER is related to the bit-energy-to-interference spectral density $\frac{E_b}{I_0}$ value, which is communicated from the User Equipment (UE) to the transmitting Node-B using the Channel Quality Indicator (CQI) value [7]. This 5-bit CQI value, ranging from 0 to 30, is calculated as

follows:

$$CQI = \begin{cases} 0 & \text{if } \frac{E_b}{I_0} \leq -16, \\ \left\lfloor \frac{E_b}{I_0}/1.02 + 16.62 \right\rfloor & \text{if } -16 < \frac{E_b}{I_0} \leq 14, \\ 30 & \text{if } 14 < \frac{E_b}{I_0}. \end{cases} \tag{2.29}$$

When the CQI value is received by Node-B, it can be converted back to an estimate of $\frac{E_b}{I_0}$.

In the previous section, the following expression was developed that explains the relationship between the transmission rate R_b and the resulting $\frac{E_b}{I_0}$ that can be expected:

$$\frac{E_b}{I_0} = \frac{P_{TX} G_c^{P_{RX}} W/R_b}{(\alpha G_c^{P_{Inter}} + \varepsilon G_c^{P_{Extra}}) P_D + N_0 W} \tag{2.30}$$

By choosing the appropriate MCS value, the transmission rate can be increased while the resulting $\frac{E_b}{I_0}$ still meets the following condition:

$$\frac{E_b}{I_0} > \left(\frac{E_b}{I_0}\right)_{\text{Threshold}}. \tag{2.31}$$

The $\left(\frac{E_b}{I_0}\right)_{\text{Threshold}}$ is a threshold that is directly related to the maximum PER threshold that each class of traffic can endure.

Reference [13] contains the required SNR-to-PER curves in a flat fading Rayleigh model for QPSK rate 1/3, rate 1/2, rate 3/4, 16QAM rate 1/2, and rate 3/4. Note that the MCS modes in Table 2.1 require QPSK rate 1/4 instead of rate 1/3. A useful rate 1/4 SNR-to-PER curve could not be found in the available literature. The rate 1/3 was therefore used instead, which results in a slightly higher PER than could have been achieved with rate 1/4.

Tables 2.2 to 2.6 were created as look-up tables from the curves in [13]. Points in between the lookup values can be found by interpolation, as long as the PER is kept in the $\log_{10}$ space and the SNR is kept in dB. Note that the packet length in [13] was 50bits, plus 4 control bits. Knowledge of the packet length is required to convert between BER and PER using the following expressions:

$$PER = 1 - (1 - BER)^L, \tag{2.32}$$

and

$$BER = 1 - (1 - PER)^{1/L}. \tag{2.33}$$

Using Tables 2.2 to 2.6 it is possible to relate the maximum BER of each class of service to a respective $\left(\frac{E_b}{I_0}\right)_{\text{Threshold}}$. The MCS that results in the highest transmission rate may then be chosen, so that the resulting $\frac{E_b}{I_0}$ is still higher than $\left(\frac{E_b}{I_0}\right)_{\text{Threshold}}$. If the channel fading does not change too rapidly during the ensuing transmission interval, the traffic class should remain within the bounds of its BER target.

Since this section is able to find a relationship between PER and bit-rate, it is possible to estimate the PER during a transmission, based on the MCS chosen. The simulation is thus able to estimate how many packets were corrupted during a typical packet transmission by generating a flat random number a, between 0.0 and 1.0. A packet error will have occurred if $a \leq PER$.

Table 2.2: QPSK, Rate 1/3, SNR-to-BER lookup-table

SNR (dB)	**PER (L=54b)**	**BER**
-4	$8 \cdot 10^{-1}$	$2.9 \cdot 10^{-2}$
-3	$3 \cdot 10^{-1}$	$6.6 \cdot 10^{-3}$
-2	$5 \cdot 10^{-2}$	$9.5 \cdot 10^{-4}$
-1	$4 \cdot 10^{-3}$	$7.4 \cdot 10^{-5}$
0	10^{-4}	$1.9 \cdot 10^{-6}$

Table 2.3: QPSK, Rate 1/2, SNR-to-BER lookup-table

SNR (dB)	**PER (L=54b)**	**BER**
-2	$9 \cdot 10^{-1}$	$4.2 \cdot 10^{-2}$
-1	$4 \cdot 10^{-1}$	$9.4 \cdot 10^{-3}$
0	$2 \cdot 10^{-1}$	$4.1 \cdot 10^{-3}$
1	$2 \cdot 10^{-2}$	$3.7 \cdot 10^{-4}$
2	$2 \cdot 10^{-4}$	$3.7 \cdot 10^{-6}$

Table 2.4: QPSK, Rate 3/4, SNR-to-BER lookup-table

SNR (dB)	**PER (L=54b)**	**BER**
1	$9 \cdot 10^{-1}$	$4.2 \cdot 10^{-2}$
2	$4 \cdot 10^{-1}$	$9.4 \cdot 10^{-3}$
3	$2 \cdot 10^{-2}$	$3.7 \cdot 10^{-4}$
4	$3 \cdot 10^{-3}$	$5.6 \cdot 10^{-5}$
5	$6 \cdot 10^{-4}$	$1.1 \cdot 10^{-5}$

Table 2.5: 16QAM, Rate 1/2, SNR-to-BER lookup-table

SNR (dB)	**PER (L=54b)**	**BER**
4	$9 \cdot 10^{-1}$	$4.2 \cdot 10^{-2}$
5	$5 \cdot 10^{-1}$	$1.3 \cdot 10^{-2}$
6	$2 \cdot 10^{-1}$	$4.1 \cdot 10^{-3}$
7	$3 \cdot 10^{-2}$	$5.6 \cdot 10^{-4}$
8	$4 \cdot 10^{-3}$	$7.4 \cdot 10^{-5}$
9	$2 \cdot 10^{-4}$	$3.7 \cdot 10^{-6}$

Table 2.6: 16QAM, Rate 3/4, SNR-to-BER lookup-table

SNR (dB)	**PER (L=54b)**	**BER**
7	$9.5 \cdot 10^{-1}$	$5.4 \cdot 10^{-2}$
8	$9 \cdot 10^{-1}$	$4.2 \cdot 10^{-2}$
9	$7 \cdot 10^{-1}$	$2.2 \cdot 10^{-2}$
10	$4 \cdot 10^{-1}$	$9.4 \cdot 10^{-3}$
11	$2 \cdot 10^{-1}$	$4.1 \cdot 10^{-3}$
12	$5 \cdot 10^{-2}$	$9.5 \cdot 10^{-4}$
13	10^{-2}	$1.9 \cdot 10^{-4}$
14	$2 \cdot 10^{-3}$	$3.7 \cdot 10^{-5}$
15	$5 \cdot 10^{-4}$	$9.3 \cdot 10^{-6}$

2.6 Schedulers to compare

The behaviour of the following schedulers is explored in this chapter:

2.6.1 Round Robin [7]

The Round Robin (RR) scheduler is one of the simplest. At the end of each TTI, it moves onto the next queue and tries to fill up the scheduling interval with as much data as possible from this queue. If a queue is empty, the scheduler simply moves to the next queue. No attempt at optimisation is made. If all queues are full, then over a prolonged period of time, each one would be given an equal number of TTIs for transmission.

2.6.2 Proportional Fair Throughput [7]

The aim of the Proportional Fair Throughput (PF-T) scheduler is to maximise throughput, but in a fair manner. The scheduling rule is given by:

$$\text{Next packet} = \max_i \frac{r_i}{\bar{r}_i}, \tag{2.34}$$

where r_i is the instantaneous transmission rate that HSDPA could assign to class i traffic, if chosen by the scheduler. $\bar{r}_i$ is the average transmission rate that was assigned to class i traffic. It can be found as follows:

$$\bar{r}_i(k+1) = \begin{cases} (1-\alpha)\bar{r}_i(k) + \alpha r_i(k) & \text{if } i \text{ is served in slot } k, \\ (1-\alpha)\bar{r}_i(k) & \text{otherwise,} \end{cases} \tag{2.35}$$

where $0 < \alpha < 1$ is a weighting factor, whose value was chosen to be 0.001.

The numerator in the scheduling rule ensures that the scheduler will take advantage of temporary throughput improvements. On the other hand, the denominator ensures that over a long-term period, the scheduler will attempt to assign equal resources to all classes.

2.6.3 Maximum Carrier to Interference ratio [7]

The Maximum Carrier to Interference ratio (Max C/I) scheduler selects packets based purely on the best channel conditions. The relative instantaneous channel quality indicator η is defined by

$$\eta_i = \frac{\zeta_i}{\bar{\zeta}}, \tag{2.36}$$

where $\zeta_i = \frac{E_b}{I_0}$ is the SNR of the channel that the head-of-queue packet of the class i queue will be transmitted through, while $\bar{\zeta} = \frac{1}{n} \cdot \sum_{j=1}^{n} \zeta_j$ is the average SNR of all channels. Here n is the total number of traffic classes.

The scheduling rule is simply given by:

$$\text{Next packet} = \max_i \eta_i. \tag{2.37}$$

2.6.4 Earliest Deadline First

The Earliest Deadline First (EDF) scheduler attempts to meet the required deadlines of traffic classes. Distributing bandwidth and achieving fair throughput among the traffic classes is not a sufficient criterion to be able to sustain real-time traffic on a packetised network. Strict deadlines need to be adhered to. The scheduling rule for EDF is given by:

$$\text{Next packet} = \min_i (d_i - D_i), \tag{2.38}$$

where D_i is the queueing delay that the head-of-queue packet of the class i queue has experienced, while d_i is the delay deadline of the packet.

2.6.5 Opportunistic Earliest Deadline First

Finally, Opportunistic EDF (O-EDF) uses the rules of EDF, but prioritises traffic classes which will be transmitted through good channel conditions.

$$\text{Next packet} = \min_i d_i \cdot \frac{\bar{G}_c}{G_c} - D_i, \tag{2.39}$$

where G_c is equivalent to the user channel gain $G_c^{P_{RX}}$ which in this context is abbreviated, while $\bar{G}_c$ is its short-term average.

2.7 Simulation parameters

A custom-made simulation package using Borland C++ was created. The analytical expressions were evaluated in MATLAB.

Throughout this thesis, custom-built simulation engines were used to produce simulation results. Initially, packages like NS-2 and OpNet were considered. However, the focus of this thesis is always on a single node which queues packets from various sources and then transmits them. Popular open source and commercial software, such as NS-2 and OpNet, is more suitable for modeling end-to-end network environments, such as typically required for investigating routing algorithms. It was decided that it would be faster and more effective to custom build a specialised simulator.

Table 2.7 lists the parameters for the simulation, which are similar to those proposed in [8]. A variable number of traffic sources were modeled, depending on the required load. The percentage load is defined as

$$\text{Percentage Load} = 100\% \cdot \frac{\text{Average traffic arriving into node}}{\text{NodeCapacity}} \tag{2.40}$$

The NodeCapacity is constant remains constant. If a long-term average sample is taken of the amount of traffic each source is generating, the sample becomes constant. The average percentage load may therefore be varied by changing the number of traffic sources.

Each traffic source generated the video, voice, and web traffic according to the model discussed in Section 2.2. Traffic was generated independently of other traffic sources.

For the HSDPA links between Node B and the UEs, 20 mobile channels were created. Each packet that was generated was assigned a flat random number ranging from 0 to 19, which implied the target channel that it would be transmitted through. Each of the 20 channels was modeled independently of all other channels. No spacial correlation among transmission channels was taken into consideration.

As mentioned already, the scheduling intervals are defined in terms of the TTI. In other words, a new packet is scheduled every TTI. Note that a range of transmission rates are

Table 2.7: Simulation parameters [8]

PARAMETER	**VALUE**
α	0.025
P_D	30 Watt
Cell radius R	500 meters
$N = N_0 W$	$2.00245 \cdot 10^{-14}$ Watt
W	5MHz
ε (close to Node B: $R \leq 10$m)	0
ε (intermediate: 10m $< R <$ 450m)	0.25
ε (cell border: 450m $\leq R \leq$ 500m)	0.5
PATHLOSS ATTENUATION $L(t)$	(in dB)
Near zone	$92.92 + 10.96 \log(R)$
($R <$ 300m)	
Far zone	$106.48 + 43.85 \log(R)$
($R \geq$ 300m)	
None-line of sight (probability = 0.2)	$151.32 + \log(R)$
(R = distance from Node B)	
SHADOWING ATTENUATION	
$s(t)$ (Gaussian variable)	(in dB)
Mean	0
Standard deviation	8
Bit Error Rate Threshold	
Video	$9 \cdot 10^{-6}$
Voice	$9 \cdot 10^{-6}$
Web	$8.4 \cdot 10^{-7}$

possible and various packet sizes are encountered. As the IP packets are passed from the network layer down to the MAC layer, they are broken into smaller frames. The scheduler is located on the MAC layer, which multiplexes the queued frames onto the physical layer, where they are transmitted onto the wireless medium. Only once the appropriate transmission rate has been chosen, can the frame size be determined. The rest of the packet stays in the queue, until another frame is chosen for transmission.

If the remainder of a packet is too small to fill an entire frame, or very small packet sizes are encountered, the effective transmission rate can be significantly decreased. Only a small proportion of the total transmission interval is used for actual transmission, while the rest of the time is wasted. To avoid this problem, packet stuffing was used. Here the packet that is next in queue is still transmitted if this packet has a packet length short enough to complete transmission in the remainder of the current transmission interval.

2.8 Results

In this chapter, the behaviour of five schedulers was simulated.

2.8.1 Relationship between mobile devices and the resulting load

Fig. 2.2(a) gives the key relationship between the number of users and what the respective measured load was for each scheduler used. The two schedulers that stand out from the rest are EDF and PF-T, where the load on the EDF scheduler grows faster than the other schedulers as the number of users increases, while the load on PF-T does the opposite and grows more slowly. The reason for the change in load is due to the average service rate that the schedulers receive, as discussed in the next section.

2.8.2 Average Service Rate

Fig. 2.2(b) shows that the reason for the different load behaviour of the various schedulers is related directly to the average service rate that they receive. The service rate is mea-

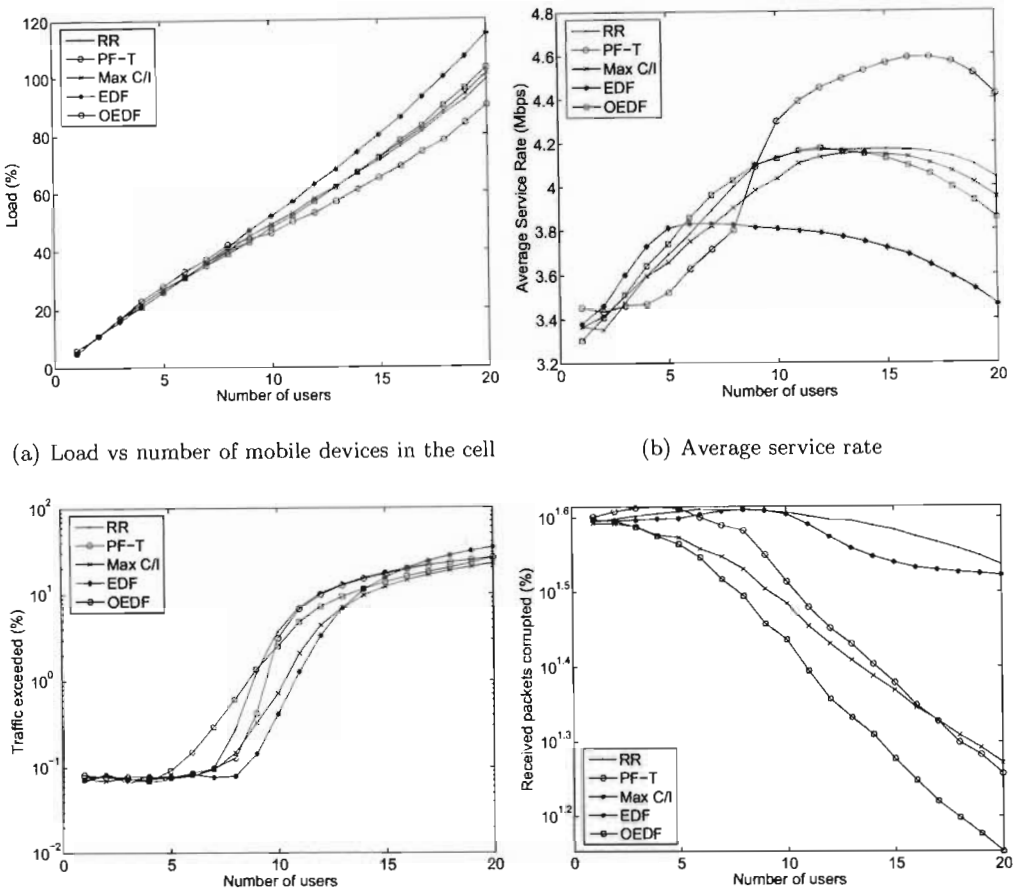

(a) Load vs number of mobile devices in the cell

(b) Average service rate

(c) Percentage traffic exceeding delay deadline

(d) Percentage traffic corrupted during transmission

Figure 2.2: Class-independent scheduler performance

sured by taking a sample of the transmission rate that a packet is scheduled with. The transmission rates are added up and at the end are divided by the total number of packets sent.

In order to understand the resultant service curves, consider the distribution of the various traffic classes. In the simulation it was measured that the video traffic makes up approximately 66% of all traffic generated, followed by approximately 30% of voice traffic and only a few percent of web traffic.

These values can also be found analytically as follows. The average video transmission

rate can be calculated as follows:

$$Video = M \cdot \frac{p}{p+q} \cdot V = 10 \cdot 0.96 \cdot 13.3 \cdot 10^3 = 128\text{kbps}. \tag{2.41}$$

The average voice transmission rate can be found:

$$Voice = \frac{p}{p+q} \cdot V = 64.3\text{kbps}. \tag{2.42}$$

For web traffic, we need to consider that

$$T_{OFF} = 2s. \tag{2.43}$$

$$T_{ON} = 300\text{packets} \cdot 0.4s \text{ inter-arrival time per packet} = 120s. \tag{2.44}$$

The average packet length is found as follows:

$$\bar{p}(x) = \int_{l_{\min}}^{l_{\max}} x \cdot p(x)\, dx \tag{2.45}$$

$$= \int_{l_{\min}}^{l_{\max}} x \cdot \left(\frac{\zeta \cdot {l_{\min}}^{\zeta}}{x^{\zeta+1}} [u(x - l_{\min}) - u(x - l_{\max})] + \delta(x - l_{\max}) \left(\frac{l_{\min}}{l_{\max}} \right)^{\zeta} \right) dx \tag{2.46}$$

$$= \int_{l_{\min}}^{l_{\max}} \zeta \cdot {l_{\min}}^{\zeta} \cdot x^{-\zeta}\, dx \tag{2.47}$$

$$= \frac{\zeta}{-\zeta+1} \cdot {l_{\min}}^{\zeta} \cdot x^{-\zeta+1} \Big|_{l_{\min}}^{l_{\max}} \tag{2.48}$$

$$= \frac{\zeta}{-\zeta+1} \cdot {l_{\min}}^{\zeta} \cdot ({l_{\max}}^{-\zeta+1} - {l_{\min}}^{-\zeta+1}) \tag{2.49}$$

Remembering that $\zeta = 1.1$, $l_{\min} = 640b$, $l_{\max} = 12kb$, one can evaluate the expression.

$$\bar{p}(x) = 1789\text{b}. \tag{2.50}$$

Finally, one can calculate the average web traffic arrival rate as follows:

$$Web = \frac{300\text{packets} \cdot 1789\text{b}}{T_{ON} + T_{OFF}} \tag{2.51}$$

Therefore

$$Web = 4398bps. \tag{2.52}$$

The analytical percentages for the various traffic classes therefore become:

$$Video = \frac{128\text{kbps}}{128\text{kbps} + 64.3\text{kbps} + 4.4\text{kbps}} = 65\%. \tag{2.53}$$

$$Voice = \frac{64.3\text{kbps}}{128\text{kbps} + 64.3\text{kbps} + 4.4\text{kbps}} = 33\%. \tag{2.54}$$

$$Web = \frac{4.4\text{kbps}}{128\text{kbps} + 64.3\text{kbps} + 4.4\text{kbps}} = 2.2\%. \tag{2.55}$$

The PF-T scheduler is aimed at choosing packets that will receive the highest possible transmission rate. Since voice packets have a very short length compared to video packets, and since both voice and video packets have the same bit error rate threshold, voice packets will on average receive a much higher transmission rate than video packets. PF-T will therefore prioritise voice traffic above video and web packets. The throughput measure in the denominator of the PF-T scheduling rule will avoid total starvation of the other traffic classes. But voice traffic still receives a disproportionately high percentage of the available resources. For high load conditions, the large number of very short voice packets that PF-T serves mean that HSDPA is able to significantly increase the transmission rate, as the probability of the corruption of small voice packets is much lower than longer video packets. As PF-T tries to limit itself exclusively to transmitting voice packets, the average throughput will therefore be much higher than for other schedulers. On the downside, this also means that video traffic will be neglected, with a large percentage being dropped.

A similar effect can be seen for Round Robin, Max C/I and O-EDF. Round Robin will distribute TTIs equally among traffic classes, if each traffic queue is filled. Max C/I chooses the packet that will be transmitted through the best channel conditions. Averaged over a long period of time, all traffic classes will experience the same channel conditions. The result is that Max C/I and Round Robin both end up assigning resources evenly among the traffic queues.

O-EDF consists of two components. On the one hand, it takes into account the delay that packets have already experienced and how close they are to their deadlines. On the other, the channel conditions play an important role, as they change the delay deadline, thereby dynamically changing the priority of the traffic. The results in Fig. 2.2(b) clearly show, how the channel conditions play a more important role in the decision making of O-EDF

than the delay, as the average service rate of O-EDF is very similar to that of Max C/I and Round Robin.

Due to the very low web traffic generation rate, Round Robin, Max C/I, and O-EDF will therefore end up sharing the available resources almost evenly between voice and video traffic, even though voice traffic only accounts for a third of the total traffic generated. Due to the high transmission rates of voice packets, the average transmission rate that these three schedulers are able to achieve will be boosted.

EDF, on the other hand, is solely interested in the delay experienced by packets, and whether the respective deadlines are being approached. Due to this fact, resources will be assigned much more fairly to the various classes of traffic, based on the arrival rate of the classes. As a result, approximately two-thirds of the resources will be assigned to video, 30% to voice and the remaining 4% to web traffic. And since video traffic is served at a much slower average rate than voice, the average transmission rate must be less than for the other schedulers, as can be seen in Fig. 2.2(b). On the positive side, video traffic will essentially no longer exclusively exceed its deadline. The deadline violations are more evenly spread among the traffic classes.

In general, Fig. 2.2(b) shows how, under low load conditions, all schedulers perform more or less the same. The reason is that the queues are fairly empty. In most cases, there simply are not enough packets of different classes available for different scheduling decisions to be made.

As the load grows, a peak is reached after which the service rate gradually decreases. The reason for this behaviour is that a sample of the service rate will only be taken once a packet has successfully completed transmission. If half a packet completes transmission and another packet is chosen for transmission in the next TTI, the remainder of the original packet will have to wait for the scheduler to choose its queue again, before the packet can complete its transmission. If, in the mean time, the packet reaches its delay deadline and it is a voice or video packet, it will be dropped before the remainder can be transmitted. The result is, that the transmission of the initial portion of the packet is wasted. The average service rate of the scheduler will therefore decrease. The probability

of partially transmitted packets being dropped increases as the load grows. Note that this transmission peak occurs much earlier with EDF than with Round Robin, Max C/I and O-EDF, while PF-T only achieves its peak at very high loads. The main reason for this is that EDF will attempt to start the transmission of video packets most frequently, compared to the other schedulers. In the case of PF-T, this effect is much less likely to occur, as video packets are largely shunned. And since multiple voice packets can be transmitted in a single TTI, the average transmission rate can grow up to very high load conditions.

For very low load conditions, this effect is reversed. PF-T will always try and serve voice packets first. By the time it attempts to serve waiting video packets, there is a much higher probability a large portion of transmission time will be wasted on the video packet, which is ultimately dropped when voice traffic is once again prioritised above it in the next TTI. On the other hand, EDF proves its worth under low load conditions, as it is the most likely scheduler to complete the video packet transmission before it reaches its deadline.

2.8.3 Deadline violations

Fig. 2.2(c) shows the percentage of traffic that exceeded its delay deadline. In the case of video and voice traffic, a delay deadline violation of a packet will result in the packet being dropped.

Up until a load of 14 users, EDF has the least number of deadline violations and therefore performs the best. As discussed in the previous section, the reason for this is that video traffic represents two-thirds of the total traffic generated. As resources are effectively assigned in proportion to the amount of traffic generated in each class, EDF is able to avoid more video delay violations than the other schedulers. This gives EDF a distinct advantage. At loads higher than around 15 users, EDF looses its advantage. The average transmission rate of EDF is so much lower, that the total number of violations across all traffic classes exceeds those of other schedulers.

For the other schedulers, Max C/I consistently has a slightly lower deadline violation probability than O-EDF. The reason is that, to a small degree, O-EDF does not distribute resources as evenly among the queues as Max C/I does. Instead, O-EDF contains a component of EDF, which measures the delay that classes experienced and therefore gives video a larger amount of resources than Max C/I would. Both Max C/I and O-EDF have a slight advantage over Round Robin, as they distribute packets based on channel conditions, while Round Robin blindly shares the resources among the queues. Max C/I and O-EDF are therefore able to achieve slightly higher transmission rates than Round Robin, as is evident in Fig. 2.2(b). As a result, both Max C/I and O-EDF will, on average, have fewer deadline violations than Round Robin.

Finally, in the case of PF-T, voice traffic is favoured due to its high transmission rates, while video traffic is largely neglected, resulting in large scale deadline violations. Due to the very high transmission rates that PF-T is able to achieve, the total number of deadline violations are relatively low for loads below 10 users. But as the load increases above this level, the deadline violations of video traffic increase to a level that brings the overall deadline violations to a similar level of Round Robin.

2.8.4 Transmission corruptions

Fig. 2.2(d) shows the percentage of packets that were corrupted during transmission. As the load increases, all three traffic queues are full for a larger proportion of time. The result is that PF-T, Max C/I and O-EDF have more packets to choose from and are able to ensure that packets are transmitted through the best possible channel conditions. This, in turn, reduces the number of corrupt packets that are received by the UE.

In the case of EDF and Round Robin, the channel conditions are ignored, and the number of corrupt packets therefore stays fairly constant as the load increases. The slight decrease in corruptions can be attributed to more voice packets being available for transmission. As the channel conditions improve, HSDPA will automatically increase the transmission rate, even for schedulers such as EDF and Round Robin. Due to the small size of voice packets, HSDPA is therefore able to transmit more voice packets during a period of improved

channel conditions. The result is that, as the load increases, the availability of voice packets increases and the number of packet transmissions during good channel conditions will increase in comparison to the number of transmissions during bad channel conditions.

2.8.5 Average delay and unfairness

Figs. 2.3(a), 2.3(c), and 2.3(e) contain the average queueing delay that video, voice and web traffic respectively experience. At first glance, EDF seems to perform the least favourable, as of all three classes it has the highest queueing delay for large portions of the load conditions. One needs to remember though that EDF schedules traffic based on the delay deadlines of the classes, which are 100ms for video traffic, 50ms for voice traffic, and 500ms for web traffic. In the case of voice traffic, EDF traffic does not reach the deadline, but is still much higher than the other schedulers under high load conditions. The reason for voice delays not reaching the deadline is due to multiple transmissions of voice packets per TTI. The delay of video and web traffic, on the other hand, approaches the deadline at relatively low loads.

The advantage of the EDF scheduler is the clear queueing delay differentiation of traffic classes. The delay deadlines of the various traffic classes create behavioral expectations with customers, which they are prepared to pay for. If no discernable difference is noticeable, the requirement for an advanced delay-targeting QoS design becomes questionable. To further illustrate the point, a form of delay unfairness is proposed that is defined as follows:

$$\text{Unfairness} = 100\% \cdot \frac{d_i - D_i}{d_i}, \tag{2.56}$$

where d_i is the delay deadline of class i and D_i is the queueing delay that the front-of-queue-i packet has experienced by the time it is served. In other words, with this expression an attempt is made to measure how close the delay was to its deadline, by the time the packet completed transmission.

Figs. 2.3(b), 2.3(d), and 2.3(f) contain the average unfairness, measured according to (2.56). This highlights, more clearly, how EDF is able to differentiate the delay of the 3

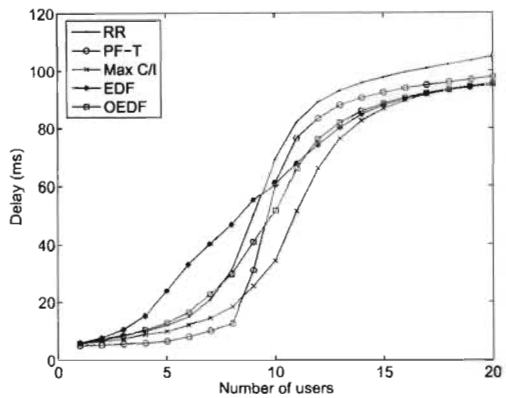

(a) Average delay of Video traffic

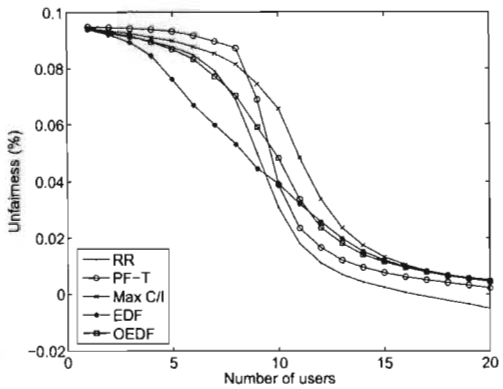

(b) Unfairness of Video traffic

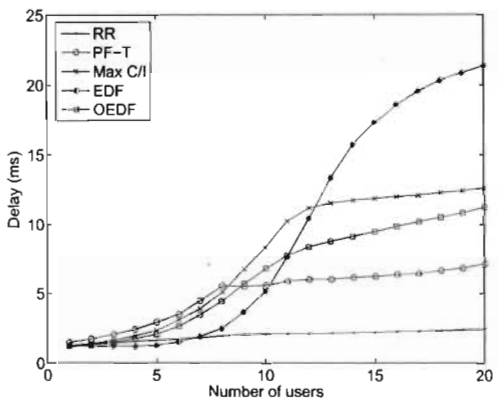

(c) Average delay of Voice traffic

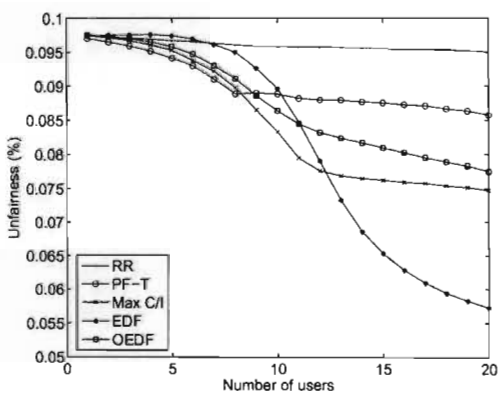

(d) Unfairness of Voice traffic

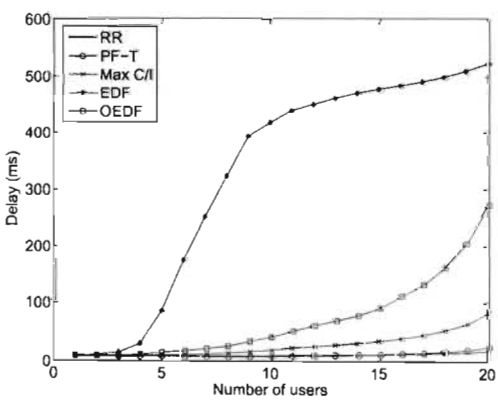

(e) Average delay of Web traffic

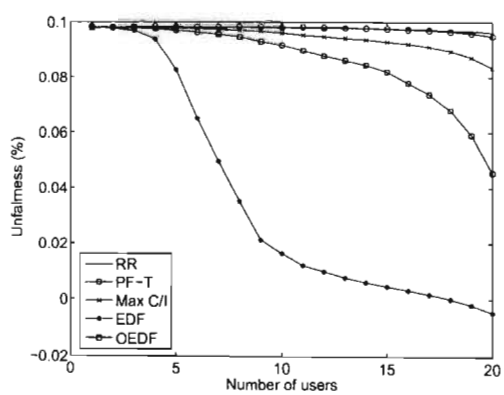

(f) Unfairness of Web traffic

Figure 2.3: Average delay and unfairness

classes, based on their respective deadlines. For all 3 classes, as the load increases, EDF approaches the deadline, marked as 0 on the unfairness graphs.

In the case of video traffic, all schedulers are able to approach the delay deadline quite well. For most of the schedulers this is due to their preference of voice over video traffic. As the video delay approaches the delay deadline, it is dropped. This creates an artificial ceiling around the delay deadline. In the case of voice and web traffic, all schedulers, except for EDF, completely ignore the delay deadline.

2.9 Conclusion

This chapter presented an HSDPA simulation environment. Video, voice, and web traffic were realistically produced by a varying number of sources. The number of sources was varied from 1 to 20, thereby achieving load-conditions varying from 0% to 100%. The model focussed on the downlink transmissions from the base-station to the mobile units, migrating around the cell. It measured the average service rate, the deadline violations, and the percentage traffic corrupted during transmissions. The average delay measure per class of traffic was also presented, accompanied by a deadline-related unfairness measure.

The particular choice of BER thresholds for the various traffic classes played an important role in this simulation. Changing the thresholds would have had a large impact on the behaviour. But, the change is predictable, and the evaluation techniques used in the discussion still apply. The underlying conclusion is that EDF is the only scheduler considered in this simulation, that attempts to enforce queueing delay behaviour on the classes of traffic. The other schedulers distributed resources evenly or in a way that maximises the transmission rate. The result is an increase in the packet loss of certain packet types. If differentiated queueing delay is seen as a sellable commodity, EDF is therefore a valuable asset.

A major concern with EDF in a HSDPA environment, is the lack of channel awareness. Unfortunately, large-scale packet corruption cannot be avoided. It was hoped that O-EDF could be a reliable bridge between the delay awareness of EDF and the channel awareness

of Max C/I. O-EDF is disappointing, as its channel awareness completely overrules the deadline awareness during the decision making process. Luckily, even if EDF chooses a packet that will be transmitted through a bad channel, HSDPA will respond with an appropriate MCS. This will at least partially make up for EDF's channel unawareness. Therefore, if deadline-based traffic differentiation is of primary importance, EDF remains the most viable solution.

Finally, various papers have concluded the following:

- In [7] the transient transmission rate from 0s to 450s was measured, but only at a single load condition. It was found that in the cases of Pedestrian A, Vehicular A, and Vehicular B environments, Max C/I had twice the transmission rate of Round Robin, followed by PF-T. In this chapter, the order of the transmission rates of the same three schedulers is equivalent, but only if the load is kept lower than seven users. At higher loads, the order of the schedulers reverses.

- In [12], a comparison is made between two scenarious. In the first case, all users are placed on the edge of the transmission cell. Here, Max C/I is able to serve around 50% more users than the PF-T scheduler is. In the second scenario, the users are distributed within close range of Node-B. The result is that the situation is reversed, and PF-T is able to support up to four times as many users as Max C/I. In the case of the load curves presented in this chapter, the load of Max C/I grows at a faster rate than that of PF-T, as the number of users is increased. In other words, PF-T is able to support more users than Max C/I. This scenario is therefore more similar to the second scenario in [12], although not as extreme. As the users in the current chapter are evenly spread across the cell, a mixture between scenarios one and two in [12] was confirmed.

- In [8], a comparison is made between three schedulers. The first is called the Opportunistic Index, and is equivalent to Max C/I. The second is called the Fairness Priority Index, which is similar to EDF and essentially finds the ratio of the queueing delay to its deadline and then chooses the traffic class with the smallest resulting ratio. Finally, the Global Priority Index is a hybrid scheme that combines the Fairness

Priority Index with Max C/I. The packet loss of Max C/I is found to be much larger than that of the Fairness Priority Index. Assuming that EDF in this chapter behaves similarly to the Fairness Priority Index in [8], this chapter compares favourably with that of [8] as long as the load in this chapter is kept below thirteen users. In the case of the cell throughput in [8], the Fairness Priority Index outperforms Max C/I up to 2.5 times at the maximum load of sixty users. This behaviour is similar to that of PF-T and EDF found in this chapter, as long as the network load is larger than eight users.

In conclusion, under the correct conditions, the results presented in this chapter therefore tie up with those presented in existing literature.

Chapter 3

EDF analysis

3.1 Introduction

Advanced scheduling has become an inevitable component of modern Quality-of-Service (QoS)-based data networks. In the past, networks contained only one class of traffic, making it possible to optimise the architecture of the network according to its specific needs. For example, the telephone network is a rigid structure with good performance guarantees, while packet switched networks are more flexible but only provide marginal performance guarantees [5]. Modern integrated services networks carry a large number of different data types, each with its own requirements.

To provide QoS guarantees, a scheduler is required. The scheduler is usually located inside every switch or router. When the router has determined what the next destination of the various packets should be, the scheduler decides in what order the packets should be transmitted and at what rate, so that delay and throughput guarantees are met. In wired networks, a large amount of research has been published on various schedulers, most of which belong to the family of *General Processor Sharing* (GPS) schedulers [5, 16, 17, 18, 19, 20, 21, 22, 23, 24, 25]. The main reason for the abundance of literature on GPS is the throughput guarantee that these schedulers adhere to, which make it possible to find delay bounds with relative ease.

This chapter focuses on another popular scheduler, known as Earliest Deadline First (EDF). Whereas GPS schedulers maximise throughput in a fair manner, making them particularly well suited for greedy traffic, EDF sorts incoming traffic in the order in which queueing time deadlines are approached. An EDF scheduler is therefore best suited for delay-sensitive real-time traffic. Telecommunication companies around the world have expressed their interest in finding ways to merge real-time traffic, such as voice conversations, video-conferencing and video-on-demand with best-effort traffic, on the same IP network. This promises to offer a cost-effective and more adaptable solution than carrying real-time and best-effort traffic on separate networks.

In order to engineer a future network, analytical models are required that predict the behaviour of the various networking components. In the case of the EDF scheduler, an exact analysis, as offered by conventional queueing theory, cannot be used to model modern networks carrying heterogeneous traffic, as these networks are generally too complicated. The problem with the EDF scheduler is that packets are not served in order of arrival, as is the case with First-In-First-Out (FIFO).

Few papers have been published that attempt to analyse the behaviour of EDF [26, 27, 28, 29, 30, 31]. As an exact analysis is not feasible, several approximation methods were used to model EDF. For example, reference [26] finds an approximate expression for the mean value of the queueing delay in an EDF queueing system. Reference [27] relies on a Chernoff bound to find an expression for the deadline violation probability. Reference [28] compares a similar Chernoff bound to an expression derived using the Effective Bandwidth theory and Large Deviation principles and finds that for heavy loads the Chernoff bound is looser than the second method.

More recent papers that offer analyses of the EDF algorithm include [32], which extends the classic response time analysis techniques to analyse tasks scheduled either with fixed priorities, or with an EDF scheduler running on top of an underlying fixed priority scheduler. [33] presents fast exact feasibility tests for uniprocessor real-time systems using preemptive EDF scheduling. An integrated schedulability theory for EDF is presented. Finally, for the multiprocessor scenario, [34] derives a new schedulability test for preemptive

deadline scheduling of periodic or sporadic real-time tasks on a single-queue m-server system. This new test allows the task deadline to be more or less than the task period, and is based on a new analysis concept, called a mu-busy interval.

This chapter makes two major contributions. Unlike other papers on the delay and fairness of schedulers, the upper or lower bound are not found, but rather the actual delay and fairness probability distributions. The Effective Bandwidth theory and Large Deviation principles are used to derive approximate expressions that describe the deadline violation probability, followed by the cumulative distribution function and the probability density function of the delay of individual traffic classes served by an Earliest Deadline First scheduler. A definition for the stochastic fairness of real-time traffic classes in an Earliest Deadline First queueing system is introduced and an expression for this fairness found. The result is a set of expressions that captures the delay and fairness behaviour of traffic in an Earliest Deadline First queueing system.

Section 3.2 introduces the system model used throughout this paper. Section 3.3.1 introduces the deadline violation probability analysis presented in [28] and extends it by deriving an expression for the individual traffic classes, as opposed to the system as a whole. Sections 3.3.2 and 3.3.3 derive expressions for the cumulative distribution function and probability density function of the queueing delay, respectively. In section 3.4 a new measure of the fairness distribution of real-time traffic is proposed, followed by a derivation of an approximate expression for the stochastic fairness bound of the various traffic classes.

3.2 System Model

Imagine that the various sources in a network produce data packets of J different classes. Examples of such data types are voice, stored video, video-conference, e-mail, FTP, and HTTP packets. Each of these has different delay, jitter (variation in delay), throughput, bit-error-rate and packet-loss-rate requirements. Only when a network is able to meet all the requirements of all the data classes, can it claim to provide quality-of-service (QoS).

The Earliest Deadline First (EDF) scheduler [35] is one of the simplest multiplexing algorithms, especially well suited for real-time traffic, as it is able to adhere to the delay deadlines that traffic classes require. Voice and video are examples of real-time traffic, as opposed to best-effort traffic, which includes e-mail, ftp and http. As a packet p_i of data class i is created, it is assigned a corresponding delay deadline d_i. This represents the amount of time that packets of data type i can afford to queue at switching nodes they pass through. The EDF scheduler picks the head-of-queue packet from queue j, which has the closest deadline $\min_j(d_j - D_j)$. Here D_j is the queueing delay that the head-of-queue packet of queue j experienced, since it arrived.

3.3 Delay Analysis

3.3.1 Deadline Violation Probability

The following deadline violation probability analysis in this subsection is based on the work presented in [28]. It has been extended by deriving an expression that describes the violation probability of individual traffic classes as opposed to the whole system, as was the case in [28].

Adopting the system model of [28], imagine that K sources produce J different data types, with corresponding upper delay bounds of $d_1, d_2, \ldots, d_J$, where $d_1 \leq d_2 \leq \ldots \leq d_J$. Let k_i be the number of sources that produce class i data. C is the link rate at which a chosen packet will be served, while L is the packet size, which is assumed to be constant. The amount of work of class i that source j produces in the time interval $[0, t]$ is represented by $A_{ij}[0, t]$. The total amount of class i traffic arriving from all J sources, is simply represented by $A_i[0, t]$.

Using the graphical timeline in Fig. 3.1, imagine that a packet p_i of class i (double boxed) arrives at time $T - d_i$. In other words, it will have to be served by time T to make its deadline. If the packets within all the queues is added up, then the total system queue length of packets already queued is hereby defined to be represented by symbol

$Q(T-d_i)$. Now, in order to calculate the total number of packets that will be transmitted before packet p_i, note that a packet p_{i-1} with deadline d_{i-1} arriving anywhere within time interval $[T-d_i, T-d_{i-1}]$ (the boxed interval in Fig. 3.1) will be served before packet p_i, since it will have an earlier deadline. Even though it arrived after packet p_i it should still be added to the queue $Q(T-d_i)$ of packets which will be served before packet p_i. The same is true for a packet p_{i-2} arriving within $[T-d_i, T-d_{i-2}]$, and so on. Note that this assumption can only be made for an EDF scheduler.

On the other hand, a packet p_{i+1} with deadline d_{i+1} that arrived before packet p_i within time interval $[T-d_{i+1}, T-d_i]$ will be served after packet p_i. This must therefore be subtracted from $Q(T-d_i)$, to find the total packets that are served before packet p_i.

As a summary, if these two processes are implemented, the expression

$$Q(T-d_i) + \sum_{j=1}^{i-1} A_j[T-d_i, T-d_j] - \sum_{j=i+1}^{J} A_j[T-d_j, T-d_i], \tag{3.1}$$

represents all packets that will be served before packet p_i. Since the system resource capacity is given by C, the maximum amount of traffic that can be served during the interval $[T-d_i, T]$ is given by Cd_i. In order for the packet to exceed its delay deadline, the following expression therefore has to be true:

$$\underbrace{Q(T-d_i)}_{\text{arrived before } p_i} + \underbrace{\sum_{j=1}^{i-1} A_j[T-d_i, T-d_j]}_{\text{arrived after } p_i\text{, served before } p_i} - \underbrace{\sum_{j=i+1}^{J} A_j[T-d_j, T-d_i]}_{\text{arrived before } p_i\text{, served after } p_i} \geq \underbrace{Cd_i}_{\text{total service}} . \tag{3.2}$$

Furthermore, assuming that the queue length $Q(T-d_i)$ has a stationary queue length distribution with mean Q, the violation probability of class i traffic multiplexed by an EDF scheduler can be directly deduced from (3.2) to be

$$P_{vio}^{i} = \Pr\{D_i > d_i\} \approx \Pr[Q + A_i - Cd_i \geq 0] = \Pr[Q \geq Cd_i - A_i], \tag{3.3}$$

where $A_i = \sum_{j=1}^{J} A_j[d_i - d_j]$, the total number of class i packets that arrived over a time period $d_i - d_j$. For $i = J$, this result is identical to that found in [28].

The problem to be solved in (3.3) is to find an expression for the stationary queue length distribution Q. Determining the exact queue length distribution is usually difficult. Reference [28] therefore suggests the use of Large Deviation estimates as an alternate solution.

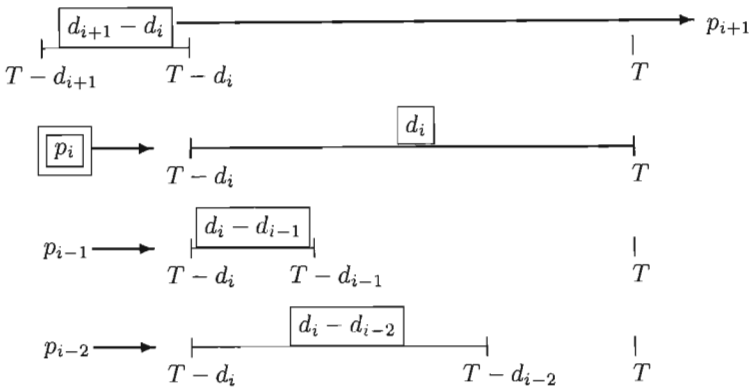

Figure 3.1: Time lines for the various traffic classes

Two such approximations, the Large Buffer and the Many Sources asymptotics have both been used to approximate queue length distributions and buffer overflow probabilities [36]. As discussed in [37] and [38], the Large Buffer asymptotic $\Pr[q \geq Q] = e^{-\delta Q}$ is used when the buffer overflow probability is determined as the buffer size varies. The Many Sources asymptotic $\Pr[\text{overflow}] = e^{-NI}$ is used when the buffer overflow probability is measured, while the number of sources is varied and the buffer capacity and service rate are kept constant. In the expression for the Large Buffer asymptotic, Q may be the total buffer size B or a queue length of interest, while for the Many Sources asymptotic, N is a scaling parameter such that $B = Nb$ and $C = Nc$, where b and c respectively denote the buffer space and bandwidth per source.

Assuming that the Large Buffer asymptotic holds for a varying queue length Q, the appropriate choice in this case is the Large Buffer asymptotic

$$\Pr[Q \geq q] = e^{-\delta q}, \tag{3.4}$$

as the assumption is that the number of sources remains constant and the aim is to calculate a distribution of the queue length Q. The only unknown in (3.4) is the queue length decay rate δ. In order to evaluate this, the Effective Bandwidth theory is introduced. As discussed in detail in [39], the Effective Bandwidth $\alpha(s,t)$ is a measure of the burstiness of a source and lies somewhere between the mean and the peak arrival rate of the source. It is given by

$$\alpha(s,t) = \frac{1}{st} \log \mathbb{E}\left[e^{sX[0,t]}\right] \qquad 0 < s,t < \infty, \tag{3.5}$$

where $X[0,t]$ represents the amount of work that arrives from a source in the interval $[0,t]$.

The characteristics of a source are fully captured by the effective bandwidth through its s and t parameters, which are the so-called space and time parameters. For any fixed value in t, $\alpha(s,t)$ is increasing in s. Therefore $\alpha(0,t) = \frac{\mathbb{E}X[0,t]}{t}$ and $\alpha(\infty,t) = \frac{\bar{X}[0,t]}{t}$. Reference [38] furthermore explains that the implication of the s and t parameters for traffic engineers is

$$s = \frac{\partial \gamma}{\partial B} \qquad \text{and} \qquad st = \frac{\partial \gamma}{\partial C},$$

where $\gamma = -\log \Pr[\text{overflow}]$. In other words, s is equal to the rate at which the logarithm of the overflow probability changes with the buffer size, for a fixed capacity. On the other hand, st is equal to the rate at which the logarithm of the overflow probability decreases with the link capacity for a fixed buffer size.

To evaluate the queue length decay rate δ in (3.4), one may use the fact that $0 < s < \delta$ and the stability limit of the system [36, 38, 28]:

$$\sum_{j=1}^{J} k_j \alpha_j(s) \leq C, \tag{3.6}$$

where $\alpha(s) = \lim_{t\to\infty} \alpha(s,t)$.

For a Poisson source [36, 40]

$$\alpha_j(s,t) = \alpha_j(s) = \frac{\lambda_j}{s}(e^s - 1), \tag{3.7}$$

since a Poisson source has independent increments, as mentioned in [39]. Here, λ_j is the mean arrival rate of the Poisson source of class j.

If (3.7) is substituted into (3.6), a non-linear expression results, which may be evaluated numerically, to find the desired δ:

$$\frac{e^\delta - 1}{\delta} = \frac{C}{\sum_{j=1}^{J} k_j \lambda_j}. \tag{3.8}$$

The deadline violation probability may thus be found using the Large Buffer asymptotic of (3.4) as an approximation for (3.3) to give

$$P_{vio}^i = \Pr[Q \geq Cd_i - A_i] \approx e^{-\delta(Cd_i - A_i)}. \tag{3.9}$$

But as mentioned earlier, $A_i = \sum_{j=1}^{J} A_j[d_i - d_j]$, which represents the total number of class i packets that arrive over a time period of $d_i - d_j$. This may also be approximated using the Effective Bandwidth theory to give

$$\sum_{j=1}^{J} A_j[d_i - d_j] \approx \sum_{j=1}^{J} k_j \alpha(s, d_i - d_j)[d_i - d_j]. \tag{3.10}$$

The expression for the deadline violation probability of class i traffic in (3.9) therefore becomes

$$P_{vio}^{i} \approx \exp\left\{ -\delta C d_i + \delta \sum_{j=1}^{J} k_j (d_i - d_j)\alpha(\delta, d_i - d_j)) \right\}. \tag{3.11}$$

In the case of Poisson sources, (3.7) may be substituted into (3.11) to give

$$P_{vio}^{i} \approx \exp\left\{ -\delta C d_i + (e^{\delta} - 1) \sum_{j=1}^{J} k_j \lambda_j (d_i - d_j) \right\}. \tag{3.12}$$

Note that the use of Poisson sources is not strictly valid. Packet-switched traffic will in general not be generated by Poisson sources. On the other hand, no statistical source model currently exists that satisfactorily captures the source behaviour of packet switched networks. Typically, traffic will have a heavy tailed nature and have long-range dependence with a self-similar fractal nature. The resultant mathematical models are very difficult to work with [41], [42]. To avoid these problems this analysis limits itself to the Poisson model. But, by changing the Large Buffer Asymptotic and using other estimates of $\alpha_j(s,t)$, one may readily change the model presented here to a more accurate source model.

In [28] in Section 4.2, Sivaraman and Chiussi show that for an ON-OFF Markovian Fluid Sources,

$$\alpha_j(s,t) = \frac{1}{t} \log\left\{ \left(\frac{\lambda_j}{\lambda_j + \mu_j}, \frac{\mu_j}{\lambda_j + \mu_j} \right) \exp\begin{pmatrix} -\mu_j t + h_j s t & \mu_j t \\ \lambda_j t & -\lambda_j t \end{pmatrix} \begin{pmatrix} 1 \\ 1 \end{pmatrix} \right\}, \tag{3.13}$$

and $a_j(s) = \lim_{t\to\infty} \alpha_j(s,t)$ is given by

$$\alpha_j(s) = \frac{1}{2}\left(h_j s - \mu_j - \lambda_j + \sqrt{(h_j s - \mu_j + \lambda_j)^2 + 4\lambda_j \mu_j} \right) \tag{3.14}$$

For the remainder of Chapter 3 and the work in Chapter 4 only the Poisson source model will be used. However, the expressions for the ON-OFF Markovian Fluid Source model can be used to extend this work to a more realistic source model.

3.3.2 Cumulative Delay Distribution

In this section the aim is to find the cumulative delay distribution of EDF. The work from this point onwards is novel and builds on the violation probability analysis of [28].

To determine the cumulative delay distribution, one can follow a similar argument to that presented in Section 3.3.1. Here it was argued that

$$P_{vio} = \Pr\{D_i > d_i\} = \Pr[Q \geq Cd_i - A_i]. \tag{3.15}$$

Instead of merely looking at the probability of whether the deadline will be exceeded, one can determine the cumulative delay distribution by finding the probability that the queueing time D_i exceeds some arbitrary time t. The resulting expression becomes:

$$\Pr\{D_i > t\} = \Pr[Q \geq Ct - A_i]. \tag{3.16}$$

Alternatively, the argument can be turned around to find the probability that packet p_i has already been served by time $T - d_i + t$, which is more convenient in this case. Similarly to Section 3.3.1, imagine that packet p_i of class i arrives at time $T - d_i$. Referring to Fig. 3.2, in order for packet p_i to be served by time $T - d_i + t$, where $t \geq 0$, the capacity C of the system will have to be sufficiently large to clear all the packets Q_{Total} that first have to be transmitted:

$$Ct > Q_{Total}. \tag{3.17}$$

The total number of packets Q_{Total} that will be served before packet p_i is given by

$$Q_{Total} = \underbrace{Q(T-d_i)}_{\text{arrived before } p_i} + \underbrace{\sum_{j=1}^{i-1} A_j(T-d_i, T^*)}_{\text{arrived after } p_i\text{, will be served before } p_i} - \underbrace{\sum_{j=i+1}^{J} A_j(T-d_j, T-d_i)}_{\text{arrived before } p_i\text{, will be served after } p_i}, \tag{3.18}$$

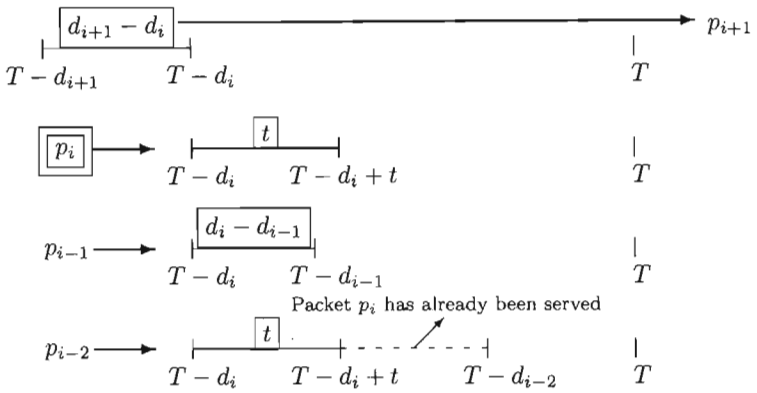

Figure 3.2: Special case: Packet p_i gets served at time $t < d_i$.

where

$$T^* = \begin{cases} T - d_i + t, & t < d_i - d_j \\ T - d_j, & t \geq d_i - d_j \end{cases}. \tag{3.19}$$

Expression (3.19) introduces a new degree of complexity. Fig. 3.2 illustrates the probability that packet p_i has already been served by time $T - d_i + t$. In this case, any packets arriving after $T - d_i + t$ cannot be served before p_i anymore, even if the EDF scheduler would have prioritised them higher if p_i was still queueing. Only packets that arrive between $T - d_i$ and $T - d_i + t$, and also have a higher priority ($j > i$) than packet p_i, therefore need to be added to the queued packets $Q(T - d_i)$.

The probability that the delay D_i experienced by a packet of class i is greater than some period $t \geq 0$ is then given by

$$\Pr\{D_i > t\} = \Pr\left\{ Q(T - d_i) > Ct - \sum_{j=1}^{i-1} A_j(T - d_i, T^*) + \sum_{j=i+1}^{J} A_j(T - d_j, T - d_i) \right\} \tag{3.20}$$

Using the Large Buffer asymptotic expressed in (3.4), equation (3.20) may thus be rewritten to give

$$\Pr\{D_i > t\} = \exp\left\{ -\delta Ct + \delta \sum_{j=1}^{i-1} A_j(T - d_i, T^*) - \delta \sum_{j=i+1}^{J} A_j(T - d_j, T - d_i) \right\} \tag{3.21}$$

Similarly, one can use the Effective Bandwidth theory to approximate any of the packets arriving before and after packet p_i

$$\sum_{j=1}^{i-1} A_j(T-d_i, T^*) - \sum_{j=i+1}^{J} A_j(T-d_j, T-d_i) = \sum_{j=1}^{i-1} T_j k_j \alpha_j(\delta, T_j), \tag{3.22}$$

where

$$T_j = \begin{cases} d_i - d_j, & d_i - d_j < t \\ t, & d_i - d_j \geq t \end{cases} \tag{3.23}$$

In (3.22), k_j are the number of sources of class j and $\alpha_j(\delta, T_j)$ is the effective bandwidth of class j sources. The probability that the delay D_i experienced by a packet of class i is greater than some period $t \geq 0$ is therefore given by

$$\Pr\{D_i > t\} = \exp\left\{-\delta C t + \delta \sum_{j=1}^{J} k_j T_j \alpha_j(\delta, T_j)\right\}. \tag{3.24}$$

For the special case that Poisson sources generate the traffic, (3.7) is substituted into (3.24), which results in

$$\Pr\{D_i > t\} = \exp\left\{-\delta C t + (e^{\delta} - 1) \sum_{j=1}^{J} k_j \lambda_j T_j\right\}. \tag{3.25}$$

To obtain the cumulative distribution function $F_i(t)$, note that

$$\begin{aligned} F_i(t) &= \Pr\{D_i \leq t\} \\ &= 1 - \exp\left\{-\delta C t + (e^{\delta} - 1) \sum_{j=1}^{J} k_j \lambda_j T_j\right\}\Bigg|_{t \geq 0}. \end{aligned} \tag{3.26}$$

3.3.3 Delay Probability Density Function

From the results in the previous section, one is able to predict the probability density function (pdf) of the queueing time, using the following argument:

Depending on the value of t, there exists a boundary value $h_i(t) \leq i$, such that

$$h_i(t) = \max_j d_i - d_j \geq t. \tag{3.27}$$

which results in

$$\begin{cases} j \in [1, h_i(t)], & \text{where } d_i - d_j \geq t, \\ j \in [h_i(t)+1, J], & \text{where } d_i - d_j < t. \end{cases} \tag{3.28}$$

Using (3.28), equation (3.23) translates to

$$T_j = \begin{cases} t, & j \in [1, h_i(t)] \\ d_i - d_j, & j \in [h_i(t)+1, J]. \end{cases} \tag{3.29}$$

With the help of (3.29), equation (3.26) can be rewritten as

$$\begin{aligned} F_i(t) &= 1 - \exp\left\{ -\delta C t + (e^\delta - 1) \left[\underbrace{\sum_{j=1}^{h_i(t)} k_j \lambda_j t}_{d_i - d_j \geq t} + \underbrace{\sum_{j=h_i(t)+1}^{J} k_j \lambda_j (d_i - d_j)}_{d_i - d_j < t} \right] \right\} \\ &= 1 - \exp\left\{ t \left[-\delta C + (e^\delta - 1) \sum_{j=1}^{h_i(t)} k_j \lambda_j \right] + (e^\delta - 1) \sum_{j=h_i(t)+1}^{J} k_j \lambda_j (d_i - d_j) \right\} \Bigg|_{t \geq 0}. \end{aligned} \tag{3.30}$$

But the probability density function of D_i for a given $t \geq 0$ is

$$f_i(t) = \frac{dF_i(t)}{dt}. \tag{3.31}$$

Therefore

$$\begin{aligned} f_i(t) = &\left(\delta C - (e^\delta - 1) \sum_{j=1}^{h_i(t)} k_j \lambda_j \right) \\ &\cdot \exp\left[-\delta C t + (e^\delta - 1) \sum_{j=1}^{h_i(t)} k_j \lambda_j t + (e^\delta - 1) \sum_{j=h_i(t)+1}^{J} k_j \lambda_j (d_i - d_j) \right] \Bigg|_{t \geq 0}. \end{aligned} \tag{3.32}$$

3.4 Fairness

3.4.1 Stochastic fairness definition

One of the first researchers to define fairness mathematically was Golestani. In [21], he defines a perfectly fair system to have the quality

$$w_k(t_1, t_2) = w_j(t_1, t_2),\ k, j \in B(t_1, t_2). \tag{3.33}$$

Here $B(t_1, t_2)$ is the set of sessions that are backlogged during the interval (t_1, t_2), while

$$w_j(t_1, t_2) = \frac{W_k(t_1, t_2)}{r_k}\ k \in K, \tag{3.34}$$

where K is the set of sessions, set up on a link. $W_k(t_1, t_2)$ are the number of bits of session k transmitted during $(0, t)$, while r_k represents the service share allocated to session k.

Effectively, what this means is that in a perfectly fair server, the amount of service a session receives normalised by its share of the available bandwidth, should be the same for all backlogged sessions. In reality, no packetised implementation of a fluid system can achieve this goal. Stiliadis in [24] and [43] therefore replaced his equivalent version of the perfect fairness definition

$$\max \left| \frac{W_a^S(\tau, t)}{r_a} - \frac{W_b^S(\tau, t)}{r_b} \right| = 0 \qquad \text{for all } a \text{ and } b, \tag{3.35}$$

with a more realistic version

$$\max \left| \frac{W_a^S(\tau, t)}{r_a} - \frac{W_b^S(\tau, t)}{r_b} \right| \leq F^S \qquad \text{for all } a \text{ and } b. \tag{3.36}$$

The bound F^S is an upper bound and indicates how unfair a scheduler is.

Stiliadis' definition is based on the assumption that the various traffic classes have been promised a throughput guarantee. This is a good system for best-effort traffic. For real-time traffic, the biggest concern is the delay that packets experience while travelling through the network. A different fairness definition is needed which takes delay deadlines into consideration, instead of throughput guarantees. Furthermore, the definition proposed by Stiliadis is deterministic — the fairness value F^S may never be exceeded. The problem

with a definition of this kind is that extremely large fairness values may be possible, but with very low probability. This means that F^S may be situated very far away from the mean fairness value and therefore does not capture the common behaviour of the scheduler. In some cases, the fairness might not be bounded at all, which means that F^S cannot be found.

A stochastic fairness bound, on the other hand, guarantees that the fairness value of class a will not exceed the bound F_a with a probability of more than δ [44]. This thesis therefore proposes the following expression as a suitable definition for the fairness of real-time class a traffic:

$$\text{Prob}\left\{\left|\frac{D_a}{d_a} - \frac{D_b}{d_b}\right| > F_a(\delta)\right\} \leq \delta, \qquad \text{for all } b, \tag{3.37}$$

where D_a is the delay that a packet of class a with delay deadline d_a experienced, while δ is the maximum probability that the fairness limit F may be exceeded by. This is an important contribution as a fairness curve dependent on the value of δ can now be drawn. Users of this curve can with ease read of the fairness bound exceeded with a probability of $\delta\%$, which allows for realistic risk assessments.

In practice the stochastic fairness $F_a(\delta)$ of *Type a* traffic can be found by rewriting (3.37) in integral form and then solving for $F_a(\delta)$, given a value of δ.

$$\int_{F_a(\delta)}^{\infty} f_{\left|\frac{D_a}{d_a} - \frac{D_b}{d_b}\right|}(t)\, dt = \delta. \tag{3.38}$$

3.4.2 Derivation of the stochastic fairness expression

In order to find an expression for the stochastic fairness of real-time traffic, the following pdf distribution must be found

$$f_{\left|\frac{D_a}{d_a} - \frac{D_b}{d_b}\right|}(t). \tag{3.39}$$

The pdf $f_{\frac{D_a}{d_a}}(t)$ is given by

$$f_{\frac{D_a}{d_a}}(t) = |d_a| \cdot f_{D_a}(d_a t). \tag{3.40}$$

The value of all delay deadlines d_a is constant and always positive, so that $|d_a| = d_a$. The pdf $f_{\frac{D_a}{d_a}}(t)$ therefore translates to

$$\begin{aligned} f_{\frac{D_a}{d_a}}(t) &= d_a \left(\delta C - (e^\delta - 1) \sum_{j=1}^{h_a(d_a t)} k_a \lambda_a \right) \\ &\cdot \exp\left[-\delta C d_a t + \left((e^\delta - 1) \cdot \sum_{j=1}^{h_a(d_a t)} k_j \lambda_j d_a t \right) + \left((e^\delta - 1) \cdot \sum_{j=h_a(d_a t)+1}^{J} k_j \lambda_j (d_i - d_j) \right) \right] \end{aligned} \tag{3.41}$$

The next step is to find $f_{\frac{D_a}{d_a} - \frac{D_b}{d_n}}(t)$. This can be obtained through the following convolution integral, which requires dummy variable τ for the integration:

$$\begin{aligned} f_{\frac{D_a}{d_a} - \frac{D_b}{d_b}}(t) &= \int_{-\infty}^{\infty} d_a d_b \cdot \left(\delta C - (e^\delta - 1) \cdot \sum_{j=1}^{h_a(d_a t + d_a \tau)} k_j \lambda_j \right) \cdot \left(\delta C - (e^\delta - 1) \cdot \sum_{j=1}^{h_b(d_b \tau)} k_j \lambda_j \right) \\ &\cdot \exp\left[-\delta C d_a (t+\tau) - \delta C d_b \tau + (e^\delta - 1) \left\{ \sum_{j=1}^{h_a(d_a t + d_a \tau)} k_j \lambda_j d_a (t+\tau) + \sum_{j=h_a(d_a t + d_a \tau)+1}^{J} k_j \lambda_j (d_a - d_j) \right. \right. \\ &\left. \left. + d \sum_{j=1}^{h_b(d_b \tau)} k_j \lambda_j d_b \tau + \sum_{j=h_b(d_b \tau)+1}^{J} k_j \lambda_j (d_b - d_j) \right\} \right] d\tau \\ &= d_a d_b \cdot \exp(-\delta C d_a t) \cdot \int_{-\infty}^{\infty} \left(\delta C - (e^\delta - 1) \cdot \sum_{j=1}^{h_a(d_a t + d_a \tau)} k_j \lambda_j \right) \cdot \left(\delta C - (e^\delta - 1) \cdot \sum_{j=1}^{h_b(d_b \tau)} k_j \lambda_j \right) \\ &\cdot \exp\left[-\delta C (d_a + d_b) \tau + (e^\delta - 1) \left\{ \sum_{j=1}^{h_a(d_a t + d_a \tau)} k_j \lambda_j d_a (t+\tau) + \sum_{j=h_a(d_a t + d_a \tau)+1}^{J} k_j \lambda_j (d_a - d_j) \right. \right. \\ &\left. \left. + \sum_{j=1}^{h_b(d_b \tau)} k_j \lambda_j d_b \tau + \sum_{j=h_b(d_b \tau)+1}^{J} k_j \lambda_j (d_b - d_j) \right\} \right] d\tau, \end{aligned} \tag{3.42}$$

In this equation it is somewhat tricky to ensure that $h_a(d_a t)$ is converted correctly during the convolution process, with dummy variable τ. Fig. 3.3 can be consulted to show that the boundary events $h_a(d_a t + d_a \tau)$ and $h_b(d_b \tau)$ in the above equation are correct.

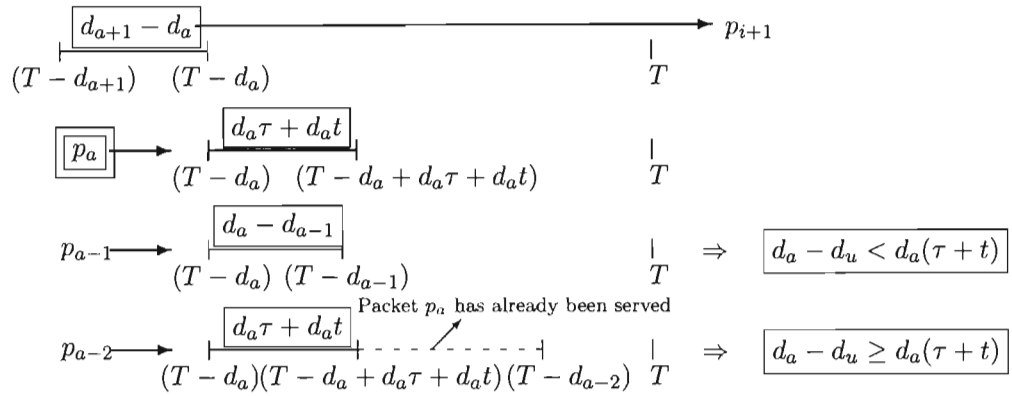

Figure 3.3: Timeline for packet p_a.

This integral consists of various discontinuous functions. Using this information, the integral must be broken down into a sum of integrals, of which the limits run between the various breaks in functions.

$$
\begin{aligned}
f_{\frac{D_a}{d_a}-\frac{D_b}{d_b}}(t) =& d_a d_b \cdot \exp(-\delta C d_a t) \cdot \sum_{n=1}^{a+b} \int_{\tau_0=0}^{\tau_n} \left(\delta C - (e^\delta - 1) \sum_{j=1}^{h_a(n)} k_j \lambda_j \right) \cdot \left(\delta C - (e^\delta - 1) \sum_{j=1}^{h_b(n)} k_j \lambda_j \right) \\
& \cdot \exp \left[-\delta C(d_a + d_b)\tau + (e^\delta - 1) \left\{ \sum_{j=1}^{h_a(n)} k_j \lambda_j d_a (t + \tau) + \sum_{j=h_a(n)+1}^{J} k_j \lambda_j (d_a - d_j) \right. \right. \\
& \left. \left. + \sum_{j=1}^{h_b(n)} k_j \lambda_j d_b \tau + \sum_{j=h_b(n)+1}^{J} k_j \lambda_j (d_b - d_j) \right\} \right] d\tau, \\
=& d_a d_b \cdot \exp(-\delta C d_a t) \sum_{n=1}^{a+b} \frac{\left(\delta C - (e^\delta - 1) \sum_{j=1}^{h_a(n)} k_j \lambda_j \right) \cdot \left(\delta C - (e^\delta - 1) \sum_{j=1}^{h_b(n)} k_j \lambda_j \right)}{-\delta C(d_a + d_b) + (e^\delta - 1) \left\{ \sum_{j=1}^{h_a(n)} k_j \lambda_j d_a + \sum_{j=1}^{h_b(n)} k_j \lambda_j d_b \right\}} \\
& \cdot \left(\exp \left[-\delta C(d_a + d_b)\tau_n + (e^\delta - 1) \left\{ \sum_{j=1}^{h_a(n)} k_j \lambda_j d_a (t + \tau_n) + \sum_{j=h_a(n)+1}^{J} k_j \lambda_j (d_a - d_j) \right. \right. \right. \\
& \left. \left. \left. + \sum_{j=1}^{h_b(n)} k_j \lambda_j d_b \tau_n + \sum_{j=h_b(n)+1}^{J} k_j \lambda_j (d_b - d_j) \right\} \right] \right. \\
& \left. - \exp \left[-\delta C(d_a + d_b)\tau_{n-1} + (e^\delta - 1) \left\{ \sum_{j=1}^{h_a(n)} k_j \lambda_j d_a (t + \tau_{n-1}) + \sum_{j=h_a(n)+1}^{J} k_j \lambda_j (d_a - d_j) \right. \right. \right. \\
& \left. \left. \left. + \sum_{j=1}^{h_b(n)} k_j \lambda_j d_b \tau_{n-1} + \sum_{j=h_b(n)+1}^{J} k_j \lambda_j (d_b - d_j) \right\} \right] \right)
\end{aligned}
$$

(3.43)

where

$$\begin{cases} j \in [1, h_a(n)], & d_a - d_j \geq d_a t + d_a \tau \\ j \in [h_a(n)+1, J], & d_a - d_j < d_a t + d_a \tau \\ \hline j \in [1, h_b(n)], & d_b - d_j \geq d_b \tau \\ j \in [h_b(n)+1, J], & d_b - d_j < d_b \tau \end{cases} \tag{3.44}$$

which may be rewritten for convenience sake to be

$$\begin{cases} j \in [1, h_a(n)], & \tau \leq \frac{d_a - d_j - d_a t}{d_a} \\ j \in [h_a(n)+1, J], & \tau > \frac{d_a - d_j - d_a t}{d_a} \\ \hline j \in [1, h_b(n)], & \tau \leq \frac{d_b - d_j}{d_b} \\ j \in [h_b(n)+1, J], & \tau > \frac{d_b - d_j}{d_b} \end{cases} \tag{3.45}$$

In order to find the fairness pdf of class-a traffic with respect to all other traffic types, the average must be found:

$$\begin{aligned} & f_{\frac{D_a}{d_a} - \frac{D_b}{d_b}}(t) \\ & = \frac{1}{J-1} \sum_{\substack{b=1 \\ b \neq a}}^{J} \left\{ d_a d_b \cdot \exp(-\delta C d_a t) \sum_{n=1}^{a+b} \frac{\left(\delta C - (e^\delta - 1) \sum_{j=1}^{h_a(n)} k_j \lambda_j\right) \cdot \left(\delta C - (e^\delta - 1) \sum_{j=1}^{h_b(n)} k_j \lambda_j\right)}{-\delta C (d_a + d_b) + (e^\delta - 1) \left\{ \sum_{j=1}^{h_a(n)} k_j \lambda_j d_a + \sum_{j=1}^{h_b(n)} k_j \lambda_j d_b \right\}} \right. \\ & \cdot \left(\exp\left[-\delta C (d_a + d_b) \tau_n + (e^\delta - 1) \left\{ \sum_{j=1}^{h_a(n)} k_j \lambda_j d_a (t + \tau_n) + \sum_{j=h_a(n)+1}^{J} k_j \lambda_j (d_a - d_j) \right.\right.\right. \\ & \left.\left.\left. + \sum_{j=1}^{h_b(n)} k_j \lambda_j d_b \tau_n + \sum_{j=h_b(n)+1}^{J} k_j \lambda_j (d_b - d_j) \right\} \right] \right. \\ & \left. - \exp\left[-\delta C (d_a + d_b) \tau_{n-1} + (e^\delta - 1) \left\{ \sum_{j=1}^{h_a(n)} k_j \lambda_j d_a (t + \tau_{n-1}) + \sum_{j=h_a(n)+1}^{J} k_j \lambda_j (d_a - d_j) \right.\right.\right. \\ & \left.\left.\left. + \sum_{j=1}^{h_b(n)} k_j \lambda_j d_b \tau_{n-1} + \sum_{j=h_b(n)+1}^{J} k_j \lambda_j (d_b - d_j) \right\} \right] \right) \Bigg\} \Bigg|_{t \geq 0} \end{aligned} \tag{3.46}$$

Instead of $f_{\frac{D_a}{d_a} - \frac{D_b}{d_b}}(t)$ the aim is actually to find $f_{\left|\frac{D_a}{d_a} - \frac{D_b}{d_b}\right|}(t)$. This is achieved by mapping the function from the negative domain into the positive domain, with symmetry around the y-axis. The problem is that the above expression is only defined for $t \geq 0$. In terms of

actual measurements performed in a simulation, it only represents values of $\frac{D_a}{d_a} - \frac{D_b}{d_b}$, where $\frac{D_a}{d_a} \geq \frac{D_b}{d_b}$. In order to find values of $\frac{D_a}{d_a} - \frac{D_b}{d_b}$, where $\frac{D_a}{d_a} < \frac{D_b}{d_b}$, one must take $f_{\frac{D_b}{d_b} - \frac{D_a}{D_a}}(t)\Big|_{t \geq 0}$ and plot this into the negative domain. The whole fairness equation therefore becomes:

$$f_{|\frac{D_a}{d_a} - \frac{D_b}{d_b}|}(t) = \left\{ \begin{array}{ll} f_{\frac{D_a}{d_a} - \frac{D_b}{d_b}}(t) & t \geq 0 \\ f_{\frac{D_b}{d_b} - \frac{D_a}{d_a}}(-t) & t < 0 \end{array} \right|_{\text{for every } b} \tag{3.47}$$

This expression makes it possible to perform the mapping of the function from the negative domain onto the function in the positive domain, thereby resulting in

$$f_{|\frac{D_a}{d_a} - \frac{D_b}{d_b}|}(t) = f_{\frac{D_a}{d_a} - \frac{D_b}{d_b}}(t) + f_{\frac{D_b}{d_b} - \frac{D_a}{d_a}}(t)\Big|_{t \geq 0, \text{ for every } b} \tag{3.48}$$

Equation (3.49) represents the complete fairness pdf:

$$\begin{aligned} f_{|\frac{D_a}{d_a} - \frac{D_b}{d_b}|}(t) = \frac{1}{J-1} \sum_{\substack{b=1 \\ n \neq a}}^{J} \Bigg\{ d_a d_b \cdot \sum_{n=1}^{a+b} & \frac{\left(\delta C - (e^\delta - 1)\sum_{j=1}^{h_a(n)} k_j \lambda_j\right) \cdot \left(\delta C - (e^\delta - 1)\sum_{j=1}^{h_b(n)} k_j \lambda_j\right)}{-\delta C(d_a + d_b) + (e^\delta - 1)\left\{\sum_{j=1}^{h_a(n)} k_j \lambda_j d_a + \sum_{j=1}^{h_b(n)} k_j \lambda_j d_b\right\}} \\ \cdot \Bigg(\exp \Bigg[& -\delta C d_a t - \delta C(d_a + d_b)\tau_n + (e^\delta - 1) \Bigg\{ \sum_{j=1}^{h_a(n)} k_j \lambda_j d_a (t + \tau_n) + \sum_{j=h_a(n)+1}^{J} k_j \lambda_j (d_a - d_j) \\ & + \sum_{j=1}^{h_b(n)} k_j \lambda_j d_b \tau_n + \sum_{j=h_b(n)+1}^{J} k_j \lambda_j (d_b - d_j) \Bigg\} \Bigg] \\ - \exp \Bigg[& -\delta C(d_a + d_b)\tau_{n-1}\Big|_{\tau_0=0} + (e^\delta - 1) \Bigg\{ \sum_{j=1}^{h_a(n)} k_j \lambda_j d_a (t + \tau_{n-1})\Big|_{\tau_0=0} + \sum_{j=h_a(n)+1}^{J} k_j \lambda_j (d_a - d_j) \\ & + \sum_{j=1}^{h_b(n)} k_j \lambda_j d_b \tau_{n-1}\Big|_{\tau_0=0} + \sum_{j=h_b(n)+1}^{J} k_j \lambda_j (d_b - d_j) \Bigg\} \Bigg] \\ + \exp \Bigg[& -\delta C d_b t - \delta C(d_b + d_a)\tau_n + (e^\delta - 1) \Bigg\{ \sum_{j=1}^{h_b(n)} k_j \lambda_j d_b (t + \tau_n) + \sum_{j=h_b(n)+1}^{J} k_j \lambda_j (d_b - d_j) \\ & + \sum_{j=1}^{h_a(n)} k_j \lambda_j d_b \tau_n \quad + \sum_{j=h_a(n)+1}^{J} k_j \lambda_j (d_a - d_j) \Bigg\} \Bigg] \\ - \exp \Bigg[& -\delta C(d_b + d_a)\tau_{n-1}\Big|_{\tau_0=0} + (e^\delta - 1) \Bigg\{ \sum_{j=1}^{h_b(n)} k_j \lambda_j d_b (t + \tau_{n-1})\Big|_{\tau_0=0} + \sum_{j=h_b(n)+1}^{J} k_j \lambda_j (d_b - d_j) \\ & + \sum_{j=1}^{h_a(n)} k_j \lambda_j d_a \tau_{n-1}\Big|_{\tau_0=0} + \sum_{j=h_a(n)+1}^{J} k_j \lambda_j (d_a - d_j) \Bigg\} \Bigg] \Bigg) \Bigg\} \Bigg|_{t \geq 0} . \end{aligned} \tag{3.49}$$

In order to find an expression for the stochastic fairness bound of EDF traffic, one could now substitute (3.49) into (3.38), which for the sake of convenience has been represented here

$$\int_{F_a(\delta)}^{\infty} f_{|\frac{D_a}{d_a}-\frac{D_b}{d_b}|}(t)\,dt = \delta. \tag{3.50}$$

The result is a non-linear equation, which is difficult to solve analytically for varying values of δ. On the other hand, it can be solved numerically with relative ease.

3.5 Results

3.5.1 Simulation Model

In order to verify the precision of the derived analytical expressions, a custom-made simulation package using Borland C++ was created. The analytical expressions were evaluated in MATLAB. The parameters used for the simulation model and analytical expressions were conveniently kept the same as in [28] and [14]. The parameters are summarised in Table 3.1.

Table 3.1: System parameters

Type of traffic	d_i (ms)	k_i	λ_i (Mbps)
T0 — Audio	6	200	0.064
T1 — Video conference	10	82	0.5
T2 — Stored video	14	15	3
Link capacity	C = 100Mbps		
Packet size	L = 10Kb		
Buffer Capacity	∞		
Serving Interval	$10\mu s$		

Note that for the deadline violation probability analysis, the number of *Type 1* sources was varied between 74 and 84, which corresponded to a load variation of between 94.8% and 99.8%, respectively. In the case of the delay and fairness distributions the results are limited to the extreme cases of 74 and 82 *Type 1* users, which translates to a load of 94.8%

and 98.8%, respectively.

The simulation was run for 24 hours of network time. As the serving interval is $10\mu s$, this corresponds to 8.64×10^9 scheduling intervals. This is a relatively long simulation time, but is required to produce meaningful error probability results at load conditions of 94.8%.

3.5.2 Comparison of Analytical and Simulation Results

Deadline violation probability

Fig. 3.4 contains the violation probabilities of class 1, 2, and 3 traffic as predicted by the analysis and measured by the simulations. During the numerical evaluation of the analytical expressions, the deadline violation probabilities for all three data types turned out to be exactly the same. Fig. 3.4 demonstrates how the analytical violation probability curves of the three classes therefore lie on top of one another for all loads. This is also the case for the simulation results, which tie up with the analytical results, although only one curve is shown here.

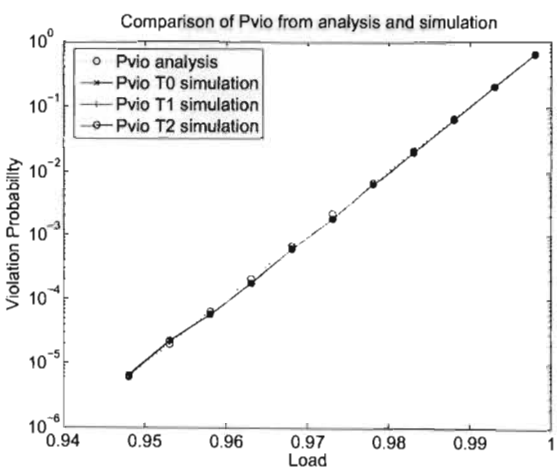

Figure 3.4: Comparison of analytical and simulation results

This result may be somewhat unexpected. It is therefore worth doing a quick verifica-

tion to show why, in the analytical expression, the class of service does not play a role. Remembering that

$$\frac{e^{\delta}-1}{\delta} = \frac{C}{\sum_{j=1}^{J} k_j \lambda_j}, \tag{3.51}$$

and remembering the expression for the violation probability

$$P_{vio}^{i} \approx \exp\left\{-\delta C d_i + (e^{\delta}-1)\sum_{j=1}^{J} k_j \lambda_j (d_i - d_j)\right\}, \tag{3.52}$$

the focus can now be narrowed to the inner portion of the exponential:

$$-\delta C d_i + (e^{\delta}-1)\sum_{j=1}^{J} k_j \lambda_j (d_i - d_j) \tag{3.53}$$

$$\propto \left(-C d_i + \frac{(e^{\delta}-1)}{\delta}\sum_{j=1}^{J} k_j \lambda_j (d_i - d_j)\right) \tag{3.54}$$

$$= -C d_i + \frac{C}{\sum_{j=1}^{J} k_j \lambda_j}\sum_{j=1}^{J}(d_i k_j \lambda_j - d_j k_j \lambda_j) \tag{3.55}$$

$$= -C \cdot \frac{\sum_{j=1}^{J} d_j k_j \lambda_j}{\sum_{j=1}^{J} k_j \lambda_j} \tag{3.56}$$

Therefore

$$P_{vio}^{i} = P_{vio} = \text{Constant with respect to } i. \tag{3.57}$$

This shows that the violation probability is independent of the traffic class i being considered.

It is quite tempting to jump to the conclusion that the EDF scheduler must be perfectly fair, since it ensures that all classes will experience the same deadline violation probability. That this is not the case will become evident from the fairness distribution results, as the three fairness distribution curves do not lie on top of one another.

Delay distributions

Figs. 3.5(a) and 3.5(b) contain the analytical and simulated cumulative distribution functions of the queueing time experienced by traffic classes 0, 1, 2 under a load of 94.8% and

98.8%. In Figs. 3.5(c) and 3.5(d), the probability density functions of the queueing time of traffic classes 0, 1, 2 are portrayed under loads of 94.8% and 98.8% as predicted by the analytical model and simulation runs. In both cases the analytical model follows the simulation results very well.

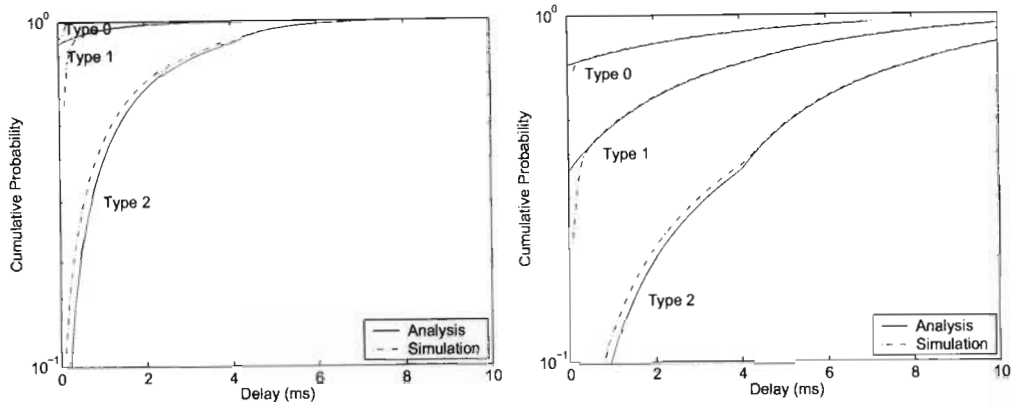

(a) Cumulative Distribution Function under 94.8% load (b) Cumulative Distribution Function under 98.8% load

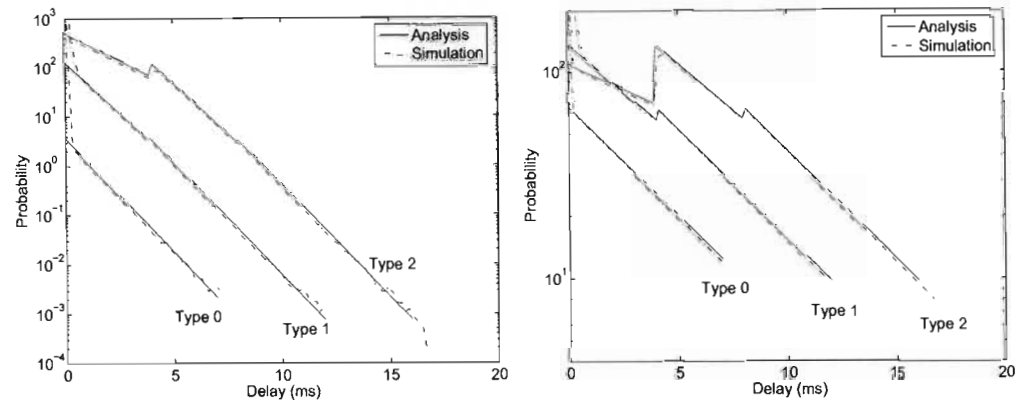

(c) Probability Density Function under 94.8% load (d) Probability Density Function under 98.8% load

Figure 3.5: Distributions of EDF scheduler

The pdf distributions in Figs. 3.5(c) and 3.5(d) show several discontinuities both within the analytical and simulated curves. The mathematical reason for this is the conditional expression

$$T_j = \begin{cases} d_i - d_j & d_i - d_j < t \\ t & d_i - d_j \geq t. \end{cases} \tag{3.58}$$

Within this expression one can clearly see, how the expression for the pdf curve will change as the various $d_i - d_j$ boundaries are transgressed. This matches up to the pdf curves in Figs. 3.5(c) and 3.5(d), which have their discontinuities wherever $t = d_i - d_j$.

From a behavioral point of view, the discontinuities can be explained with the help of

Fig. 3.2 in Section 3.3.2. When a packet p_i enters its queue, packets of a lower traffic class will still be served before packet p_i, up until the boundary condition $d_i - d_j$, at which point packet p_i's priority is higher than any packet p_j that arrived after it. The probability that packet p_i is chosen and transmitted therefore jumps up to a higher level at this specific time. This repeats itself for every $d_j > d_i$.

In both cases the analytical model follows the simulation results very well, except for the area around 0ms where the simulation deviates from the analysis. The reason for this is that the analytical model relies on the large buffer asymptotic, which assumes that the number of sources does not change. In order for the asymptotic to be accurate, all queues have to remain backlogged. When a packet experiences a delay close to 0ms, there is a fairly high probability that at least some of the other queues are empty. The closer the delay is to 0ms, the higher the probability that the queues will be empty and that the analytical model will fail. The analytical model starts tracking the simulation fairly accurately for delay values higher than 1ms.

Fairness results

In Fig. 3.6, the 3 diagrams in the left-hand column contain the pdf distributions of $f_{\frac{D_a}{d_a} - \frac{D_b}{d_b}}(t)$ for the 3 traffic classes. Whereas, the right-hand column in Fig. 3.6, contains the folded pdf distributions of $f_{\left|\frac{D_a}{d_a} - \frac{D_b}{d_b}\right|}(t)$. Finally, Fig. 3.7 contains the stochastic fairness bound distributions for varying values of δ. In other words, Fig. 3.7 shows how the Fairness bound F_a decreases, as the acceptable percentage of violations δ is increased up to 5%.

In the case of all 9 diagrams, there was a slight shift between the analytical curves and the simulated distributions. The reason for this is that the delay pdf distributions deviate from the corresponding simulated distributions for values close to 0. Since the analytical fairness pdf distributions are basically comprised of the convolution of two delay pdf distributions, the error is in each case spread across the entire distribution. The result is that the area underneath the pdf is less than 1. To reduce the discrepancy between the analytical and the simulation results, the expressions were normalised. The result can be seen in Fig. 3.7.

Slight differences still exist, but the simulation and analytical curves track one another very well.

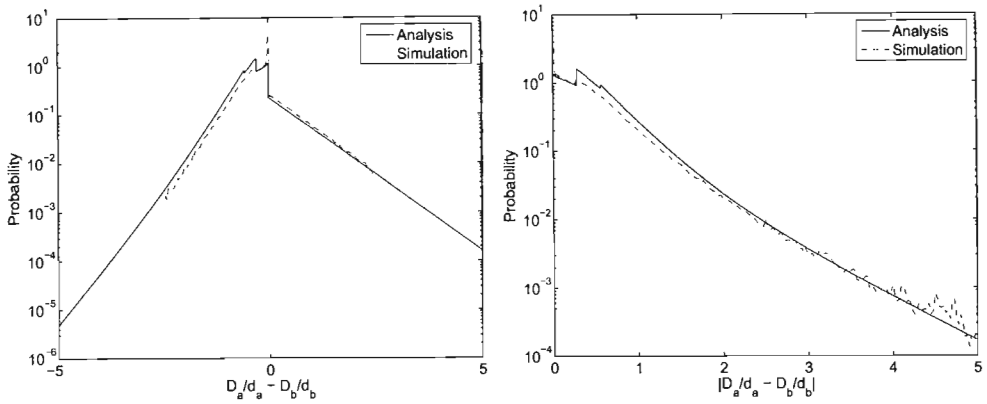

(a) $f_{\frac{D_a}{d_a} - \frac{D_b}{d_b}}(t)$ for Type 0 traffic

(b) $f_{|\frac{D_a}{d_a} - \frac{D_b}{d_b}|}(t)$ for Type 0 traffic

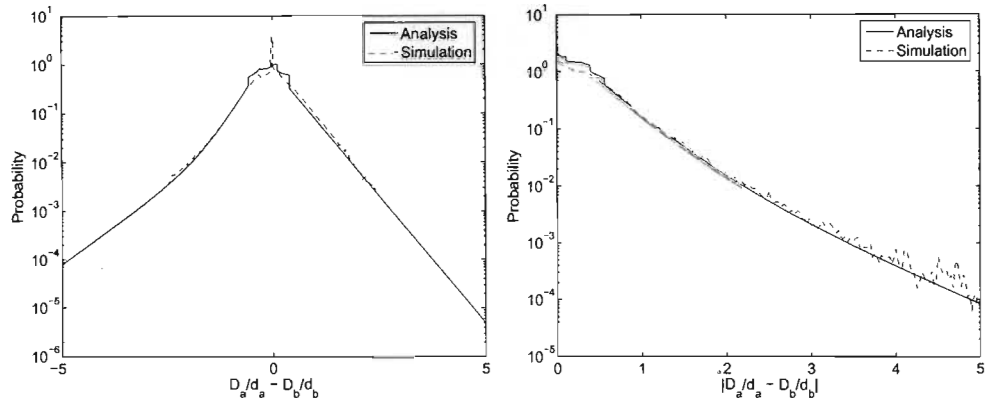

(c) $f_{\frac{D_a}{d_a} - \frac{D_b}{d_b}}(t)$ for Type 1 traffic

(d) $f_{|\frac{D_a}{d_a} - \frac{D_b}{d_b}|}(t)$ for Type 1 traffic

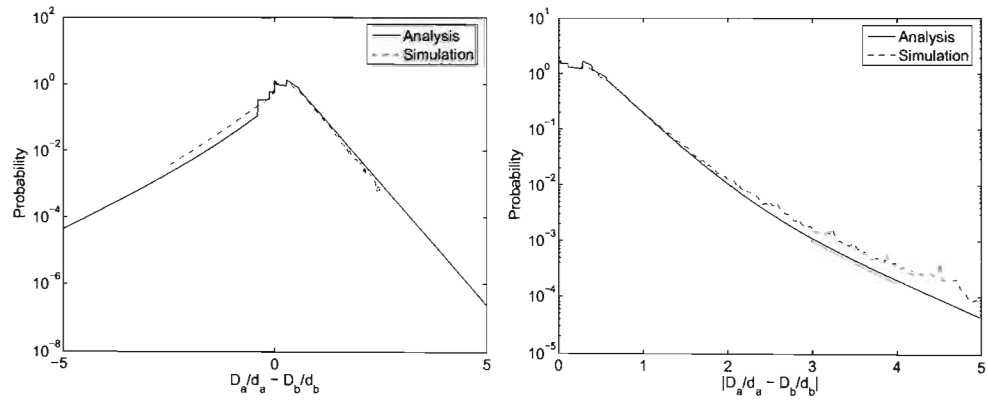

(e) $f_{\frac{D_a}{d_a} - \frac{D_b}{d_b}}(t)$ for Type 2 traffic

(f) $f_{|\frac{D_a}{d_a} - \frac{D_b}{d_b}|}(t)$ for Type 2 traffic

Figure 3.6: Fairness densities and folded counterparts

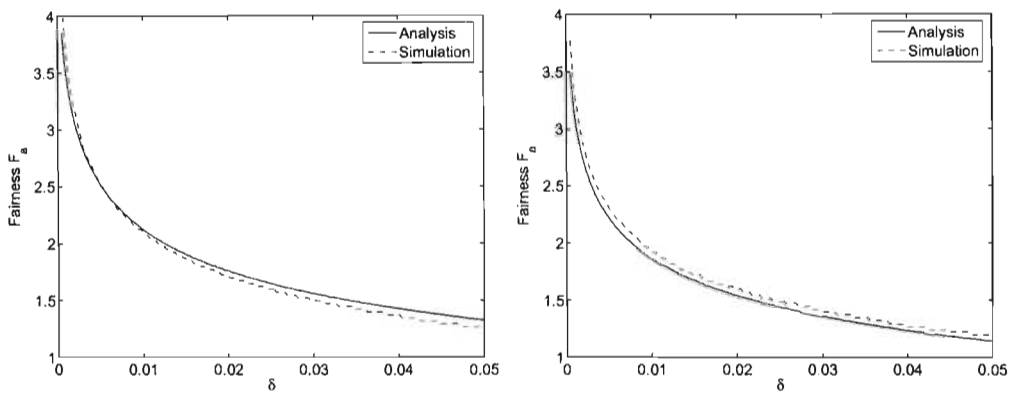

(a) Type 0 statistical fairness distribution

(b) Type 1 statistical fairness distribution

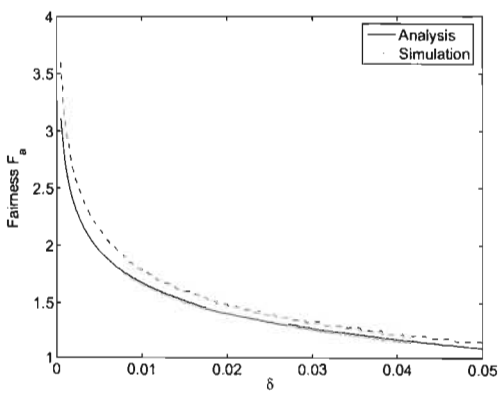

(c) Type 2 statistical fairness distribution

Figure 3.7: Normalised fairness curves

3.6 Conclusion

This chapter derived four approximate analytical expressions that capture the delay and fairness behaviour of real-time traffic classes in an EDF queueing system. The analysis relied on the Effective Bandwidth theory and the Large Buffer asymptotic. It was able to predict the deadline violation probability of individual traffic classes, the CDF and pdf of the queueing time that packets may expect, and the stochastic fairness distributions of the various traffic classes.

The analytical expression follows the delay CDF and pdf generated through simulation very well. As the fairness pdf basically consists of the convolution of two delay pdf distributions, the short-coming of the Large Buffer asymptotic is spread over the entire range of the fairness pdf. The problem can be overcome by normalising the area underneath the fairness pdf to 1.

The expressions of the delay curves that were found in this chapter are very useful to telecommunication operators. Not only do they give a fast way to predict the latency behaviour of heterogeneous traffic scheduled by EDF, but the cumulative distribution function can easily be converted into a risk curve, as follows

$$\text{Risk}_i(t) = 1 - F_i(t). \tag{3.59}$$

The result is that an operator now has a way to predict the risk of exceeding a given latency threshold under various load conditions that he would like to guarantee in a Service Level Agreement contract. Based on delay thresholds that are guaranteed and the risk profile an operator is willing to accept, this expression may furthermore be used to find a threshold that will trigger the requirement for a capacity upgrade.

3.6.1 Future Work

3.6.2 Variable Packet Sizes

The work presented in both Chapters 3 and 4 limits itself to constant packet sizes for the various traffic classes. In future work this will be expanded to variable packet sizes.

3.6.3 ON-OFF Markovian Fluid Sources

In both Chapters 3 and 4, a Poisson source model was used, which is not an accurate representation of multimedia traffic. In [28] in Section 4.2 Sivaraman and Chiussi show how a model with ON-OFF Markovian Fluid Sources could be used instead. Instead of using the effective bandwidth of a Poisson source $\alpha_j(s,t) = \frac{\lambda_j}{s}(e^s - 1)$, the effective bandwidth for an ON-OFF Markovian Fluid Source may be used:

$$\alpha_j(s,t) = \frac{1}{t}\log\left\{\left(\frac{\lambda_j}{\lambda_j+\mu_j}, \frac{\mu_j}{\lambda_j+\mu_j}\right)\exp\begin{pmatrix} -\mu_j t + h_j s t & \mu_j t \\ \lambda_j t & -\lambda_j t \end{pmatrix}\begin{pmatrix} 1 \\ 1 \end{pmatrix}\right\}, \quad (3.60)$$

and $a_j(s) = \lim_{t\to\infty}\alpha_j(s,t)$ is given by

$$\alpha_j(s) = \frac{1}{2}\left(h_j s - \mu_j - \lambda_j + \sqrt{(h_j s - \mu_j + \lambda_j)^2 + 4\lambda_j\mu_j}\right). \quad (3.61)$$

Chapter 4

Opportunistic EDF Analysis

4.1 Introduction

In this chapter, an analytical model is presented of heterogeneous traffic scheduled by an Opportunistic Earliest Deadline First (O-EDF) scheduler. The model is able to predict the cumulative distribution function (CDF) and probability density function (pdf) of the queueing delay that individual classes of service experience. The final expressions for the CDF and pdf are found by graphical curve fitting means, as calculus does not offer a closed-form solution and Gaussian quadrature approximations are not of sufficient accuracy.

4.1.1 Literature review

Numerous papers have appeared that investigate the behaviour of wireless opportunistic schedulers. In [45] the authors propose an analytical model of the EDF scheduler specifically implemented in 802.11. The paper assumes that the scheduler acts on layer 2, where it interacts with the MAC protocol. A Markov chain model is proposed that is able to model the back-off process of EDF. To achieve this, the model assumes that there are always packets to serve, and that the conditions remain stationary. This model is extended to predict the saturation throughput of EDF. The analytical models are validated with a

NS-2 simulation.

Reference [46] finds the throughput gain and delay performance versus SR of a newly proposed Packet Fair Queueing-based Opportunistic Scheduling combination (PFQ-OS), compared to the simple RR and MR-FQ schedulers. For the channel model, a path-loss (Two-Ray Ground Model) and multipath-fading (Rayleigh distribution) channel is used. The PFQ-OS algorithm introduces the concept of a search radius into the framework of PFQ and uses a maximum relative SNR (Max-rSNR) scheduling rule. The resulting algorithm offers a short-term temporal fairness guarantee and improves user throughput.

In [47] a simulation is used to show that opportunistic schedulers are not optimal when frame aggregation is used. The Aggregate Opportunistic Scheduling (AOS) algorithm, which uses frame aggregation to increase MAC efficiency, is compared to Capacity Queue Scheduling (CQS). This combines channel states with queue states and is able to offer a good compromise between throughput and fairness.

In [48] the Access Probability-based Assignment Opportunistic Scheduling (APAOS) algorithm is proposed for wireless networks with Rayleigh channels supporting multimedia services. A statistical model is proposed that mirrors the users' QoS constraints into fixed probabilities of accessing the system. The scheduler is designed to assign users access, based on these probabilities. The proposal is that this can offer high throughput performance, yet is able to satisfy the user's QoS requirements.

Reference [49] uses simulations to compare the performance of three opportunistic schedulers with that of Round Robin in an environment similar to CDMA2000 and WCDMA. A two constraint model is proposed where there is a processor sharing constraint for users in set A and a minimum throughput rate constraint for users in set B. The PS_CEBOS algorithm estimates the processor sharing constraint values for users in set B. The aim is to simplify the two constraint problem with a single processor sharing constraint for all users in the system. The MTR_CEBOS estimates minimum throughput rate constraint values for users in set A to simplify the two-constraint case into a single-constraint case. Finally, CNBOS allocates a slot according to performance values and control parameters to achieve the high system performance and updates the control parameter to guarantee

the constraints.

4.1.2 Overview of Log-normal random variables

In this chapter log-normal random variables play a vital role. Log-normal random variables are widely used among a large number of disciplines. The reason for this is that the Central Limit Theorem [50] states that the re-averaged sum of a sufficiently large number of identically distributed independent random variables each with finite mean and variance will be approximately normally distributed. Because of this characteristic of the Central Limit Theorem, Nature has an abundance of processes, which statistically turn out to be normally distributed.

A log-normal distribution is simply the exponential of a normal random variable. In other words, if a normal random variable is transformed from the log-scale into the linear scale, where the variable only exists in the positive domain, the resultant curve is log-normally distributed. The log and linear scales are both extensively used, but often in different contexts. The result is that various metrics in numerous disciplines have normal and log-normal distributions, depending on the context in which they are used. Some examples of log-normal random variables commonly used in science include [51]:

- Geology and mining (concentration of elements)
- Human medicine (latency periods of diseases, survival times after cancer diagnosis)
- Environmental (rainfall, air pollution)
- Aerobiology (airborne contamination by bacteria and fungi)
- Ecology (species abundance)
- Linguistics (length of spoke words / sentences)
- Social sciences and economics (age of marriage, farm size in England, income)

In the following sections, an attempt was made to generalise the modeling approach. The hope is that the result is an approach that may be useful to many other disciplines and not

just to the field that this thesis belongs to. Dealing with log-normal distributions turned out to be much more complicated than was first envisaged, which is summarised by [52]:

> "The lognormal distribution has become a common choice to represent intrinsically positive and often highly skewed environmental data in statistical analysis. However the implications of its use are often not carefully considered."

4.2 Introduction to O-EDF

Imagine that the various sources in a network produce data packets of J different classes. Examples of such data classes are voice, stored video, video-conference, e-mail, ftp, and http packets. Each of these has different delay, jitter (variation in delay), throughput, bit-error-rate and packet-loss-rate requirements.

Unlike the previous chapter, this chapter considers a mobile environment. Queued up traffic is transmitted through a wireless channel, which depends on the location of the target node and varies with time. To take advantage of any temporary improvements in channel quality, this chapter proposes the use of an Opportunistic Earliest Deadline First (O-EDF) scheduler. As a packet of traffic class i is created, it is assigned a corresponding delay deadline d_i, which represents the amount of time that packets of type i can afford to queue at each switching node they pass through. When packet p_i arrives at a node at some time t, it will be time-stamped with a delay deadline of $t + (\bar{\Psi}_m/\Psi_m)\, d_i$, by when the packet will have to be served according to the O-EDF scheduler.

Factor Ψ_m is the channel gain and is used to weight the deadline d_i in the O-EDF algorithm, to give preference to packets with temporary channel gain improvements. As the channel gain increases, so deadline d_i is artificially decreased, which means that this packet seems to be closer to its deadline (or further past its deadline) than it actually is. Its priority therefore increases. Note that channel gain Ψ_m is modeled to be a log-normal random variable. In the simulation, the time between channel changes was modeled to be exponentially distributed, with a mean of 1ms. $\bar{\Psi}_m$ is its short-term average. By nor-

malising the channel gain indicator by its short-term average, a comparison of channel conditions is made with respect to each channel's average behaviour and not that of other users. This alleviates the near-far problem, where mobile users close to Node B receive exclusive service.

The O-EDF scheduler picks the front-of-queue packet out of all J queues, which has the closest weighted deadline: $\min_j((\bar{\Psi}_m/\Psi_m)\,d_j - D_j)$. Here D_j is the queueing delay that packet p_j has endured.

4.3 Cumulative distribution function of delay

As is illustrated in Fig. 4.1, imagine packet p_i of class i arrives at time $\tau - (\bar{\Psi}_m/\Psi_m)\,d_i$. In order for packet p_i to be served by time $\tau - (\bar{\Psi}_m/\Psi_m)\,d_i + t$, the capacity of the system C will have to be sufficiently large to clear all the packets Q_{Total} that first have to be transmitted:

$$Ct > Q_{Total}. \tag{4.1}$$

The total number of packets Q_{Total} that will be served before packet p_i is given by

$$\begin{aligned} Q_{Total} &= (\text{all packets that arrived before } p_i) \\ &+ (\text{packets that arrived after } p_i, \text{ but will be served before } p_i) \\ &- (\text{packets that arrived before } p_i, \text{ but will be served after } p_i) \qquad (4.2) \\ &= Q(\tau - \frac{\bar{\Psi}_m}{\Psi_m}\,d_i) + \sum_{\substack{j=1 \\ j\neq i}}^{J} A_j(\tau - \frac{\bar{\Psi}_m}{\Psi_m}\,d_i, T^*) \qquad (4.3) \end{aligned}$$

where

$$T^* = \begin{cases} \tau - \frac{\bar{\Psi}_m}{\Psi_m}\,d_i + t, & t < \frac{\bar{\Psi}_m}{\Psi_m}\,d_i - \frac{\bar{\Psi}_k}{\Psi_k}\,d_j \\ \tau - \frac{\bar{\Psi}_k}{\Psi_k}\,d_j, & t \geq \frac{\bar{\Psi}_m}{\Psi_m}\,d_i - \frac{\bar{\Psi}_k}{\Psi_k}\,d_j \end{cases}. \tag{4.4}$$

To understand how this expression was created, a similar approach is used to the one in the previous chapter. Imagine that the packets that are waiting in the queue by time $\tau - (\bar{\Psi}_m/\Psi_m)\,d_i$ are represented by $Q(\tau - (\bar{\Psi}_m/\Psi_m)d_i)$. The total number of packets of

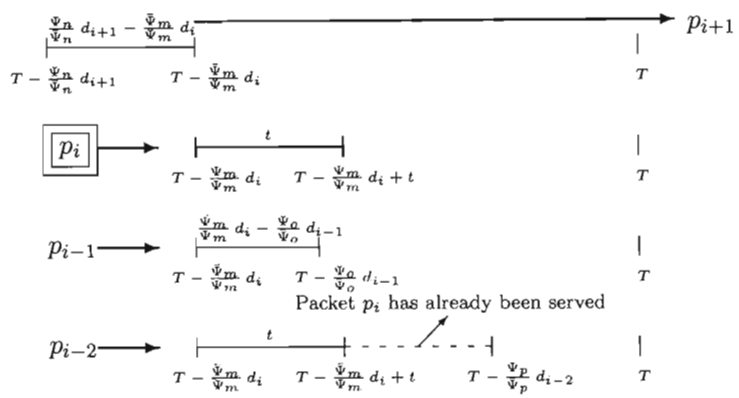

Figure 4.1: Special case: Packet p_i gets served at time $t < \bar{\Psi}_m/\Psi_m\, d_i$.

type $i-1$ that arrive after packet p_i, yet will be served before packet p_i are represented by $A_{i-1}(\tau-(\bar{\Psi}_m/\Psi_m)\, d_i, \tau-(\bar{\Psi}_o/\Psi_o)\, d_{i-1})$. In general, any packet p_j with a smaller weighted delay deadline, that arrives between $(\tau-(\bar{\Psi}_m/\Psi_m)\, d_i)$ and $(\tau-(\bar{\Psi}_k/\Psi_k)\, d_j)$ will be served before packet p_i. Equivalently, any packet p_j with a larger weighted delay deadline, that arrives between $(\tau-(\bar{\Psi}_k/\Psi_k)\, d_j)$ and $(\tau-(\bar{\Psi}_m/\Psi_m)\, d_i)$ will be served after packet $p-i$.

A special case exists for packets of traffic class j if $(t < (\bar{\Psi}_m/\Psi_m)\, d_i - (\bar{\Psi}_k/\Psi_k)\, d_j)$ and the capacity of the system C is sufficiently large to clear all the packets before time $\tau - (\bar{\Psi}_m/\Psi_m)\, d_i + t$. As Fig. 4.1 illustrates, a packet p_i will then be served by time $\tau - (\bar{\Psi}_m/\Psi_m)\, d_i + t$. Only packets that arrive between $\tau-(\bar{\Psi}_m/\Psi_m)\, d_i$ and $\tau-(\bar{\Psi}_m/\Psi_m)\, d_i+t$, and also have a higher priority than packet p_i, therefore need to be added to the queued packets $Q(\tau-(\bar{\Psi}_m/\Psi_m)\, d_i)$. One also needs to subtract from $Q(\tau-(\bar{\Psi}_m/\Psi_m)\, d_i)$ any packets that will be served after packet p_i. These are the same as in the first case discussed.

The probability that the delay D_i experienced by a packet of class i is greater than some period t is then given by

$$\begin{aligned}&\Pr\{D_i > t\}\\ &= \Pr\left\{ Q(\tau - \frac{\bar{\Psi}_m}{\Psi_m} d_i) + \sum_{\substack{j=1\\ j\neq i}}^{J} A_j(\tau - \frac{\bar{\Psi}_m}{\Psi_m} d_i, T^*) > Ct \right\},\end{aligned} \tag{4.5}$$

or rewriting,

$$\begin{aligned}&\Pr\{D_i > t\}\\&= \Pr\Bigg\{ Q(\tau - \frac{\bar{\Psi}_m}{\Psi_m} d_i) > Ct - \sum_{\substack{j=1\\ j\neq i}}^{J} A_j(\tau - \frac{\bar{\Psi}_m}{\Psi_m} d_i, T^*). \end{aligned} \tag{4.6}$$

The Large Buffer asymptotic is once again required:

$$\Pr[Q > q] = e^{-\delta q}, \tag{4.7}$$

where the assumption is that (4.7) still holds when queue length Q varies.

The only unknown in (4.7) is the queue length decay rate δ. To find this, the Effective Bandwidth theory is used together with the fact that $0 < s < \delta$ and the stability limit of the system [36] [38] [28]:

$$\sum_{j=1}^{J} k_j \alpha_j(s) \leq C, \tag{4.8}$$

where $\alpha(s) = \lim_{t\to\infty} \alpha(s,t)$. In equation (4.8), k_j are the number of sources of class j and $\alpha_j(\delta, T_j)$ is the effective bandwidth of class j sources.

For a Poisson source,

$$\alpha_j(s,t) = \alpha_j(s) = \frac{\lambda_j}{s}(e^s - 1). \tag{4.9}$$

If (4.9) is substituted into (4.8), a non-linear expression results, which may be evaluated numerically, to find the desired δ:

$$\frac{e^\delta - 1}{\delta} = \frac{C}{\sum_{j=1}^{J} k_j \lambda_j}. \tag{4.10}$$

Using the Large Buffer asymptotic expressed in (4.7), equation (4.6) may thus be rewritten to give

$$\Pr\{D_i > t\} = \exp\left\{ -\delta Ct + \delta \sum_{\substack{j=1\\ j\neq i}}^{J} A_j(\tau - \frac{\bar{\Psi}_m}{\Psi_m} d_i, T^*) \right\}. \tag{4.11}$$

The Effective Bandwidth theory characterises the arrivals. The Effective Bandwidth theory is thus able to approximate the packets arriving before and after packet p_i. To be

consistent with the rest of the analysis one must look at the extreme case where $s = \delta$, to get

$$\sum_{j=1}^{J} A_j(\tau - \frac{\bar{\Psi}_m}{\Psi_m} d_i, T^*) = \sum_{j=1}^{i-1} T_j k_j \alpha_j(\delta, T_j), \tag{4.12}$$

where

$$T_j = \frac{\bar{\Psi}_m}{\Psi_m} d_i - \frac{\bar{\Psi}_k}{\Psi_k} d_j \leq t. \tag{4.13}$$

The probability that the delay D_i experienced by a packet of class i is greater than some period t is therefore given by

$$\Pr\{D_i > t\} = \exp\left\{ -\delta C t + \delta \sum_{\substack{j=1 \\ j \neq i}}^{J} k_j T_j \alpha_j(\delta, T_j) \right\}. \tag{4.14}$$

For the special case that Poisson sources generate the traffic, (4.9) is substituted into (4.14), which results in

$$\Pr\{D_i > t\} = \exp\left\{ -\delta C t + (e^{\delta} - 1) \sum_{\substack{j=1 \\ j \neq i}}^{J} k_j \lambda_j T_j \right\}. \tag{4.15}$$

4.4 Finding the CDF

To obtain the cumulative distribution function $F_i(t)$, note that

$$\begin{aligned} F_i(t) &= 1 - \Pr\{D_i > t\} \\ &= 1 - \exp\left\{ -\delta C t + (e^{\delta} - 1) \sum_{\substack{j=1 \\ j \neq i}}^{J} k_j \lambda_j T_j \right\}. \end{aligned} \tag{4.16}$$

The problem here is that, unlike the previous chapter, T_j is now a random variable that varies as the channel gain Ψ_m changes.

To find an expression for the CDF, note that random variable T_j is given by

$$T_j = \begin{cases} d_i \frac{\bar{\Psi}_m}{\Psi_m} - d_j \frac{\bar{\Psi}_k}{\Psi_k} & \text{for } d_i \frac{\bar{\Psi}_m}{\Psi_m} - d_j \frac{\bar{\Psi}_k}{\Psi_k} < t, \\ t & \text{for } d_i \frac{\bar{\Psi}_m}{\Psi_m} - d_j \frac{\bar{\Psi}_k}{\Psi_k} \geq t, \end{cases} \tag{4.17}$$

where, the channel pdf in dBW is given by

$$f_{\Psi_m}(y) = \frac{1}{\sigma_m \sqrt{2\pi}} \cdot \exp\left[-\frac{(y - \mu_m)^2}{2{\sigma_m}^2} \right] \qquad \text{(dBW)} \tag{4.18}$$

and, the channel pdf in Watts is given by

$$f_{\Psi_m}(y) = \frac{1}{\sigma_m y \sqrt{2\pi}} \cdot \exp\left[-\frac{(\log_{10} y - \mu_m)^2}{2{\sigma_m}^2} \right] \qquad \text{(W)} \tag{4.19}$$

In the case of this analysis, the pdf in Watts is of importance, which is a log-normal distribution. In order to evaluate this, an expression for T_j must first be derived. Once this is known, the pdf of random variable $F_i(t, T_j)$ can be found, which has the following definition:

$$F_i(t, T_j) = 1 - \exp\left\{ -\delta C t + (e^{\delta} - 1) \sum_{\substack{j=1 \\ j \neq i}}^{J} k_j \lambda_j T_j \right\}. \tag{4.20}$$

Finally, the marginal distribution of $F_i(t, T_j)$, averaged with respect to T_j, is the CDF of O-EDF. This is the expression that this chapter attempts to find.

4.5 Curve fitting T_j

To find an expression that describes the CDF, the pdf of random variable $f_{T_j}(t)$ must first be found. To generalise the problem further, the following expression is used. This is a more generalised expression:

$$Y = a \cdot (X(\mu_1, \sigma_1))^b - c \cdot (X(\mu_2, \sigma_2))^d, \tag{4.21}$$

which can be rewritten using a more convenient syntax:

$$Y = a \cdot X^b(\mu_1, \sigma_1) - c \cdot X^d(\mu_2, \sigma_2). \tag{4.22}$$

To develop this expression mathematically is difficult. The problem here are the two log-normal random variables $X(\mu_1, \sigma_1)$ and $X(\mu_2, \sigma_2)$. As they are independent of one another, it should be possible to use a convolution to find the expression for Y. The problem is that the resultant integral does not have a closed-form solution.

Numerous approaches were attempted to solve this problem. Firstly, the trapezoidal method was used, which turned out to be highly unsuccessful due to the non-linear nature of the log-normal random variables. In [53], the authors show how one may attempt to solve the sum of log-normal variables with a Gauss-Hermite function. Accordingly, attempts were made to solve the problem with a combination of a Gauss-Hermite and Gauss-Laguerre approximation.

The Gauss-Laguerre Quadrature method [54] is a simple approximation for integrals containing exponential factors of the form

$$\int_0^\infty e^{-x} f(x)\, dx \approx \sum_{a=1}^{n} w_a f(x_a). \tag{4.23}$$

The weights w_i are given by

$$w_i = \frac{x_i}{(n+1)^2 [L_{n+1}(x_i)]^2} \tag{4.24}$$

and the Laguerre polynomial $L_n(x)$ of degree n is defined by

$$L_n(x) = \frac{e^x}{n!} \frac{d^n}{dx^n} (e^{-x} x^n) \tag{4.25}$$

The first couple of points of x_i and w_i can be found in Table 4.1. If the degree of the function is very high, various algorithms are available for programs like MATLAB. These are able to generate a much larger set of points than is usually listed in published tables.

The Gauss-Hermite quadrature method [54] is very similar to the Gauss-Laguerre, except that the exponential factor is of the form e^{-x^2} and the integral has different bounds:

$$\int_{-\infty}^\infty e^{-x^2} f(x)\, dx \approx \sum_{a=1}^{n} w_a f(x_a). \tag{4.26}$$

Similarly to the Gauss-Laguerre method, algorithms are available for download which are able to determine the x_i and w_i pairs for the Gauss-Hermite quadrature method.

Table 4.1: Gauss-Laguerre nodes and weights

n	x_i	w_i
2	0.585786	0.853553
	3.41421	0.146447
3	0.415775	0.711093
	2.29428	0.278518
	6.28995	0.0103893
4	0.322548	0.603154
	1.74576	0.357419
	4.53662	0.0388879
	9.39507	0.000539295
5	0.26356	0.521756
	1.4134	0.398667
	3.59643	0.0759424
	7.08581	0.00361176
	12.6408	0.00002337

It was decided that graphical curve-fitting would be the most suitable approach, as the Gauss-quadrature methods were unable to accurately estimate the behaviour of f_{T_j}. In general this approach produces precise results with relative ease.

To develop an approximate expression for the pdf of (4.22), the problem was first broken down into its simplest form. To start off, the aim was to find the pdf of the generalised expression $Y = aX$, where X is a log-normal random variable and a is some constant. More and more complexities were added, until the resulting expression for random variable Y represented the pdf of (4.22). In each case, a suitable expression for the pdf was found by fitting a curve onto simulated results. The validity of the expression was tested by varying the parameters of the resultant curves. A few diagrams of the resultant curve fitted solutions have been represented in this chapter as examples.

The following subsections are a summary of the step-wise development towards (4.22). By keeping the problem as generic as possible, the resultant expressions are a tool set for

dealing with normal and log-normal random variables.

4.5.1 Finding the pdf of $Y = aX(\mu_1, \sigma_1)$

For this scenario, the resulting pdf can be approximated to be

$$f_Y(x) \sim \frac{1}{a} \cdot \text{log-N}\left(\frac{x}{a}, \mu, \sigma\right). \tag{4.27}$$

Here log-N(x, μ, σ) represents a log-normal distribution, where the associated normal distribution has a mean of μ and a standard deviation of σ. Note that this may also be expressed as log-N(μ, σ), if the range does not need to be scaled.

4.5.2 Finding the pdf of $Y = aX^b(\mu_1, \sigma_1)$

For this scenario, the resulting pdf can be approximated to be

$$f_Y(x) \sim \frac{1}{a} \cdot \text{log-N}\left(\frac{x}{a}, b\mu_1, |b|\sigma_1\right). \tag{4.28}$$

4.5.3 Finding the pdf of $Y = X(\mu_1, \sigma_1) - X(\mu_2, \sigma_2)$

In this case, the resulting pdf can be approximated to be

$$f_Y(x) \sim \text{N}\left(x, e^{\mu_1} - e^{\mu_2}, \frac{1}{3} \cdot (\sigma_1 + \sigma_2)(e^{\mu_1} + e^{\mu_2})\right), \tag{4.29}$$

where N(x, μ, σ) represents a normal distribution, with a mean of μ and standard deviation of σ. This may also be expressed as N(μ, σ), if the range does not need to be scaled.

Some example curves for various combinations of μ_1, σ_1 and μ_2, σ_2 can be seen in the first diagram of Fig. 4.2. In each case, the squiggly curve is the one achieved through simulation, while the smooth curve is the normal distribution that was fitted. This is true for all four diagrams in Fig. 4.2.

Note that Cramer's theorem [55] states that if the sum of two random variables results in a normal distribution, then the two random variables must be normally distributed

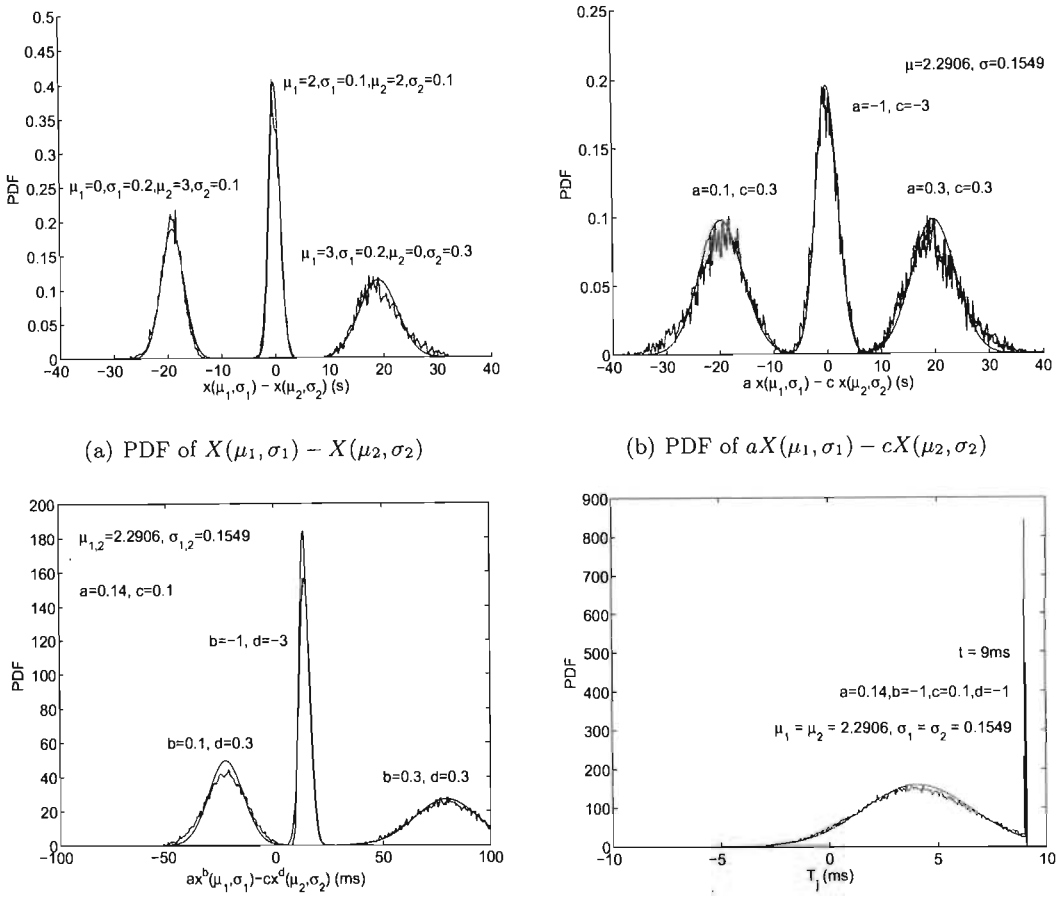

(a) PDF of $X(\mu_1, \sigma_1) - X(\mu_2, \sigma_2)$

(b) PDF of $aX(\mu_1, \sigma_1) - cX(\mu_2, \sigma_2)$

(c) PDF of $aX^b(\mu_1, \sigma_1) - cX^d(\mu_2, \sigma_2)$

(d) PDF of T_j

Figure 4.2: Difference of two log-normal random variables

themselves. Even though this analysis deals with the difference and not the sum of two log-normally distributed random variables, it is important to acknowledge that the resultant curve is not normally distributed. The normal approximation is only an approximation and only accurate if μ_1 and σ_1 are similar to μ_2 and σ_2, respectively. As the difference between the μ or σ values of the two contributing log-normal distributions starts deviating, the skewness of the resultant curve increases, and the normal approximation proposed will deviate further.

4.5.4 Finding the pdf of $Y = aX(\mu_1, \sigma_1) - cX(\mu_2, \sigma_2)$

Here, the resulting pdf can be approximated to be

$$f_Y(x) \sim \mathrm{N}\left(x, ae^{\mu_1} - ce^{\mu_2}, (\sigma_1 + \sigma_2)(e^{\mu_1} + e^{\mu_2}) \cdot \frac{a+c}{6}\right). \tag{4.30}$$

The second diagram presented in Fig. 4.2 contains sample curves for various values of a and c. Once again, the values of a and c may not vary too much, as they will otherwise cause skewness in the resulting curve, which would deviate from the proposed normal distribution.

4.5.5 Finding the pdf of $Y = aX^b(\mu_1, \sigma_1) - cX^d(\mu_2, \sigma_2)$

For this scenario, the resulting pdf can be approximated to be

$$f_Y(x) \sim \mathrm{N}\left[x, (ae^{b\mu_1} - ce^{d\mu_2}), (e^{b\mu_1} + e^{d\mu_2}) \cdot \frac{a+c}{6} \cdot \left(\sigma_1 \cdot \frac{b^2}{|b|} + \sigma_2 \cdot \frac{d^2}{|d|}\right)\right]. \tag{4.31}$$

The third diagram in Fig. 4.2 presents scenarios for varying values of b and d. The skewness problem again needs to be considered as b and d start deviating. Please note though, that the proposed normal distribution fits the actual curve quite well for both positive and negative values of b and d, as long as these are kept fairly similar.

4.5.6 Finding the pdf of $T_j(\Psi_m, \Psi_k, t)$

For this scenario, the resulting pdf can be approximated to be

$$f_{T_j}(x < t) \sim \mathrm{N}\left[x, ae^{b\mu_1} - ce^{d\mu_2}, (e^{b\mu_1} + e^{d\mu_2}) \cdot \frac{a+c}{6} \cdot \left(\sigma_1 \cdot \frac{b^2}{|b|} + \sigma_2 \cdot \frac{d^2}{|d|}\right)\right], \tag{4.32}$$

$$f_{T_j}(x > t) = 0. \tag{4.33}$$

The special case of $f_{T_j}(x = t)$ poses a slight problem, as the rest of the area to the right of t falls on this specific spot. Therefore

$$f_{T_j}(t) = \delta(x - t) \cdot \left[1 - \mathrm{CDF}_N\left(t, ae^{b\mu_1} - ce^{d\mu_2},\right.\right.$$
$$\left.\left.(e^{b\mu_1} + e^{d\mu_2}) \cdot \frac{a+c}{6} \cdot \left(\sigma_1 \cdot \frac{b^2}{|b|} + \sigma_2 \cdot \frac{d^2}{|d|}\right)\right)\right], \tag{4.34}$$

where $\delta(x-t)$ is the Dirac delta function and the $\mathrm{CDF}_N(t)$ is the CDF of the same normal distribution at point t.

The last diagram in Fig. 4.2 presents an example curve, where $t = 9$ms. Note that it is difficult finding the derivative of the simulated values. Instead, a Δt value was used, where Δt is equal to the difference between points plotted on the x-axis. The last diagram in Fig. 4.2 is therefore not totally correct, as the y-value at t should actually spike to infinity. But the principle is still apparent.

At this point it is good to remember that this derivation is actually dealing with the special case

$$a = d_i \cdot \bar{\Psi}_m = d_i \cdot \exp(\mu_1 + \sigma_1^2/2), \tag{4.35}$$
$$b = -1, \tag{4.36}$$
$$c = d_j \cdot \bar{\Psi}_k = d_j \cdot \exp(\mu_2 + \sigma_2^2/2), \tag{4.37}$$
$$d = -1, \tag{4.38}$$

where, in the case of the O-EDF scheduler model

$$\mu_1 = \mu_2 \tag{4.39}$$

and

$$\sigma_1 = \sigma_2. \tag{4.40}$$

Therefore

$$f_{T_j}(x < t) \sim \mathrm{N}\left[x, d_i \cdot \bar{\Psi}_m e^{-\mu} - d_j \cdot \bar{\Psi}_k e^{-\mu}, \frac{4}{6} \cdot e^{-\mu}\sigma \cdot (d_i \cdot \bar{\Psi}_m + d_j \cdot \bar{\Psi}_k)\right], \tag{4.41}$$
$$f_{T_j}(x > t) = 0, \tag{4.42}$$

and

$$f_{T_j}(t) = \delta(x-t) \cdot \left[1 - \mathrm{CDF}_N\left(t, d_i \cdot \bar{\Psi}_m e^{-\mu} - d_j \cdot \bar{\Psi}_k e^{-\mu}, \frac{4}{6} \cdot e^{-\mu}\sigma \cdot (d_i \cdot \bar{\Psi}_m + d_j \cdot \bar{\Psi}_k)\right)\right]. \tag{4.43}$$

The next section carries on with the development of a more generalised model for the CDF of O-EDF using the same constants a, b, c, and d.

4.6 Curve fitting the CDF

In the previous section the pdf of T_j was found. One can use this result to develop an expression for the CDF of O-EDF. To achieve this, note that

$$F_i(t) = 1 - \exp\left\{-\delta C t + (e^{\delta} - 1) \sum_{\substack{j=1 \\ j \neq i}}^{J} k_j \lambda_j T_j\right\}. \tag{4.44}$$

To develop a mathematical expression that describes this CDF, the various T_j are weighted by $k_j\lambda_j$ and then summed.

4.6.1 Finding the pdf of $k_j\lambda_j T_j$

From [56] it is apparent that if $X \sim \mathrm{N}(\mu, \sigma^2)$ is a normal distribution and x_1 and x_2 are real numbers, then

$$x_1 X + x_2 \sim \mathrm{N}\left(x_1\mu + x_2, x_1\sigma\right). \tag{4.45}$$

In the case of the O-EDF model, $x_1 = k_j\lambda_j$ and $x_2 = 0$. Therefore

$$f_{k_j\lambda_j T_j}(x < k_j\lambda_j t) \sim \mathrm{N}(x, k_j\lambda_j\mu_N, k_j\lambda_j\sigma_N), \tag{4.46}$$

$$f_{k_j\lambda_j T_j}(x > k_j\lambda_j t) = 0, \tag{4.47}$$

and

$$f_{k_j\lambda_j T_j}(k_j\lambda_j t) = \delta(x - k_j\lambda_j t) \cdot (1 - \mathrm{CDF}_N(k_j\lambda_j t, k_j\lambda_j\mu_N, k_j\lambda_j\sigma_N)), \tag{4.48}$$

where, for simplicity sake,

$$\mu_N = ae^{b\mu_i} - ce^{d\mu_j} \tag{4.49}$$

and

$$\sigma = (e^{b\mu_i} + e^{d\mu_j}) \cdot \frac{a+c}{6} \cdot \left(\sigma_i \cdot \frac{b^2}{|b|} + \sigma_N \cdot \frac{d^2}{|d|} \right). \tag{4.50}$$

Note, for interest sake, that

$$\begin{aligned} \mathrm{CDF}_N(k_j\lambda_j t) &= \frac{1}{2}\left[1 + \mathrm{erf}\left(\frac{k_j\lambda_j t - k_j\lambda_j\mu_N}{k_j\lambda_j\sigma_N\sqrt{2}}\right)\right] \\ &= \mathrm{CDF}_N(t). \end{aligned} \tag{4.51}$$

The first diagram in Fig. 4.3 contains some example curves that show how the approximation is able to follow the simulated behaviour of $k_0\lambda_0 T_0$, $k_1\lambda_1 T_1$, and $k_2\lambda_2 T_2$.

4.6.2 Finding the pdf of $\sum_{j\neq i}^{J} k_j\lambda_j T_j$

The properties of a normal distribution [57] require that, if $X \sim \mathrm{N}(\mu_X, \sigma_X^2)$ and $Y \sim \mathrm{N}(\mu_Y, \sigma_Y^2)$ are independent normal random variables, then the sum is normally distributed with:

$$U = X + Y \sim \mathrm{N}(\mu_X + \mu_Y, \sigma_X^2 + \sigma_Y^2) \tag{4.52}$$

Note that the variance was used here and not the standard deviation, as was previously done. This is to simplify the resulting expression. If this is used as an initial approximation for the required sum, the result is

$$f_{\sum_{j\neq i} k_j\lambda_j T_j}\left(x < \sum_{j\neq i} k_j\lambda_j t\right) \sim \mathrm{N}\left[\sum_{j\neq i} k_j\lambda_j\mu_N, \sum_{j\neq i} (k_j\lambda_j\sigma_N)^2\right], \tag{4.53}$$

$$f_{\sum_{j\neq i} k_j\lambda_j T_j}\left(x > \sum_{j\neq i} k_j\lambda_j t\right) = 0, \tag{4.54}$$

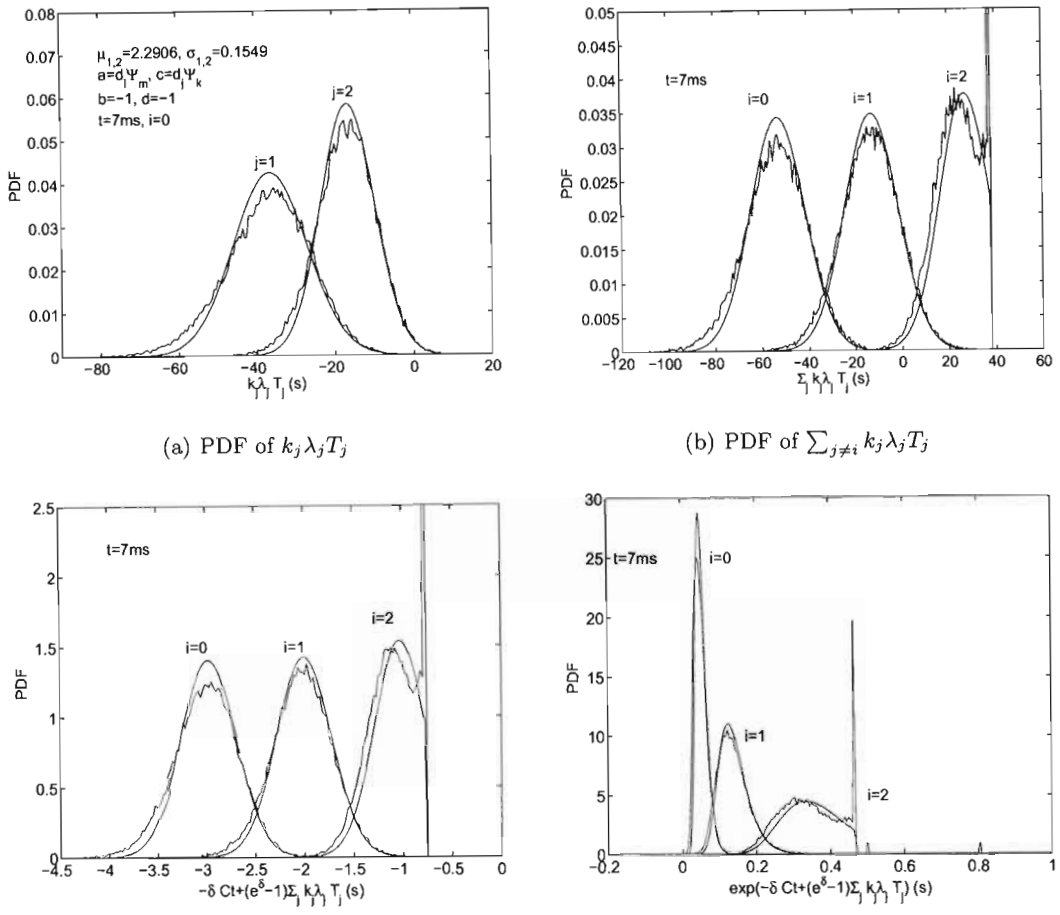

(a) PDF of $k_j\lambda_j T_j$

(b) PDF of $\sum_{j\neq i} k_j\lambda_j T_j$

(c) PDF of X

(d) PDF of $\exp(X)$

Figure 4.3: PDF of $k_j\lambda_j T_j$ and $\sum_{j\neq i} k_j\lambda_j T_j$

and

$$f_{\sum_{j\neq i} k_j\lambda_j T_j}\left(\sum_{j\neq i} k_j\lambda_j t\right)$$
$$= \delta\left(x - \sum_{j\neq i} k_j\lambda_j t\right) \cdot \left[1 - \mathrm{CDF}_N\left(\sum_{j\neq i} k_j\lambda_j t, \sum_{j\neq i} k_j\lambda_j\mu_N, \sum_{j\neq i}(k_j\lambda_j\sigma_N)^2\right)\right], \quad (4.55)$$

Note that in a simulation environment, the values of a, b, c, and d are not constant, but change for different values of i and j. In other words, during the summation $\sum_j k_j\lambda_j T_j$, the values of c and d will change as j changes. This will become more apparent right at the end of this development process, when the values of a, b, c, and d will be replaced.

The second diagram in Fig. 4.3 contains some example curves that show how the approximation is able to follow the simulated behaviour of $\sum_{j\neq i} k_j\lambda_j T_j$, for $i = 0$, $i = 1$ and $i = 2$.

4.6.3 Finding the pdf of $X_i = -\delta Ct + (e^\delta - 1)\sum_{j\neq i}^{J} k_j\lambda_j T_j$

As was already mentioned, from the properties of a normal distribution in [56] it is known that if $X \sim \mathrm{N}(\mu, \sigma^2)$ and x_1 and x_2 are real numbers, then

$$x_1 X + x_2 \sim \mathrm{N}\left(x_1\mu + x_2, (x_1\sigma)^2\right). \tag{4.56}$$

In the case of O-EDF $x_1 = e^\delta - 1$ and $x_2 = -\delta Ct$. Therefore

$$\begin{aligned}
&f_{X_i}\left(x < -\delta Ct + (e^\delta - 1)\sum_{j\neq i} k_j\lambda_j t\right) \\
&\sim \mathrm{N}\Bigg[(e^\delta - 1)\sum_{j\neq i} k_j\lambda_j(ae^{b\mu_i} - ce^{d\mu_j}) - \delta Ct, \\
&(e^\delta - 1)^2 \cdot \sum_{j\neq i}\left(\frac{k_j\lambda_j}{6}\cdot(a+c)\cdot(e^{b\mu_i} + e^{d\mu_j})\cdot\left(\sigma_i\cdot\frac{b^2}{|b|} + \sigma_j\cdot\frac{d^2}{|d|}\right)\right)^2\Bigg], \qquad (4.57) \\
&f_{X_i}\left(x > -\delta Ct + (e^\delta - 1)\sum_{j\neq i} k_j\lambda_j t\right) = 0, \qquad (4.58)
\end{aligned}$$

and

$$\begin{aligned}
&f_{X_i}\left(-\delta Ct + (e^\delta - 1)\sum_{j\neq i} k_j\lambda_j t\right) \\
&= \delta\left(x + \delta Ct - (e^\delta - 1)\sum_{j\neq i} k_j\lambda_j t\right)\cdot\left[1 - \mathrm{CDF}_N\left(-\delta Ct + (e^\delta - 1)\sum_{j\neq i} k_j\lambda_j t\right)\right],
\end{aligned} \tag{4.59}$$

The third diagram in Fig. 4.3 contains some example curves that show how the approximation is able to follow the simulated behaviour of $X_i = -\delta Ct + (e^\delta - 1)\sum_{\substack{j=1\\ j\neq i}}^{J} k_j\lambda_j T_j$, for $i = 0$, $i = 1$ and $i = 2$.

4.6.4 Finding the pdf of $Z_i = \exp\left[-\delta Ct + (e^\delta - 1)\sum_{j\neq i}^{J} k_j\lambda_j T_j\right]$

In the previous section it was shown that $X_i = -\delta Ct + (e^\delta - 1)\sum_{j\neq i}^{J} k_j\lambda_j T_j$ can be reasonably estimated by a normal distribution. In this section it is useful to note that $\exp(X_i)$ must by definition therefore be log-normal. The result is that the previous normal expressions now change to log-normal equivalents.

$$
\begin{aligned}
&f_{Z_i}\left(x < \exp\left[-\delta Ct + (e^\delta - 1)\sum_{j\neq i} k_j\lambda_j t\right]\right) \\
&\sim \text{log-N}\left[(e^\delta - 1)\sum_{j\neq i} k_j\lambda_j(ae^{b\mu_i} - ce^{d\mu_j}) - \delta Ct,\right. \\
&\left.(e^\delta - 1)^2 \cdot \sum_{j\neq i}\left(\frac{k_j\lambda_j}{6}\cdot(a+c)\cdot(e^{b\mu_i} + e^{d\mu_j})\cdot\left(\sigma_i\cdot\frac{b^2}{|b|} + \sigma_j\cdot\frac{d^2}{|d|}\right)\right)^2\right], \qquad (4.60)
\end{aligned}
$$

$$
f_{Z_i}\left(x > \exp\left[-\delta Ct + (e^\delta - 1)\sum_{j\neq i} k_j\lambda_j t\right]\right) = 0, \qquad (4.61)
$$

and

$$
\begin{aligned}
&f_{Z_i}\left(\exp\left[-\delta Ct + (e^\delta - 1)\sum_{j\neq i} k_j\lambda_j t\right]\right) \\
&= \delta\left(x - \exp\left[-\delta Ct + (e^\delta - 1)\sum_{j\neq i} k_j\lambda_j t\right]\right) \\
&\cdot\left[1 - \text{CDF}_{log-N}\left(\exp\left[-\delta Ct + (e^\delta - 1)\sum_{j\neq i} k_j\lambda_j t\right]\right)\right]. \qquad (4.62)
\end{aligned}
$$

where, in this case, reference is made to the CDF of a log-normal distribution. Note also that for both the log-normal pdf log-N and the CDF_{log-N} functions, the mean μ and standard deviation σ values are defined to be those of the equivalent normal distribution. During the conversion from normal to log-normal, these values therefore do not have to be changed.

The last diagram in Fig. 4.3 contains some example curves that show how the approximation is able to follow the simulated behaviour of $Z_i = \exp(-\delta Ct + (e^\delta - 1)\sum_{\substack{j=1\\ j\neq i}}^{J} k_j\lambda_j T_j)$, for $i = 0$, $i = 1$ and $i = 2$.

4.7 Cumulative distribution function of O-EDF

In this section it is finally possible to determine an expression for the cumulative distribution function $F_{D_i}(t)$ for the Opportunistic Earliest Deadline First (O-EDF) scheduler. This can be achieved by realising that

$$F_{D_i}(t) = 1 - \bar{Z}_i(t). \tag{4.63}$$

Here $\bar{Z}_i(t)$ is the marginal distribution of random variable Z_i. To find $\bar{Z}_i(t)$, note that the marginal distribution is defined to be

$$f(a) = \int_b f_{A,B}(a,b)\,db = \int_b f_{A|B}(a|b) f_B(b)\,db. \tag{4.64}$$

In the case of the O-EDF model, the resulting expression is therefore given by

$$\bar{Z}_i(t) = \int_x f_{Z_i|X}(t|x) \cdot f_X(x)\,dx, \tag{4.65}$$

where, quite simply, $f_X(x) = x$. In other words, the marginal distribution effectively requires one to find the mean of $Z_i(t)$ across the values of x at the specified value of t. Therefore

$$\bar{Z}_i(t) = \int_0^z x \cdot \text{log-N}[\mu,\sigma]\,dx + \int_0^\infty x \cdot \delta(x-z) \cdot [1 - \text{CDF}_{log-N}(z,\mu,\sigma)]\,dx, \tag{4.66}$$

where

$$\mu = (e^\delta - 1)\sum_{j\neq i} k_j\lambda_j(ae^{b\mu_i} - ce^{d\mu_j}) - \delta Ct, \tag{4.67}$$

$$\sigma^2 = (e^\delta - 1)^2 \cdot \sum_{j\neq i}\left(\frac{k_j\lambda_j}{6} \cdot (a+c) \cdot (e^{b\mu_i} + e^{d\mu_j}) \cdot \left(\sigma_i \cdot \frac{b^2}{|b|} + \sigma_j \cdot \frac{d^2}{|d|}\right)\right)^2. \tag{4.68}$$

and

$$z = \exp\left[-\delta Ct + (e^\delta - 1)\sum_{j\neq i} k_j\lambda_j t\right]. \tag{4.69}$$

Note that the first term in the expression for $\bar{Z}_i(t)$ is of the form

$$g(k) = \int_k^\infty xf(x)\,dx = \int_{-\infty}^\infty xf(x)\,dx - \int_0^k xf(x)\,dx. \tag{4.70}$$

$g(k)$ is known as the partial expectation of the left truncated density $f(x)$, which for a lognormal density can be shown to be [58]:

$$g(k) = \exp\left(\mu + \frac{\sigma^2}{2}\right) \cdot \Phi\left(\frac{-\ln(k) + \mu + \sigma^2}{\sigma}\right), \tag{4.71}$$

where Φ is the CDF of the standard normal, in other words with a mean of 0 and standard deviation of 1. Now, in the case of a Gaussian distribution, it is known that

$$\int_{-\infty}^{\infty} x f(x)\, dx = \exp\left(\mu + \frac{\sigma^2}{2}\right), \tag{4.72}$$

which is simply the mean of the log-normal function. Therefore

$$\int_{0}^{k} x f(x)\, dx = \exp\left(\mu + \frac{\sigma^2}{2}\right) - \exp\left(\mu + \frac{\sigma^2}{2}\right) \cdot \Phi\left(\frac{-\ln(k) + \mu + \sigma^2}{\sigma}\right) \tag{4.73}$$

$$= \exp\left(\mu + \frac{\sigma^2}{2}\right) \cdot \left[1 - \Phi\left(\frac{-\ln(k) + \mu + \sigma^2}{\sigma}\right)\right] \tag{4.74}$$

To work out the second term, containing the delta function, note that the following may be true, depending on the function $f(x)$ [59]:

$$\int_{-\infty}^{\infty} f(x)\delta(x - a)\, dx = f(a) \tag{4.75}$$

Therefore, one can try

$$\int_{-\infty}^{\infty} x \cdot \delta(x - z) \cdot [1 - \mathrm{CDF}_{log-N}(z, \mu, \sigma)]\, dx$$

$$= z \cdot [1 - \mathrm{CDF}_{log-N}(z, \mu, \sigma)]. \tag{4.76}$$

One can thus conclude that the Cumulative Distribution Function of the delay of traffic scheduled by O-EDF is given by

$$F_{D_i}(t) = 1 - \bar{Z}_i(t)$$

$$= 1 - \exp\left(\mu + \frac{\sigma^2}{2}\right) \cdot \left[1 - \Phi\left(\frac{-\ln(z) + \mu + \sigma^2}{\sigma}\right)\right] + z \cdot [1 - \mathrm{CDF}_{log-N}(z, \mu, \sigma)]. \tag{4.77}$$

And since,

$$a = d_i \cdot \bar{\Psi}_m = d_i \cdot \exp(\mu_i + \sigma_i^2/2), \tag{4.78}$$

$$b = -1, \tag{4.79}$$

$$c = d_j \cdot \bar{\Psi}_k = d_j \cdot \exp(\mu_j + \sigma_j^2/2), \tag{4.80}$$

$$d = -1, \tag{4.81}$$

where

$$\mu_i = \mu_j \tag{4.82}$$

and

$$\sigma_i = \sigma_j, \tag{4.83}$$

therefore

$$\mu = (e^{\delta} - 1) \sum_{j \neq i} k_j \lambda_j (d_i \cdot \bar{\Psi}_m e^{-\mu_i} - d_j \cdot \bar{\Psi}_k e^{-\mu_j}) - \delta C t, \tag{4.84}$$

$$\sigma^2 = (e^{\delta} - 1)^2 \cdot \sum_{j \neq i} \left(\frac{k_j \lambda_j}{6} \cdot (d_i \cdot \bar{\Psi}_m + d_j \cdot \bar{\Psi}_k) \cdot (e^{-\mu_i} + e^{-\mu_j}) \cdot (\sigma_i + \sigma_j) \right)^2. \tag{4.85}$$

4.8 Probability density function of O-EDF

The pdf of a random variable is simply the derivative of its CDF. But in the case of O-EDF in the previous section it was shown that the CDF of O-EDF can be suitably approximated by

$$F_{D_i}(t) = 1 - \exp\left(\mu + \frac{\sigma^2}{2}\right) \cdot \left[1 - \Phi\left(\frac{-\ln(z) + \mu + \sigma^2}{\sigma}\right)\right]$$
$$+ z \cdot [1 - \mathrm{CDF}_{log-N}(z, \mu, \sigma)]. \tag{4.86}$$

Here, as in the previous section,

$$\mu = (e^{\delta} - 1) \sum_{j \neq i} k_j \lambda_j (d_i \cdot \bar{\Psi}_m e^{-\mu_i} - d_j \cdot \bar{\Psi}_k e^{-\mu_j}) - \delta C t, \tag{4.87}$$

$$\sigma^2 = (e^{\delta} - 1)^2 \cdot \sum_{j \neq i} \left(\frac{k_j \lambda_j}{6} \cdot (d_i \cdot \bar{\Psi}_m + d_j \cdot \bar{\Psi}_k) \cdot (e^{-\mu_i} + e^{-\mu_j}) \cdot (\sigma_i + \sigma_j) \right)^2, \tag{4.88}$$

$$z = \exp \left[-\delta C t + (e^{\delta} - 1) \sum_{j \neq i} k_j \lambda_j t \right]. \tag{4.89}$$

The pdf is then given by

$$f_{D_i}(t) = \frac{d}{dt} F_{D_i}(t). \tag{4.90}$$

Now,

$$\mathrm{CDF}_{log-N}(z, \mu, \sigma) = \frac{1}{2} + \frac{1}{2} \mathrm{erf} \left[\frac{\ln(z) - \mu}{\sigma \sqrt{2}} \right]. \tag{4.91}$$

Here it is useful to know that

$$\frac{d}{dx} \mathrm{erf}(x) = \frac{2}{\sqrt{\pi}} e^{-x^2} \tag{4.92}$$

Therefore

$$\frac{d}{dt} \mathrm{CDF}_{log-N}(z, \mu, \sigma) = \frac{d}{dt} \cdot \left(\frac{1}{2} + \frac{1}{2} \mathrm{erf} \left[\frac{\ln(z) - \mu}{\sigma \sqrt{2}} \right] \right) \tag{4.93}$$

$$= \frac{1}{2} \frac{d}{dt} \left(\frac{2}{\sqrt{\pi}} \cdot \int_0^{(\ln(z) - \mu)/\sigma\sqrt{2}} e^{-x^2} \, dx \right) \tag{4.94}$$

$$= \frac{1}{\sqrt{\pi}} \cdot \exp \left[- \left(\frac{\ln(z) - \mu}{\sigma \sqrt{2}} \right)^2 \right] \cdot \left(\frac{1}{z \sigma \sqrt{2}} - \frac{1}{\sigma \sqrt{2}} \cdot \frac{d\mu}{dt} \right) \cdot \frac{dz}{dt} \tag{4.95}$$

$$= \frac{1}{\sigma \sqrt{2\pi}} \cdot \exp \left[- \left(\frac{\ln(z) - \mu}{\sigma \sqrt{2}} \right)^2 \right] \cdot \left(\frac{1}{z} - \frac{d\mu}{dt} \right) \cdot \frac{dz}{dt} \tag{4.96}$$

where

$$\frac{dz}{dt} = \left[-\delta C + (e^{\delta} - 1) \sum_{j \neq i} k_j \lambda_j \right] \cdot \exp \left[-\delta C t + (e^{\delta} - 1) \sum_{j \neq i} k_j \lambda_j t \right], \tag{4.97}$$

$$\frac{d\mu}{dt} = -\delta C, \tag{4.98}$$

and

$$\frac{d\sigma}{dt} = 0. \tag{4.99}$$

Similarly,

$$\mathrm{CDF}_N(x, \mu, \sigma) = \frac{1}{2} + \frac{1}{2}\mathrm{erf}\left(\frac{x-\mu}{\sigma\sqrt{2}}\right), \tag{4.100}$$

therefore,

$$\Phi\left(\frac{-\ln(z)+\mu+\sigma^2}{\sigma}, 0, 1\right) = \frac{1}{2} + \frac{1}{2}\mathrm{erf}\left(\frac{-\ln(z)+\mu+\sigma^2}{\sigma\sqrt{2}}\right) \tag{4.101}$$

Remembering once again that

$$\frac{d}{dx}\mathrm{erf}(x) = \frac{2}{\sqrt{\pi}}e^{-x^2}, \tag{4.102}$$

one can solve this as follows

$$\frac{d}{dt}\Phi\left(\frac{-\ln(z)+\mu+\sigma^2}{\sigma}\right) = \frac{1}{2}\cdot\frac{d}{dt}\mathrm{erf}\left[\frac{-\ln(z)+\mu+\sigma^2}{\sigma\sqrt{2}}\right] \tag{4.103}$$

$$= \frac{1}{\sqrt{\pi}}\exp\left[-\left(\frac{-\ln(z)+\mu+\sigma^2}{\sigma\sqrt{2}}\right)^2\right]\cdot\left(\frac{-1}{z\sigma\sqrt{2}} + \frac{1}{\sigma\sqrt{2}}\cdot\frac{d\mu}{dt}\right)\cdot\left(-\frac{dz}{dt}\right) \tag{4.104}$$

$$= -\frac{1}{\sigma\sqrt{2\pi}}\cdot\exp\left[-\left(\frac{-\ln(z)+\mu+\sigma^2}{\sigma\sqrt{2}}\right)^2\right]\cdot\left(\frac{-1}{z} + \frac{d\mu}{dt}\right)\cdot\frac{dz}{dt} \tag{4.105}$$

Therefore, the probability density function of the delay of traffic scheduled by O-EDF is given by

$$\begin{aligned} f_{D_i}(t) = &-\exp\left(\mu+\frac{\sigma^2}{2}\right)\cdot\frac{d\mu}{dt} + \exp\left(\mu+\frac{\sigma^2}{2}\right)\cdot\frac{d\mu}{dt}\cdot\Phi\left(\frac{-\ln(z)+\mu+\sigma^2}{\sigma}\right) \\ &+ \exp\left(\mu+\frac{\sigma^2}{2}\right)\cdot\frac{d}{dt}\Phi\left(\frac{-\ln(z)+\mu+\sigma^2}{\sigma}\right) \\ &+ \frac{dz}{dt}\cdot[1-\mathrm{CDF}_{log-N}(z,\mu,\sigma)] - z\cdot\frac{d}{dt}\mathrm{CDF}_{log-N}(z,\mu,\sigma). \end{aligned} \tag{4.106}$$

4.9 Results

4.9.1 Simulation Model

In order to verify the precision of the derived analytical expressions, a custom-made simulation package using Borland C++ was created. The analytical expressions were evalu-

ated in MATLAB. The parameters used for the simulation model and analytical expressions were conveniently kept similar to those in [28]. The parameters are summarised in Table 4.2.

In this chapter a channel model was added. As mentioned in the analytical model, a channel gain indicator Ψ was used, which for all channels was chosen to be identically log-normally distributed. For channel m the probability distribution of the channel gain is given by

$$f_{\Psi_m}(y) = \frac{1}{\sigma_m\sqrt{2\pi}} \cdot \exp\left[-\frac{(y-\mu_m)^2}{2{\sigma_m}^2}\right] \quad \text{(dBW)}, \tag{4.107}$$

where all $\mu = 0.1549$ and $\sigma = 2.2906$.

Table 4.2: System parameters

Type of traffic	d_i (ms)	k_i	λ_i (Mbps)
T0 — Audio	6	200	0.064
T1 — Video conference	10	82	0.5
T2 — Stored video	14	15	3
Link capacity	$C = 100$Mbps		
Packet size	$L = 10$Kb		
Buffer Capacity	∞		
Serving Interval	$10\mu s$		
Mean value of channel gain	$\mu = 0.1549$		
Standard deviation of channel gain	$\sigma = 2.2906$		

In the simulation, an attempt was made to estimate the average channel gain value $\bar{\Psi}_m$ of each channel m as an actual router may do, by recording the last 100 channel gain values and averaging across them.

In total 20 different channels were created. The target channel that packets were destined to be transmitted through were chosen, according to a flat random distribution. The time durations $t_{channel}$ between individual channel changes were exponentially distributed, with an average duration of $\bar{t}_{channel} = 1ms$.

Note that for the deadline violation probability analysis, the number of *Type 1* sources

was varied between 74 and 84, which corresponded to a load variation of between 94.8% and 99.8%, respectively. In the case of the delay and fairness distributions, the users were limited to 74 and 82 *Type 1* users, which translates to a load of 94.8% and 98.8%, respectively.

The simulation was run for 24 hours of network time. As the serving interval is $10\mu s$, this corresponds to 8.64×10^9 scheduling intervals. This is a relatively long simulation time, but is required to produce meaningful error probability results at load conditions of 94.8%.

4.9.2 Comparison of Analytical and Simulation Results

The results in Fig. 4.4 indicate that the analytical CDF curves fit the simulated curves very closely, for both 94.8% and 98.8% loads.

For a 98.8% load, the predicted pdf values track the simulated values for large delay values. For small delay values, the analytical model deviates and is unable to capture the subtleties of the simulation. The deviation is especially apparent for Type 2 traffic. The reason for the deviation is that the analytical pdf curve is a derivative of the CDF curve. Even minor deviations of the analytical CDF curve from the simulated values are greatly amplified as the slope of the analytical CDF curve varies from the simulation. This is the unfortunate disadvantage of using curve fitting techniques. Even minor deviations of the approximations, which may have seemed negligible are greatly amplified once the derivative is applied to derive the pdf curve.

In the case of the 94.8% load, a further scaling factor separates the analytical model from the simulation. The reason for this difference is that the simulation has a heavy tail for delay values approaching 0. As the total area under the pdf must equal 1, the rest of the simulated pdf curve lies lower than the analytical curve.

Although discrepancies exist between the analysis and the simulation, the analytical model still remains a good approximation of the delay behaviour that can be expected for various classes of traffic scheduled by O-EDF.

Note that the resulting curves presented here are very similar to those presented in Chapter 3, except that the discontinuities that were present on the Chapter 3 pdf curves have been smeared out. This is to be expected, as the channel gain variables Ψ_m and Ψ_k effectively vary the deadline d_i, thereby varying the hand-over points, which cause the discontinuities.

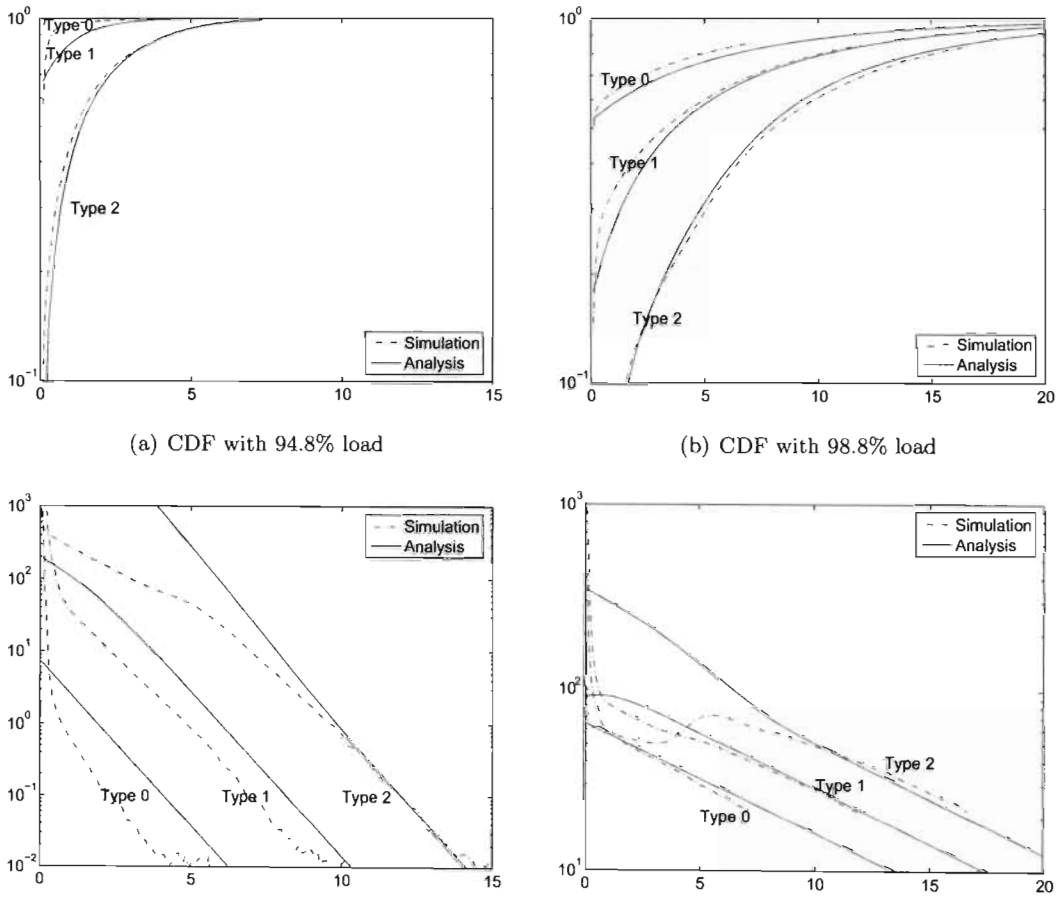

(a) CDF with 94.8% load

(b) CDF with 98.8% load

(c) pdf with 94.8% load

(d) pdf with 98.8% load

Figure 4.4: Delay behaviour of O-EDF scheduler

4.10 Conclusion

In this chapter, an attempt was made to develop an analytical model of the delay experienced by Voice, Video and Web traffic scheduled by an Opportunistic Earliest Deadline

First (O-EDF) scheduler. Log-normally distributed channel quality indicators were assumed for the various wireless channels.

During the development of the mathematical expressions of the Cumulative Distribution Functions (CDFs) and the probability density functions (pdfs), integrals with no closed-form solution were encountered. Various attempts were made to find quadrature approximations. Graphical curve fitting techniques resulted in expressions that were able to match the simulated queueing delay closely. The model is therefore able to predict the delay behaviour of O-EDF.

Chapter 5

Conclusion

Corporate virtual private networks (VPNs) require strict QoS adherence, as these companies not only rely on web access and electronic mail, but on their VPNs to enable business critical data exchange between branches and the head-office. In more recent times, these companies now also rely on IP telephony and even video conferencing facilities to reduce telephone costs and decrease traveling. One of the most important components employed to achieve QoS in VPNs are advanced schedulers. At present, even top-end routers will offer at most a hierarchical combination of deficit round-robin and priority schedulers. To achieve the latency requirements of delay-sensitive traffic, a combination of random dropping algorithms and traffic policers are used to limit the queue lengths. Although these methods will always be required as a last resort, the reliance on them can be decreased if delay-sensitive schedulers are used, as is proved in this thesis.

In recent years, advanced wireless and mobile standards, such as WiFi and HSDPA, have been developed, which have proved to be attractive technical solutions for the so-called last mile, the network component that interconnects the customer with the operator's core network. Fixed last-mile infrastructure requires massive capital investments. Furthermore, the fixed-line infrastructure is difficult to relocate, and therefore requires careful planning, with very limited subsequent freedom of movement. Reliable wireless and mobile infrastructure in the last mile has become a hot topic among researchers, as telecommunications

operators around the world are making large investments into their wireless and mobile infrastructure.

5.1 Thesis Summary

The introductory chapter gives a brief overview of Virtual Private Networks and explains the need for Quality of Service. An overview of the evolution of the wireless network is given, which is an attractive replacement for the expensive last mile. A motivation for the research that was conducted and an overview of this thesis are given. Finally, the original contributions in this thesis are listed.

Chapter 2 presents the behaviour of three traffic classes scheduled by a variety of schedulers across an HSDPA air interface. A custom-built C++ simulator was used to measure the average delay, the amount of traffic that exceeded its deadline, and the percentage traffic corrupted during the down-stream data transmission from a base-station to mobile units in its cell. The units were geographically scattered across the cell and were able to move around within a 500m radius. Based on the load that the network was placed under, a maximum of 20 mobile units were able to request voice, video, and web traffic via the base-station.

The video traffic was modeled to have constant-sized packets, which were generated by ten On-Off Markov sources, each one generating traffic at a constant rate. Similarly, voice traffic was generated by a single Markov source. On the other hand, web traffic was modeled to have information request and reading periods, the durations of which were geometrically distributed. During the reading periods, no traffic was generated, while during the request period packets with Pareto distributed packet lengths were produced, where the inter-arrival times of these packets were geometrically distributed. The transmission channel was modeled to be distance dependent and have a slow-fading log-normally distributed shadowing component. The transmission rate was varied, based on the various modulation and coding schemes that HSDPA uses in an effort to reduce bit-error rates, as the fading of the channel varies over time.

Out of the five schedulers considered, EDF was the only one that attempted to adjust the queueing delay of each class of service according to its respective imposed deadline. O-EDF, Round Robin, Max C/I and PF-T all achieved higher average transmission rates than EDF, as their scheduling rules do not require them to distribute as large a proportion of the available resources to video traffic. Video traffic has very long packets, which requires slower transmission rates to avoid packet corruption. Under similar simulation conditions, the results presented in this chapter were comparable to those published in the referenced papers.

In Chapter 3, Large Deviation principles and the Effective Bandwidth Theory were used to model the delay and fairness distributions of Earliest Deadline First. This model was based on a simple Deadline Violation analysis performed in [28]. This analysis was enhanced to be class-of-service aware. It was then further extended to predict the delay cumulative distribution functions and the delay probability density functions that various classes of traffic with different delay deadlines can expect. A definition for the fairness of delay-sensitive schedulers was proposed. The analytical model was extended to predict the fairness distribution, according to the fairness definition. The limitation of the proposed models is that Poisson traffic sources are assumed. Enough information was given though, to show how more realistic traffic distributions could be used instead. The problem with such distributions is that none of them capture the behaviour of real packet-switched traffic, which seems to have a self-similar fractal nature. Furthermore, the resulting mathematical models are difficult to deal with. As an example, consider [28], which contains an Appendix that develops the violation probability of traffic generated by On-Off Markovian fluid sources. In all cases, the predicted curves were very similar to those found by means of the Monte Carlo simulations. They clearly showed the discontinuities that occur at the priority boundaries on the pdf curves.

Chapter 4 extended the analytical model proposed in Chapter 3 into a wireless scenario. The scheduling rule of the EDF algorithm was changed to take channel conditions into consideration. This was achieved by weighting the delay deadline of each front-of-line packet in each queue, by the current propagation gain of the channel that this packet is transmitted through. The same modeling parameters were used as in Chapter 3. The

newly introduced wireless channels were assumed to have propagation gains that are log-normally distributed. The complexity of the resulting expressions does not offer a closed-form solution. Even mathematical approximations were difficult to find, due to the non-linear nature of the expressions involved. Instead graphical curve fitting techniques were used to present a generalised approach of dealing with log-normal expressions. These commonly appear in various disciplines, ranging from Biology and Meteorology, to the financial sector. The resulting expressions may therefore be useful to a large research community.

The resulting queueing delay CDF curves were very similar to those predicted by the Monte Carlo simulation. Slight differences between the analytical and simulated curves were amplified when they were converted to pdfs by means of differentiation. Thus, the resulting pdf curves did not track their simulated counterparts as well as in Chapter 3. However, the resulting curves are a good approximation of the expected queueing delay.

5.2 Future Directions

The following are potential research projects that could build on the work presented in this thesis:

- An attempt could be made to include spatial correlation in Chapter 2, to make the simulation model even more realistic.
- The analytical methodologies presented in Chapters 3 and 4 could be used to model the queueing delay of traffic scheduled by Largest Weighted Delay First (LWDF) and possibly Modified-Largest Weighted Delay First (M-LWDF).
- An attempt could be made to incorporate variable packet lengths into the analyses presented in Chapters 3 and 4.
- The analyses of Chapters 3 and 4 could be enhanced by replacing the Poisson traffic source model with the ON-OFF Markovian Fluid Source model.

- Further attempts could be made to solve the analytical expression in Chapter 4 and avoid using the curve fitting technique.

Bibliography

[1] R. Gallaher, "An introduction to MPLS." URL = www.convergedigest.com/Bandwidth/archive/010910TUTORIAL-rgallaher1.htm, September 10, 2001.

[2] J. Schutte, "Technical service component — clear quality of service (ClearQoS)," *Internal Documentation of Telkom South Africa*, 2008.

[3] C.-K. Toh, *Wireless ATM and ad-hoc networks.* Kluwer Academic Publishers, ISBN 0-7923-9822-X, 1997.

[4] H. Holma and A. Toskala, *WCDMA for UMTS, second edition.* Jon Wiley and Sons Ltd, ISBN 0-407-84467-1, 2002.

[5] A. Parekh and R. Gallager, "A generalized processor sharing approach to flow control in integrated services networks: the single-node case," *IEEE/ACM Transactions on Networking*, vol. 1, no. 3, pp. 344–357, 1993.

[6] ETSI, "UMTS UTRA high speed downlink packet access (HSDPA) — overall description: Stage 2," Tech. Rep. V5.7.0 Release 5, ETSI TS 125 308 (3GPP TS 25.308), 2004-12.

[7] A. Haider and R. Harris, "A novel proportional scheduling algorithm for HSDPA in UMTS networks," in *The 2nd International Conference on Wireless Broadband and Ultra Wideband Communications* (I. C. Society, ed.), 2007.

[8] F. D. Angelis, I. Habib, G. Giambene, and S. Giannetti, "Scheduling for differentiated traffic types in HSDPA cellular systems," in *IEEE Globecom '05*, 2005.

[9] Wikipedia, "High-speed downlink packet access." URL: *en.wikipedia.org/wiki/Hsdpa.*

[10] Y. seok Kim, "An efficient scheduling scheme for HSDPA system in mixed traffic environments," *Communications Letters, IEEE*, vol. 12, no. 9, pp. 624–626, September 2008.

[11] R. Kwan, M. Aydin, C. Leung, and J. Zhang, "Multiuser scheduling in HSDPA using simulated annealing," in *Wireless Communications and Mobile Computing Conference, 2008. IWCMC 08 International*, pp. 236–241, 6–8 Aug. 2008.

[12] A. Farrokh, F. Blomer, and V. Krishnamurthy, "A comparison of opportunistic scheduling algorithms for streaming media in high-speed downlink packet access (HSDPA)," in *Proc. of MIPS 2004, Grenoble, France*, November 16–19, 2004.

[13] A. Harada, S. Abeta, and M. Sawahashi, "Adaptive radio parameter control considering QoS for forward link OFCDM wireless access," in *IEEE VTC*, pp. 1175–1179, 2002.

[14] S. M. Scriba and F. Takawira, "Packet violation probability analysis of the earliest deadline first scheduler," *South African Telecommunication Networks and Applications Conference 2004 (SATNAC2004)*, September 2004.

[15] C. W. Helstrom, *Probability and stochastic processes for engineers.* Macmillan Publishing Company, 1 ed., 1984.

[16] A. Elwalid and D. Mitra, "Design of generalized processor sharing schedulers which statistically multiplex heterogeneous QoS classes," in *INFOCOM (3)*, pp. 1220–1230, 1999.

[17] K. Kumaran, G. Margrave, D. Mitra, and K. Stanley, "Novel techniques for the design and control of generalized processor sharing schedulers for multiple QoS classes," *Proceedings of IEEE INFOCOM 2000*, 2000.

[18] O. Yaron and M. Sidi, "Generalized processor sharing networks with exponentially bounded burstiness arrivals," in *INFOCOM (2)*, pp. 628–634, 1994.

[19] Z.-L. Zhang, D. F. Towsley, and J. F. Kurose, "Statistical analysis of generalized processor sharing scheduling discipline," *IEEE Journal on Selected Areas in Communications*, vol. 13, no. 6, pp. 1071–1080, 1995.

[20] P. Barta, F. Nehmeth, R. Szabo, and J. Biro, "An approach for traffic characterization in generalized processor sharing networks," *IEEE International Conference on Communications 2001*, vol. 2, pp. 625–629, June 2001.

[21] S. Golestani, "A self-clocked fair queueing scheme for broadband applications," *Proceedings of INFOCOM '94*, pp. 636–646, 1994.

[22] S. J. Golestani, "Network delay analysis of a class of fair queueing algorithms," *IEEE Journal on Selected Areas in Communications*, vol. 13, no. 6, pp. 1057–1070, 1995.

[23] N. Pekergin, "Stochastic bounds on delays of fair queueing algorithms," in *INFOCOM (3)*, pp. 1212–1219, 1999.

[24] D. Stiliadis and A. Varma, "Latency-rate servers: a general model for analysis of traffic scheduling algorithms," *IEEE/ACM Transactions on Networking*, vol. 6, no. 5, pp. 611–624, 1998.

[25] D. Stiliadis and A. Varma, "Rate-proportional servers: a design methodology for fair queueing algorithms," *IEEE/ACM Transactions on Networking*, vol. 6, no. 2, pp. 164–174, 1998.

[26] K. Chen and L. Decreusefond, "An approximate analysis of waiting time in multi-class M/G/1/./EDF queues," in *Proceedings of the 1996 ACM SIGMETRICS international conference on Measurement and modeling of computer systems*, pp. 190–199, ACM Press, 1996.

[27] M. Andrews, "Probabilistic end-to-end delay bounds for earliest deadline first scheduling," *Proc. IEEE Infocom 2000*, pp. 603–612, 2000.

[28] V. Sivaraman and F. M. Chiussi, "Statistical analysis of delay bound violations at an earliest deadline first (EDF) scheduler," *Performance Evaluation*, vol. 36-37, no. 1-4, pp. 457–470, 1999.

[29] K. Elsayed, "Enhancing the end-to-end schedulability condition of EDF scheduling for real-time applications," *Proc. IEEE ATM Workshop Proceedings*, pp. 75–79, 1998.

[30] K. Zhu, Y. Zhuang, and Y. Viniotis, "Achieving end-to-end delay bounds by EDF scheduling without traffic shaping," *IEEE INFOCOM*, pp. 1493–1501, 2001.

[31] J. Lopez, M. Garcia, J. Diaz, and D. Garcia, "Worst-case utilization bound for edf scheduling on real-time multiprocessor systems," *12th Euromicro Conference on Real-Time Systems, 2000 (Euromicro RTS 2000)*, pp. 25–33, June 2000.

[32] M. G. Harbour and J. Palencia, "Response time analysis for tasks scheduled under EDF within fixed priorities," *24th IEEE Real-Time Systems Symposium*, pp. 200–209, 2003.

[33] K. Albers and F. Slomka, "Efficient feasibility analysis for real-time systems with EDF scheduling," *IEEE Computer Society, Proceedings of the Design, Automation and Test in Europe Conference and Exhibition*, pp. 492–497, 2005.

[34] T. P. Baker, "An analysis of EDF schedulability on a multiprocessor," *IEEE Transactions on Parallel and Distributed Systems*, vol. 16, August 2005.

[35] H. Zhang and S. Keshav, "Comparison of rate-based service disciplines," in *SIGCOMM*, pp. 113–121, 1991.

[36] G. Kesidis, J. Walrand, and C.-S. Chang, "Effective bandwidths for multiclass markov fluids and other ATM sources," *IEEE Transactions on Networking*, vol. 1, no. 4, pp. 424–428, August 1993.

[37] C. Courcoubetis and R. Weber, "Buffer overflow asymptotics for a buffer handling many traffic sources," *Journal of Applied Probability*, vol. 33, 1996.

[38] C. Courcoubetis, V. A. Siris, and G. D. Stamoulis, "Application of the many sources asymptotic and effective bandwidths for traffic engineering," *Telecommunications Systems*, pp. 167–191, Dec. 1999.

[39] F. Kelly, *Stochastic Networks: Theory and Applications*, vol. 4 of Royal Statistical-Society Lecture Notes Series, ch. Notes on effective bandwidths, pp. 141–168. Oxford University Press, 1996.

[40] D. Abendroth and U. Killat, "Effective bandwidth shaping: a framework for resource dimensioning," in *ICON2003, the 11th IEEE International Conference on Networks 2003*, pp. 361–366, Oct. 2003.

[41] J. Abate, G. L. Chourdhury, and W. Whitt, "Waiting-time tail probabilities in queues with long-tail service-time distributions," in *Queueing Systems*, vol. 16, pp. 311–338, 1994.

[42] J. Abate, G. L. Choudhury, and D. M. Lucantoni, "Asymptotic analysis of tail probabilities based on the computation of moments," in *Annals of Applied Probability*, vol. 5, pp. 983–1007, 1995.

[43] D. Stiliadis and A. Varma, "Frame-based fair queueing: A new traffic scheduling algorithm for packet-switched networks," Tech. Rep. UCSC-CRL-95-39, 1995.

[44] Y. Liu, S. Gruhl, and E. W. Knightly, "WCFQ: An opportunistic wireless scheduler with statistical fairness bounds," *IEEE Transactions on Wireless Communications*, vol. 2, no. 5, pp. 1017–1028, September 2003.

[45] I. E. Korbi and L. Saidane, "Analytical model of the earliest deadline first policy over 802.11," in *Fourth Advanced International Conference on Telecommunications, 2008. AICT '08*, pp. 180–187, 8–13 June 2008.

[46] Y. Wu, J. bo Wei, B.-S. Kim, Y. Xi, and D. tang Ma, "Opportunistic scheduling for delay sensitive flows in wireless networks," in *Proceedings of 16th International Conference on Computer Communications and Networks, 2007. ICCCN 2007*, pp. 7–12, 13–16 Aug. 2007.

[47] E. Ciftcioglu and O. Gurbuz, "Opportunistic scheduling with frame aggregation for next generation wireless LANs," in *IEEE International Conference on Communications, 2006*, pp. 5228–5233, June 2006.

[48] T. Kastrinogiannis and S. Papavassiliou, "Probabilistic resource allocation under opportunistic scheduling in wireless networks with multimedia services," in *12th IEEE Symposium on Computers and Communications, 2007. ISCC 2007*, pp. 699–705, 1–4 July 2007.

[49] D. Liao and L. Li, "Opportunistic scheduling for multiclass users with different QoS constraints in wireless data networks," in *International Conference on Wireless Communications, Networking and Mobile Computing, 2006. WiCOM 2006*, pp. 1–4, 22–24 Sept. 2006.

[50] L. L. Cam, "The central limit theorem around 1935," in *Statistical Science*, vol. 1, pp. 78–91, 1986.

[51] E. Limpert, W. A. Stahel, and M. Abbt, "Log-normal distributions across the sciences: Keys and clues," *BioScience*, vol. 51, no. 5, pp. 341–352, May 2001.

[52] L. G. Blackwood, "The lognormal distribution, environmental data, and radiological monitoring," *Environmental Monitoring and Assessment*, vol. 21, no. 3, pp. 193–210, June 1992.

[53] J. Wu, N. Mehta, and J. Zhang, "A flexible lognormal sum approximation method," *Mitsubishi Electric Research Laboratories www.merl.com*, pp. TR2005–099, December 2005.

[54] M. Abramowitz and I. A. Stegun, *Handbook of Mathematical Functions with Formulas, Graphs, and Mathematical Tables*. New York: Dover, ninth dover printing, tenth gpo printing ed., 1964.

[55] E. W. Weisstein, "Cramer's theorem." From MathWorld–A Wolfram Web Resource. URL: *mathworld.wolfram.com/CramersTheorem.html*.

[56] D. Downing and J. Clark, *Statistics the Easy Way*. Barron's Educational Series, 1997.

[57] W. W. Weisstein, "Normal sum distribution." From MathWorld–A Wolfram Web Resource. URL: *mathworld.wolfram.com/NormalSumDistribution.html*.

[58] S. Stone, "Understanding the black-scholes equation," *Risks and Rewards — Investment Section "A knowledge community for the society or actuaries"*, no. 50, August 2007.

[59] W. W. Weisstein, "Delta function." From MathWorld–A Wolfram Web Resource. URL: *mathworld.wolfram.com/DeltaFunction.html*.